รายงานวิจัยฉบับสมบูรณ์

โครงการพัฒนาอนุภาคระดับนาโนจากสารโพอลิไฮดรอกซีบิวทิวเรทให้เป็นตัวส่งถ่ายยาเพื่อใช้ในการบำบัดโรคมะเร็งด้วยวิธีโฟโต้ไดนามิกเทราปี

(Development of Polyhydroxyalkanoate Nanoparticles as Anti-Cancer Drug Carriers for Photodynamic Therapy)

โดย

ดร. ณัฏฐวี เนียมศิริ และคณะ

กันยายน 2556

สัญญาเลขที่ MRG 5380110

รายงานวิจัยฉบับสมบูรณ์

โครงการพัฒนาอนุภาคระดับนาโนจากสารโพอลิไฮดรอกซีบิวทิวเรทให้เป็นตัวส่งถ่ายยาเพื่อใช้ในการบำบัดโรคมะเร็งด้วยวิธีโฟโต้ไดนามิกเทราปี

(Development of Polyhydroxyalkanoate Nanoparticles as Anti-Cancer Drug Carriers for Photodynamic Therapy)

ผู้วิจัย	สังกัด
1. ดร. ณัฏฐวี เนียมศิริ	คณะวิทยาศาสตร์ มหาวิทยาลัยมหิดล
2. นางสาว ศศิวิมล ประมวล	คณะวิทยาศาสตร์ มหาวิทยาลัยมหิดล

สนับสนุนโดยสำนักงานคณะกรรมการการอุดมศึกษา สำนักงานกองทุนสนับสนุนการวิจัย และ มหาวิทยาลัยมหิดล

บทคัดย่อ

รหัสโครงการ: MRG 5380110

ชื่อโครงการ: โครงการพัฒนาอนุภาคระดับนาโนจากสารโพอลิไฮดรอกซีบิวทิวเรทให้เป็นตัวส่งถ่ายยาเพื่อใช้ในการบำบัดโรคมะเร็งด้วยวิธีโฟโต้ไดนามิกเทราปี

ชื่อนักวิจัย และสถาบัน: ดร. ณัฏฐวี เนียมศิริ
ภาควิชาเทคโนโลยีชีวภาพ คณะวิทยาศาสตร์ มหาวิทยาลัยมหิดล

อีเมล์: nuttawee.nia@mahidol.ac.th, niamsiri@gmail.com

ระยะเวลาโครงการ: 2 ปี (ขยายเวลาเพิ่มอีก 1 ปี)

บทคัดย่อ:

การรักษาแบบโฟโต้ไดนามิคเป็นวิธีรักษาแบบใหม่ที่นำมาใช้รักษาโรคมะเร็งหลายชนิด การใช้วิธีดังกล่าวเพียงอย่างเดียวหรือใช้ควบคู่กับการรักษาแบบอื่นจะทำให้การรักษาโรคโดยรวมมีประสิทธิภาพสูงสุด เนื่องจากมีความจำเพาะในการทำลายเนื้อร้าย หลักการพื้นฐานของการรักษาแบบโฟโต้ไดนามิค คือ การใช้สารโฟโต้เซนซิไทเซอร์หรือยาที่มีคุณสมบัติเป็นสารไวแสงฉีดเข้าไปในเนื้อเยื่อมะเร็ง สารไวแสงนี้จะสามารถสะสมได้ดีในเนื้อเยื่อมะเร็ง จากนั้นกระตุ้นสารไวแสงด้วยแสงที่มีความความยาวคลื่นจำเพาะ สารไวแสงจะออกฤทธิ์สร้างอนุมูลอิสระที่เป็นอนุพันธ์ของออกซิเจนเพื่อทำลายเนื้อร้าย ในขณะเดียวกันเนื้อเยื่อส่วนที่ดีจะได้รับผลกระทบน้อยมาก สารไวแสงมีคุณสมบัติไม่ชอบน้ำจึงทำให้สามารถสะสมได้ดีในเซลล์มะเร็ง แต่ก็เป็นปัญหาสำคัญเพราะตัวยาอาจไม่ละลายเมื่อฉีดเข้าไปในร่างกายผู้ป่วย

ในงานวิจัยนี้ทำการพัฒนาตัวนำส่งยาแบบนาโนพาร์ทิเคิลเพื่อใช้ในการส่งยาต้านมะเร็ง p-THPP ในการรักษาแบบโฟโต้ไดนามิคได้เป็นผลสำเร็จ โดยใช้พอลิเมอร์ที่ย่อยสลายได้รวมทั้งมีความเข้ากันได้ทางชีวภาพชนิดพอลิไฮดรอกซีอัลคาโนเอท หรือ PHAs ซึ่งผลิตได้จากเชื้อแบคทีเรียสายพันธุ์ *Cupriavidus necator* H16 โดยชนิดของ PHAs ที่สนใจ คือ พอลิไฮดรอกซีบิวทีเรทโคไฮดรอกซีวาเลอเรท P(HB-co-HV) ซึ่งเป็นโคพอลิเมอร์ซึ่งผ่านกระบวนการทำให้บริสุทธิ์ จากนั้นนาโนพาร์ทิเคิลสำหรับการนำส่งยาได้ถูกสร้างขึ้นโดยวิธีอีมัลซิฟิเคชั่นดิฟฟิวชันจาก PHAs 3 ชนิด โดยใช้สารพอลิไวนิลอัลกอฮอล์ 2 ชนิดเป็นสร้างความเสถียร นาโนพาร์ทิเคิลหุ้มยาสูตรต่างๆที่เตรียมได้มีขนาดเส้นผ่านศูนย์กลางระหว่าง 191-211 นาโนเมตร โดยที่มีปริมาณยาที่บรรจุในนาโนพาร์ทิเคิลอยู่ในระดับ 4 ถึง 9 เปอร์เซนต์และมีประสิทธิภาพในการกักเก็บยาอยู่ระหว่าง 41 ถึง 47 เปอร์เซนต์ ผลวิจัยเบื้องต้นในระดับห้องปฏิบัติการ พบว่านาโนพาร์ทิเคิลที่เตรียมจาก P(HB-co-65%HV) และกักเก็บยา p-THPP สามารถฆ่าเซลล์มะเร็งลำไส้ใหญ่ของมนุษย์ชนิดเอชที 29 ได้มากกว่า 70% ที่ความเข้มข้นของยา 6 µg/ml ภายหลังจากพรีอินคิวเบชั่น (Pre-incubation) เซลล์กับนาโนพาร์ทิเคิลเป็นเวลา 6 ชั่วโมงและฉายแสงที่ความเข้มแสง 6 J/cm^2 ซึ่งเทียบได้กับผลของ p-THPP อิสระที่ความเข้มข้นสูงกว่าคือ 8 µg/ml การทดลองนี้นับเป็นครั้งแรกที่ได้มีการศึกษากระบวนการผลิตนาโนพาร์ทิเคิลจาก PHAs เพื่อเป็นตัวนำส่งสารไวแสงสำหรับวิธีรักษาแบบโฟโต้ไดนามิค โดยมีข้อดีในการปลอดปล่อยยาอย่างช้าในลักษณะที่ถูกควบคุมเพื่อให้ยาอยู่ในร่างกายได้นานขึ้น

คำหลัก : พอลิไฮดรอกซีอัลคาโนเอท, การส่งถ่ายยา, นาโนพาร์ทิเคิล, วิธีรักษาแบบโฟโต้ไดนามิค, โรคมะเร็ง

Abstract

Project Code: MRG 5380110

Project Title: Development of Polyhydroxyalkanoate Nanoparticles as Anti-Cancer Drug Carriers for Photodynamic Therapy

Investigator: Dr. Nuttawee Niamsiri

E-mail Address: nuttawee.nia@mahidol.ac.th, niamsiri@gmail.com

Project Period: 2 years (with 1 year extension)

Abstract:

Photodynamic therapy (PDT) has been considered as one of promising strategy for various cancer treatments. The function of PDT depends on a special drug known as photosensitizer (PS) that can be activated by light at a particular wavelength to destroy the targeted cancer tissues, while leaving the nearby normal cells unharmed. Although the hydrophobicity of PS molecules is preferable for allowing them to localize towards cancer tissues, it often leads to low solubility of the PS drug molecules in blood stream, hampering their availability at cancer sites for PDT. To overcome this issue, the PS drugs are often encapsulated in a specialized carrier to improve the solubility of the PS, thus prolonging the drugs circulation while still maintaining their preferential accumulation at the tumor sites for PDT.

In this study, a new type of core-shell polymeric carrier to deliver meso-tetra(p-hydroxyphenyl)porphin (p-THPP) anti-cancer PS drug for PDT has been successfully developed from biodegradable and biocompatible polyesters polyhydroxyalkanoates (PHAs). Here, three different types of PHA known as poly(hydroxyburytrate-co-hydroxyvalerate) or P(HB-co-HV) having similar molecular weights, but varied in their %HV mole compositions were synthesized and purified from Cupriavidus necator H16. These PHAs copolymers were used for making nanoparticles in combination with two different sets of polyvinylalcohol (PVA) shell polymers via a modified emulsification-diffusion method. The different formulations of p-THPP-loaded PHA nanoparticles were subjected to various characterizations. The sizes of all p-THPP-loaded PHA nanoparticles were ranging from 191 to 211 nm in diameter. The % drug loadings of PHA nanoparticles was also optimized to be ranging from 4% to 9% with % entrapment efficiencies ranging from 41% to 47%. The preliminary in vitro photocytotoxicity against HT-29 colon cancer cells showed that the p-THPP-loaded P(HB-co-65%HV) nanoparticles could lead to almost 70% cell death at the equivalent drug dose of 6 μg/ml, after 6 h pre-incubation and the irradiated light dose at 6 J/cm^2, which was comparable to the effect of free p-THPP drug at higher concentration (i.e. 8 μg/ml). Thus far, this is the first report employing PHA nanoparticles as a PS drug carrier for PDT that also demonstrates their potentially beneficial effect of slow and controlled-release PS drugs for PDT.

Keywords: Polyhydroxyalknoates, Drug delivery, Nanopartilcles, Photodynamic therapy, Cancers

เอกสารแนบหมายเลข 3

บทคัดย่อ

การพัฒนากระบวนการผลิตอนุภาคระดับนาโนจากสารพอลิไฮดรอกซีอัลคาโนเอทเพื่อใช้เป็นตัวนำส่งยารักษาโรคมะเร็งแบบโฟโต้ไดนามิค

การรักษาแบบโฟโต้ไดนามิคเป็นวิธีรักษาแบบใหม่ที่นำมาใช้รักษาโรคมะเร็งหลายชนิด การใช้วิธีดังกล่าวเพียงอย่างเดียวหรือใช้ควบคู่กับการรักษาแบบอื่นจะทำให้การรักษาโรคโดยรวมมีประสิทธิภาพสูงสุด เนื่องจากมีความจำเพาะในการทำลายเนื้อร้าย หลักการพื้นฐานของการรักษาแบบโฟโต้ไดนามิค คือ การใช้สารโฟโต้เซนซิไทเซอร์หรือยาที่มีคุณสมบัติเป็นสารไวแสงฉีดเข้าไปในเนื้อเยื่อมะเร็ง สารไวแสงนี้จะสามารถสะสมได้ดีในเนื้อเยื่อมะเร็ง จากนั้นกระตุ้นสารไวแสงด้วยแสงที่มีความความยาวคลื่นจำเพาะ สารไวแสงจะออกฤทธิ์สร้างอนุมูลอิสระที่เป็นอนุพันธ์ของออกซิเจนเพื่อทำลายเนื้อร้าย ในขณะเดียวกันเนื้อเยื่อส่วนที่ดีจะได้รับผลกระทบน้อยมาก สารไวแสงมีคุณสมบัติไม่ชอบน้ำจึงทำให้สามารถสะสมได้ดีในเซลล์มะเร็ง แต่ก็เป็นปัญหาสำคัญเพราะตัวยาอาจไม่ละลายเมื่อฉีดเข้าไปในร่างกายผู้ป่วย

ในงานวิจัยนี้ทำการพัฒนาตัวนำส่งยาแบบนาโนพาร์ทิเคิลเพื่อใช้ในการส่งยาต้านมะเร็ง p-THPP ในการรักษาแบบโฟโต้ไดนามิคได้เป็นผลสำเร็จ โดยใช้พอลิเมอร์ที่ย่อยสลายได้รวมทั้งมีความเข้ากันได้ทางชีวภาพชนิดพอลิไฮดรอกซีอัลคาโนเอท หรือ PHAs ซึ่งผลิตได้จากเชื้อแบคทีเรียสายพันธุ์ *Cupriavidus necator* H16 โดยชนิดของ PHAs ที่สนใจ คือ พอลิไฮดรอกซีบิวทีเรทโคไฮดรอกซีวาเลอเรท P(HB-*co*-HV) ซึ่งเป็นโคพอลิเมอร์ซึ่งผ่านกระบวนการทำให้บริสุทธิ์ จากนั้นนาโนพาร์ทิเคิลสำหรับการนำส่งยาได้ถูกสร้างขึ้นโดยวิธีอีมัลซิฟิเคชั่นดิฟฟิวชันจาก PHAs 3 ชนิด โดยใช้สารพอลิไวนิลอัลกอฮอล์ 2 ชนิดเป็นสร้างความเสถียร นาโนพาร์ทิเคิลหุ้มยาสูตรต่างๆ ที่เตรียมได้มีขนาดเส้นผ่านศูนย์กลางระหว่าง 191-211 นาโนเมตร โดยที่มีปริมาณยาที่บรรจุในนาโนพาร์ทิเคิลอยู่ในระดับ 4 ถึง 9 เปอร์เซนต์และมีประสิทธิภาพในการกักเก็บยาอยู่ระหว่าง 41 ถึง 47 เปอร์เซนต์ *ผล*วิจัยเบื้องต้นในระดับห้องปฏิบัติการ พบว่านาโนพาร์ทิเคิลที่เตรียมจาก P(HB-*co*-65%HV) และกักเก็บยา p-THPP สามารถฆ่า*เซลล์*มะเร็งลำไส้ใหญ่ของมนุษย์ชนิดเอชที 29 ได้มากกว่า 70% ที่ความเข้มข้นของยา 6 μg/ml ภายหลังจากพรีอินคิวเบชั่น (Pre-incubation) เซลล์กับนาโนพาร์ทิเคิลเป็นเวลา 6 ชั่งโมงและฉายแสงที่ความเข้มแสง 6 J/cm ซึ่งเทียบได้กับผลของ p-THPP อิสระที่ความเข้มข้นสูงกว่าคือ 8 μg/ml การทดลองนี้นับเป็นครั้งแรกที่ได้มีการศึกษากระบวนการผลิตนาโนพาร์ทิเคิลจาก PHAs เพื่อเป็นตัวนำส่งสารไวแสงสำหรับวิธีรักษาแบบโฟโต้ไดนามิค โดยมีข้อดีในการปลอดปล่อยยาอย่างช้าในลักษณะที่ถูกควบคุมเพื่อให้ยาอยู่ในร่างกายได้นานขึ้น

I. ABSTRACT

DEVELOPMENT OF POLYHYDROXYALKANOATE NANOPARTICLES FOR ANTI-CANCER DRUG DELIVERY IN PHOTODYNAMIC THERAPY

Photodynamic therapy (PDT) has been considered as one of promising strategy for various cancer treatments. The function of PDT depends on a special drug known as photosensitizer (PS) that can be activated by light at a particular wavelength to destroy the targeted cancer tissues, while leaving the nearby normal cells unharmed. Although the hydrophobicity of PS molecules is preferable for allowing them to localize towards cancer tissues, it often leads to low solubility of the PS drug molecules in blood stream, hampering their availability at cancer sites for PDT. To overcome this issue, the PS drugs are often encapsulated in a specialized carrier to improve the solubility of the PS, thus prolonging the drugs circulation while still maintaining their preferential accumulation at the tumor sites for PDT.

In this study, a new type of core-shell polymeric carrier to deliver meso-tetra(p-hydroxyphenyl)porphin (p-THPP) anti-cancer PS drug for PDT has been successfully developed from biodegradable and biocompatible polyesters polyhydroxyalkanoates (PHAs). Here, three different types of PHA known as poly(hydroxyburytrate-*co*-hydroxyvalerate) or P(HB-*co*-HV) having similar molecular weights, but varied in their %HV mole compositions were synthesized and purified from *Cupriavidus necator* H16. These PHAs copolymers were used for making nanoparticles in combination with two different sets of polyvinylalcohol (PVA) shell polymers via a modified emulsification-diffusion method. The different formulations of p-THPP-loaded PHA nanoparticles were subjected to various characterizations. The sizes of all p-THPP-loaded PHA nanoparticles were ranging from 191 to 211 nm in diameter. The % drug loadings of PHA nanoparticles was also optimized to be ranging from 4% to 9% with % entrapment efficiencies ranging from 41% to 47%. The preliminary *in vitro* photocytotoxicity against HT-29 colon cancer cells showed that the p-THPP-loaded P(HB-co-65%HV) nanoparticles could lead to almost 70% cell death at the equivalent drug dose of 6 µg/ml, after 6 h pre-incubation and the irradiated light dose at 6 J/cm^2, which was comparable to the effect of free p-THPP drug at higher concentration (i.e. 8 µg/ml). Thus far, this is the first report employing PHA nanoparticles as a PS drug carrier for PDT that also demonstrates their potentially beneficial effect of slow and controlled-release PS drugs for PDT.

KEY WORDS: POLYHYDROXYALKANOATES/ NANAOPARTICLES/ DRUG DELIVERY/ PHOTODYNAMIC THERAPY/

II. EXECUTIVE SUMMARY

Cancer is a group of human diseases caused by out-of-control growth of abnormal cells, which may eventually result in death. Many medical applications have been studied for more than century, yet there is no perfect treatment for cancers. The primary problem is that cancer cells are truly like other general healthy cells, both in their main components and their sites. Such troubles make patients a lot of torturous side effects when undergone the cancer therapy process, and bring about difficulty in therapy achievement. For elimination of the problems mentioned, many combination therapies have been employed as the feasible ways to treat cancers because such combinations would integrate the advantages of each therapeutic principal [1].

One of the most interesting therapies for cancer is photodynamic therapy (PDT), which is a method of clinical treatment whereby diseased cells and tissues are destroyed by a combination of light and special drugs known as photosensitizers (PS) [1-4]. PS is a chemical compound that readily undergoes photo-excitation and then transfers its energy to other molecules (i.e. oxygen) under the influence of irradiation of light with appropriate wavelength. In biological environment, photosensitization is a simple and controllable method for the production of singlet oxygen ($^1O_2$), since PS is capable of absorbing and using light energy to excite oxygen to its singlet state [2, 4]. It is generally known that singlet oxygen is a cytotoxic agent responsible for photo-biological activity, and capable of damaging nucleic acids, proteins, and lipids in the cellular environment [5].

The concept of PDT for cancer treatment is based on the fact that the PS molecules can be preferentially localized in tumor tissues after systemic administration. Then, upon the illumination of light with specific wavelength, it leads to the generation of cytotoxic reactive oxygen species (ROS) [5]. When combined in proper dosage and concentration, ROS can irreversibly damage the treated tissues. Compared to current treatments including surgery, radiation therapy and chemotherapy, PDT appears to offer the advantages of an effective and selective method for destroying the diseased tissues, especially tumors, without damaging the surrounding healthy tissues [2, 4, 5]. The high selectivity of PDT is controlled by both

the preferential uptake of PS by the cancer cells and the ability to confine the activation of PS only to the tumor region by restricting the illumination of light to that specific region. Other advantages of PDT over the conventional cancer therapies include cost-effectiveness and higher cure rates (i.e. in palliative treatment of head and neck cancer or Barrett's esophagus) and the repetition of therapy can be done without cumulative toxicity [6]. Furthermore, PDT is very often an outpatient therapy (i.e. does not require long-term hospitalization), in contrast to the weeks to months of radiotherapy and chemotherapy or prolonged hospitalization of surgery [4, 7]. In addition, several studies have shown that PDT can also induce patient's immunity, even against less immunogenic tumors, thus leading to better treatment of cancers [4, 7].

Although PDT is becoming an established modality of treatment for various kinds of cancer with several advantages, the widespread clinical applications of PDT still remain hampered. This is mainly due to the hydrophobic property of the commonly used PS molecules, such as haemotoporphyrin derivatives (e.g. Photofrin®) [7]. Although the hydrophobicity is somewhat desirable because it is a key parameter responsible for the affinity of the PS molecules for the tumor issues, however this hydrophobicity often leads to poor solubility of the drug molecules in physiologically media, leading to impede their parenteral administration [7]. To overcome this issue, several strategies have been tried including the development of second-generation PS molecules including meso-tetra(4-hydroxyphenyl) porphyrin (p-THPP) that is slightly less hydrophobic, but still potent in its ability to photosensitize skin, brain and implanted plasma cell tumors [6, 8]. Another strategy involves chemically modification of the conventional porphyrin with polar substituents including sulphonic acid, carboxylic acid and hydroxyl groups [9].

Alternatively, hydrophobic PS molecules have been incorporated into colloidal carriers such as liposomes, ceramic- and metallic-based nanoparticles, as well as biodegradable polymeric-based nanoparticles [6, 8, 10, 11]. Another rationale for using such delivery systems is also related to their targeting ability. The PS-incorporated nanoparticles have been proved to exhibit greater efficacy for tumor treatment when compared with the free PS administered. They become even more

selective and potent to the cancer cells, especially when the surface of these nanoparticles is tailored with specific cancer targeting biomarkers [8, 10]. Several studies have shown that the size of the PS-nanoparticles carriers is also important, in which using the particles with smaller diameter mean size (i.e. less than 200 nm) are better suited for effective PDT than the particles with diameter mean size greater than 200 nm [6]. This is because the smaller nanoparticles are more effective blood-to-tumor transfer of colloidal delivery systems and have longer retention in tumor tissues [12]. In addition, such small particle size can help escaping the recognition of the particles by opsonins in the bloodstream, resulting in a reduction of their uptake by the mononuclear phagocytic system [13].

Using biodegradable polymers for making these PS-nanoparticle carriers are currently of great interest for PDT because of the way, in which the physical properties and degradation characteristics of these biodegradable polymers can be tailored and controlled. As a result, they have attracted much attention in the recent years, especially in relation to their applications in biomedical devices, drug delivery systems and tissue engineering scaffolds. Aliphatic polyesters such as polyglycolic acid) (PGA), polylactic acid (PLA), polycaprolactone (PCL), polyhydroxyalkanoates (PHAs) are the most important biodegradable polymers in the biomedical fields with frequent applications as the components in prosthesis and the controlled drug release systems [6, 8, 10, 14]. However, only PGA, PLA and PCL have been extensively studied and used for making PS-nanoparticle carriers for PDT [10], while only few research works have been reported for using PHA as the polymeric nanoparticle carrier for PS molecules [15].

Polyhydroxyalkanoates (PHAs) are aliphatic polyesters of various hydroxyalkanoates, which are synthesized by numerous microorganisms as an energy reserve material [16]. PHAs are considered to be extremely useful biomaterials for medical applications due to four important reasons. First, PHAs can be produced under a sustainable closed-cycle biotechnological process for the large-scale production and use of such polyesters and can be synthesized from renewable and cheap carbon sources based on agricultural or even on industrial wastes. Second, PHAs can be synthesized into either homopolymers, copolymers, or even heteropolymers, thus they

can provide a wide range of material properties that can match to various synthetic polymers currently in use for medical applications. Third, PHAs are biodegradable. The polymers can be broken down into monomer units simply via chemical hydrolysis in human body, especially under acidic and/or basic conditions. In addition, their biodegradation rate can also be varied depending on their monomer compositions depending. Lastly, PHAs also have an excellent biocompatible property [17]. Some of the monomers incorporated into PHA polymers are already found to be present in all higher animals. For example, the monomer components of poly(3-hydroxybutyrate), (*R*)-3-hydroxybutyric acid, is a common intermediate metabolite found in human blood [18], while the monomer component of poly(4-hydroxybutyrate), 4-hydroxybutanoic acid, is also a naturally occurring substance that is widely distributed in the mammalian body, being present in brain, kidney, heart, liver, lung, and muscle [19]. Therefore, PHAs are highly biocompatible with human body tissue, and have great potential in biomedical applications, especially for the controlled release drug delivery [20].

Here, we proposed to develop novel sub-200 nm nanoparticles as vehicles for the delivery of PS molecules used in PDT from different types of PHAs. This is because most of anti-cancer PS drugs are generally hydrophobic, which bring about less proficiency in cancer treatment via PDT. Therefore, these PS drugs need to be encapsulated in a special carrier, preferably one that is biodegradable and biocompatible with human body, as well as being able to facilitate cell penetrating while escaping host endocytosis as shown in **Figure 2.1**. Since the clinical applicability of these PHA nanoparticles have been considered as the primary importance, specific types of PHAs; poly(3-hydroxybutyrate) and poly(3-hydroxybutyrate-co-valerate) with varying %HV content, were selected for our formulation. This is mainly because their biodegradable and biocompatible properties have been extensively studied and proved to be quite suitable in drug delivery applications. In addition, the strategies for producing these PHAs are already well-studied, and can be produced in a large quantity simply via bacterial fermentation. These PHA nanoparticles was then be loaded with meso-tetra(p-hydroxyphenyl)porphin (p-THPP), a second-generation PS that is popularly used in

PDT of cancer. Furthermore, in order to assess the influence of the monomer ratio on the physiochemical and pharmacokinetic properties of the PHA nanoparticles, PHA polymers with similar molecular weight, but varied in % mole of HV monomer (i.e. 0%, 12% and 65% HV) were used for making different p-THPP-loaded PHA nanoparticles. These different formulations of p-THPP-loaded PHA nanoparticles were prepared by the emulsification-diffusion technique, which is a known method for generating sub-200 nm polymeric nanoparticles. They were subsequently studied and compared with respect to their size, surface characteristics, drug loading, entrapment efficiency, as well as profile of drug release. Finally, they were tested for *in vitro* cytotoxicity study via PDT against human colon cancer HT29 cell line.

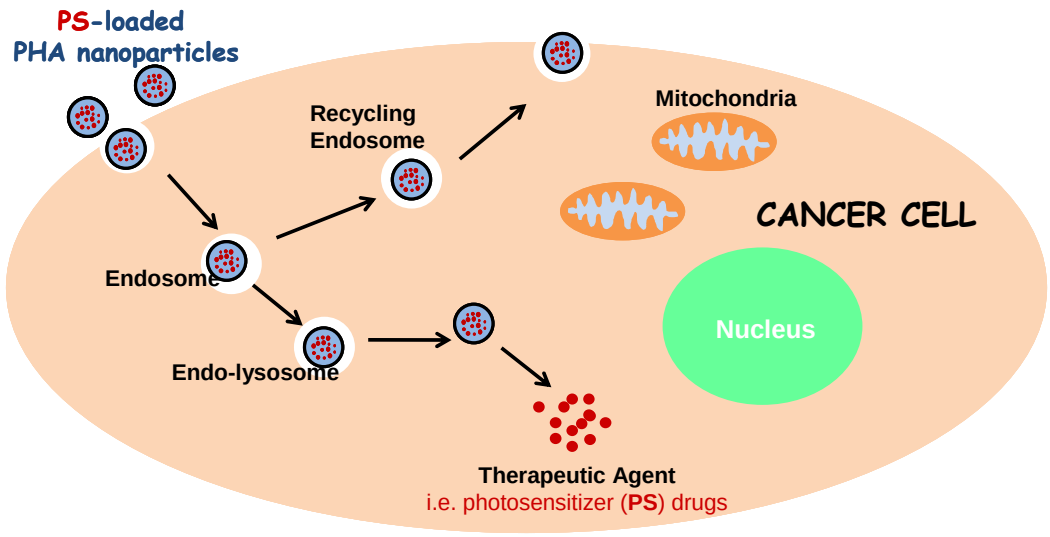

Figure 2.1 Intracellular trafficking of nanoparticles. Following their uptake, the sub-200 nm PS-loaded PHA nanoparticles are transported through early endosomes to the sorting endosomes. A fraction of nanoparticles recycles back to the cell exterior while another fraction is transported to secondary endosomes/lysosomes from where nanoparticles escape into the cytoplasm. The nanoparticles that escape into the cytoplasm could act as intracellular reservoirs for sustained release of the encapsulated therapeutic agent.

References:

1) Wright, F.C., et al., Multidisciplinary cancer conferences: A systematic review and development of practice standards. *European Journal of Cancer*, **2007**. 43: p. 1002-1010.
2) Schuitmaker, J.J., et al., Photodynamic therapy: a promising new modality for the treatment of cancer. *J. Photochem. Photobiol. B*, **1996**. 34: p. 3–12.
3) Vargas, A., et al., *In vivo* photodynamic activity of photosensitizer-loaded nanoparticles: Formulation properties, administration parameters and biological issues involved in PDT outcome. *Eur. J. Pharm. Biopharm.*, **2008**. 69: p. 43–53.
4) Wilson, B.C., Advanced photodynamic therapy. *Biophotonics*, **2008**: p. 315-334.
5) Dougherty, T.J., et al., Photodynamic therapy. *J. Natl. Cancer Inst.,* **1998**. 90: p. 889–905.
6) Chatterjee, D.K., L.S. Fong, and Y. Zhang, Nanoparticles in photodynamic therapy: An emerging paradigm. *Advanced Drug Delivery Reviews*, **2008**. 60: p. 1627-1637.
7) Brown, S.B., E.A. Brown, and I. Walker, The present and future role of photodynamic therapy in cancer treatment. *Lancet Oncol.*, **2004**. 5: p. 497–508.
8) Brannon-Peppas, L. and J.O. Blanchette, Nanoparticle and targeted systems for cancer therapy. *Adv. Drug Del. Rev.,* **2004**. 56: p. 1649– 1659.
9) Wolde, A., et al., Stability and scanning electron microscopy of Photofrin-II and Photosan-3. *J. Photochem. Photobiol. B: Biol.*, **1996**. 36: p. 139–142.
10) Bechet, D., et al., Nanoparticles as vehicles for delivery of photodynamic therapy agents. *Trends Biotechnol*, **2009**. 26: p. 612-621.
11) Gao, E., et al., Nanoparticles for two-photon photodynamic therapy in living cells. *Nano Lett.,* **2006**. 6: p. 2383-2386.
12) Kong, G., R.D. Braun, and M.W. Dewhirst, Hyperthermia enables tumor specific nanoparticle delivery: effect of particle size. Cancer Res., 2000. 60: p. 4440-4445.

13) Nagayasu, A., K. Uchiyama, and H. Kiwada, The size of liposomes: a factor which affects their targeting efficiency to tumors and therapeutic activity of liposomal antitumor drugs. *Adv. Drug Deliv. Rev.,* **1999**. 40: p. 75-87.

14) Brannon-Peppas, L., Recent advances on the use of biodegradable microparticles and nanoparticles in controlled drug deliver. *Int. J. Pharm.,* **1995**. 116: p. 1-9.

15) Simioni, A.R., et al., PHBHV/PCL microspheres as biodegradable drug delivery systems (DDS) for photodynamic therapy (PDT). *J. Mater. Sci.,* **2008**. 43: p. 580–584.

16) Anderson, A.J. and E.A. Dawes, Occurence, metabolism, metabolic rate, and industrial uses of bacterial polyhydroxyalkanoates. *Microbiological Reviews,* **1990**. 54: p. 450-472.

17) Ueda, H. and Y. Tabata, Polyhydroxyalkanonate derivatives in current clinical applications and trials. *Adv.Drug Del. Rev.,* **2003**. 55: p. 501–518.

18) Wiggam, M.I., et al., Treatment of diabetic ketoacidosis using normalization of blood 3-hydroxybutyrate concentration as the endpoint of emergency management. *Diabetes Care,* **1997**. 20: p. 1347-1352.

19) Bessman, S.P. and W.N. Fishbein, Gamma-hydroxybutyrate, a normal brain metabolite. *Nature,* **1963**. 200: p. 1207-1208.

20) Pauton, C.W. and S. Akhtar, Biosynthetic polyhydroxyalkanoates and their potential in drug delivery. *Adv. Drug Del. Rev.*, **1996**. 18: p. 133-162.

III. RESEARCH OBJECTIVES

Because most of anti-cancer PS drugs are generally hydrophobic, which bring about less proficiency in cancer treatment via PDT, therefore, these PS drugs need to be encapsulated in a special carrier, preferably one that is biodegradable and biocompatible with human body, as well as being able to facilitate cell penetrating while escaping host endocytosis.

The overall research aim is to develop sub-200 nm polymeric nanoparticles from PHA as a novel carrier for PS drugs used in PDT for the treatment of cancers. Therefore, the objectives of this research work were divided into four steps as follow:

3.1 To biosynthesize P(HB-*co*-65%HV) copolymer via bacterial cultivation and characterize the produced PHA copolymer

3.2 To prepare and characterize various nanoparticles made from three different types of PHA polymers and two different types of poly(vinyl alcohol) (PVA) stabilizer:

3.3.1 Types of PHAs used in the study:

- PHB
- P(HB-*co*-12%HV)
- P(HB-*co*-65%HV)

3.2.2 Types of PVA stabilizer used in the study:

- Low molecular weight PVA (MW 13,000-23,000)
- High molecular weight PVA (MW 30,000-70,000)

3.3 To prepare various types of the PS-loaded PHA nanoparticles and characterize for physical properties of the PS-loaded PHA nanoparticles

3.4 To perform bioassays to evaluate *in vitro* cytotoxicity and photocytotoxicity for each type of PS-loaded PHA nanoparticles via PDT on the human colon adenocarcinoma cell line HT-29.

IV. MATERIALS AND METHODS

4.1 Materials

4.1.1 Chemicals and Reagents

Chemicals and reagents used in this study were analytical and biotechnological grade and obtained from companies as listed in Table 3.1.

Table 4.1 List of chemical and reagents.

Chemicals and Reagents	**Company**	**Molecular formula**
Ammonium sulfate	Scharlau, EU	$(NH_4)_2SO_4$
Benzoic acid	Fisher Scientific, UK	C_6H_5COOH
Calcium chloride	Sigma-Aldrich, Germany	$CaCl_2$
Chloroform	RCI Labscan, Japan	$CHCl_3$
Chromium (III) chloride hexahydrate	Sigma-Aldrich, Germany	$CrCl_3.6H_2O$
Cobalt (II) chloride hexahydrate	Sigma-Aldrich, Germany	$CoCl_2.6H_2O$
Copper (II) sulfate pentahydrate	Sigma-Aldrich, Germany	$CuSO_4.5H_2O$
D-Fructose	BDH, England	$C_6H_{12}O_6$
D-Glucose	Ajax, Australia	$C_6H_{12}O_6$
Dimethy sulfoxide	Sigma, USA	$(CH_3)_2SO$
Di-Sodium hydrogen phosphate dodecahydrate	Merk, Germany	$Na_2HPO_4.12H_2O$
Ethanol	RCI Labscan, Japan	CH_3CH_2OH
Glycerol	Ajax, Australia	$C_3H_5(OH)_3$
Iron (III) chloride	Sigma-Aldrich, Germany	$FeCl_3$
Magnesium sulfate heptahydrate	Merck, Germany	$MgSO_4.7H_2O$
Methanol	RCI Labscan, Japan	CH_3OH

Table 4.1 List of chemical and reagents (Cont.)

Chemicals and Reagents	Company	Molecular formula
Nikel (II) chloride hexahydrate	Sigma-Aldrich, Germany	$NiCl_2.6H_2O$
Poly(3-hydroxybutyric acid-*co*-3-hydroxyvaleric acid) 12% HV	Sigma-Aldrich, Germany	$C_9H_{18}O_6$
Potassium dihydrogen phosphate	Merck, Germany	KH_2PO_4
Potassium chloride	BDH, England	KCl
Tetrahydrofuran	RCI Labscan, Japan	C_4H_8O
Sodium D-gluconate	Merck, Germany	$C_6H_{11}NaO_7$
Sodium chloride	Ajax, Australia	NaCl
Sodium propionate	Merck, Germany	CH_3CH_2COONa
Sulfuric acid	RCI Labscan, Japan	H_2SO_4
Valeric acid	Sigma-Aldrich, Germany	$CH_3(CH_2)_3COOH$
3-(4,5-Dimethylthiazol-2-yl)-2,5-diphenyltetrazolium bromide (MTT)	Sigma, USA	$C_{18}H_{16}BrN_5S$
5,10,15,20-Tetrakis(4-hydroxyphenyl)-21H,23H-porphine (p-THPP)	Sigma-Aldrich, Germany	$C_{44}H_{30}N_4O_4$

4.1.2 Microbiological culture media

Table 4.2 List of microbiological culture media.

Ingredients of culture media	Company
Agar	Difco-Lab, France
Tryptone	Difco-Lab, France
Yeast extract	Difco-Lab, France

4.1.3 Mammalian cell culture media

Table 4.3 List of mammalian cell culture media.

Ingredients of culture media	Company
Dulbecco's Modified Eagle Medium (DMEM)	Gibco-Invitrogen, USA
Antibiotics/Antimycotics	Gibco-Invitrogen, USA
Fetal Bovine Serum (FBS)	Gibco-Invitrogen, USA

4.2 Methods

The aim of this study is to develop the suitable delivery system for anti-cancer drug to be used in PDT. In particular, we are focusing on the preparation of a sub-200 nm PS-loaded polymeric nanoparticles that can be made from three different types of polyhydroxyalkanoates (PHAs) as a vehicle to deliver the hydrophobic second generation PS drug molecules. To accomplish our research, the research work was divided into three phase. First (PHASE I.), the desired PHA polymer with appropriate composition was synthesized via bacterial cultivation and characterized. Second (PHASE II.), various types of both PHA nanoparticles and PS-loaded PHA nanoparticles were prepared and characterized. Lastly (PHASE III.), a preliminary *in vitro* cytotoxicity and photocytotoxicity studies of PS-loaded PHA nanoparticles on HT-29 colon cancer cell line was performed.

4.2.1 Biosynthesis of polyhydroxyalkanoate (PHAs) via bacterial cultivation and characterization of the produced PHA polymers

4.2.1.1 Inoculum preparation and cultivation conditions for P(HB-co-HV) production

In this study, *Cupriavidus necator* H16 (or formally known as *Ralstonia eutropha* H16) was used mainly for the production of PHA copolymers. The inoculum of this bacterium was prepared by inoculating a single colony from a 2-days old culture grown on Lauria Bertani (LB) agar plate; 10 g/L tryptone, 5 g/L yeast extract, 10 g/L NaCl and 15 g/L agar, into 5 mL LB broth and incubated on a rotary shaker at 200 rpm at 30ºC for 20 h. Then, the 5-mL cultured inoculum was transferred

into 45 mL LB broth in a 250-mL Erlenmeyer flask. After cultivation for 16 h, the bacterial culture was centrifuged at 4,000 rpm at 4ºC for 15 min. The cell pellet was obtained and then washed once with phosphate buffer saline (PBS) solution; 8 g/L NaCl, 0.2 g/L KCl, 1.44 g/L Na_2HPO_4 and 0.24 g/L KH_2PO_4. Then, The bacterial inoculum was prepared by adjusting to have OD_{600} around 5.0-6.0 prior to inoculate at 10% (v/v) into Mineral Salt (MS) medium; 11 g/L $Na_2HPO_4.12H_2O$, 1.2 g/L KH_2PO_4, 1.4 g/L $MgSO_4.7H_2O$ and 1 g/L $(NH_4)_2SO_4$, The MS also contains 1 mL/L of trace elements; 0.22 g/L $CoCl_2.6H_2O$, 9.7 g/L $FeCl_3$, 7.8 g/L $CaCl_2$, 0.12 g/L $NiCl_2.6H_2O$, 0.11 g/L $CrCl_3.6H_2O$ and 0.16 g/L $CuSO_4.5H_2O$, which is used as a PHA production medium after adding the respective carbon source. The MS medium was prepared with a working volume of 100 mL in 500-mL flask. Various carbon substrates that were subjected to the investigation included glucose, fructose, sodium gluconate, sodium propionate and sodium valerate. Each of carbon sources was aseptically added to each culturing conditions in MS medium at the respective concentrations. The initial pH was measured and adjusted to be around 7.0. Then, the flasks were incubated on a rotary shaker at 200 rpm at 30ºC for 48 h. After the end of cultivation, the bacterial growth was monitored by measuring the OD_{600}. To harvest the PHA-accumulating cells, the cells were centrifuged at 4,000 rpm, 4ºC for 15 min. The cell pellets were washed twice with PBS buffer and further frozen at -80ºC for 1 h. Then, the frozen cells were subjected to drying via lyophilization. The values of biomass were obtained by weighing dried cells in the unit of g/L of cell dried weight (CDW).

4.2.1.2 Detection of PHA accumulation in bacterial cells via fluorescent microscopy

The PHA accumulated in bacterial cells were detected by staining the bacterial cells with a lipophilic dye known as Nile-Blue A (Ostle and Holt, 1982) to visualize the lipophilic PHA inclusion bodies inside the bacterial cells under fluorescence microscopy. To do this, the heat-fixed smears of bacterial cells were stained with Nile-Blue A solution for 2 min. Then, the slides were washed with water followed by an 8% acetic acid solution for 1 min, washed once again. Finally, the stained slides were air dried and covered with a cover slip before observed under

microscope (Olympus Model BX51, Olympus optical Co., Ltd., Japan) with fluorescence attachment using a green filter.

4.2.1.3 Determination of %HV monomer content and overall % P(HB-co-HV) content per cell dried weight (CDW) via Gas Chromatography (GC) analysis

The method of PHA determination that widely used is based on a standard methanolysis in chloroform as previously described elsewhere (Huijberts *et al*., 1994). Briefly, 20 mg of lyophilized cells was added into 18x160 mm screw capped tube and mixed with 2 mL chloroform. Then, methanol solution containing 85% (v/v) methanol, 15% (v/v) sulfuric acid and 2 mg/mL benzoic acid as an internal GC standard were added to the mixture of cells and chloroform. After incubation of mixture solution for 3.5 h at 85^{o}C, 2 mL of distilled water was added and mixed vigorously for 5 min. The mixture was separated into two layers: the aqueous layer on top of the chloroform layer. The resulting hydroxyacyl methyl esters in the bottom chloroform layer was further analyzed using Gas chromatography (Model 6890 plus, Agilent Technology, USA) equipped with HP-INNOWAX 30.0 m, 0.25 mm, 0.25 μm capillary columns and flame deionization detector (FID).

Gas chromatography condition:

Injection port temperature	:	250^{o}C
Detector temperature	:	250^{o}C
Pressure of gas carrier (He)	:	26.01 psi
Column flow	:	2 mL/min

Column oven temperature program:

Rate (^{o}C/min)	Temperature (^{o}C)	Hold time (min)
-	130	6.00
5	180	0.00
-	200.0	2.00

The PHA concentration of each sample was determined by comparison to the standard curves of HB and HV, which was constructed based on the relation between the peak area ratio of HV to benzoate and the concentrations of P(HB-*co*-12%HV).

4.2.1.4 PHA extraction

To purify PHA polymers, various recovery technologies have already been employed to extract the polymers out from the bacterial cells in the laboratory as well as at the industrial scale. The extraction strategies include solvent extraction, enzymatic treatments, and mechanical disruption (Jacquel *et al*., 2008; Kunasundari & Sudesh, 2011; Valappil *et al*., 2007). However, since the ultimate applications for our research is to extract polymer for the use of making drug-encapsulated nanoparticles for medical application, the clean separation of PHA polymers from the rest of the cellular materials at the highest level of purity (~100% purity) is a very important criteria. As a result, the solvent extraction and precipitate of pure PHA polymers using organic solvents was selected to be our means of purifying PHAs from the bacterial cells.

The solvent extraction process was performed by a standard solvent extraction technique that has used routinely in our laboratory in order to obtain pure PHB and P(HB-*co*-65%HV) for nanoparticle preparation. In brief, the bacterial cells were collected by centrifugation, washed twice with PBS and further lyophilized 24 h using Lyophilizer (Freeze zone plus 6, Labconco, USA). The polymer was isolated from the lyophilized cells using hot chloroform as the main organic solvent using the ratio of weight of dried cells (i.e. gram) to volume of solvent (i.e. mL) at 1:25. After the refluxing for 24 h at 60°C under stirring condition, the cell-chloroform mixture was filtered through a Whatman No. 1 paper filter to remove debris. The PHA polymer which dissolved in chloroform was precipitated with 10-fold volume of cold methanol. The extracted PHA was dried at room temperature for 48 h to completely remove the solvent from the collected polymer. Then, the % purity and the composition of %HV monomer content were also re-confirmed through GC analysis.

4.2.1.5 Chemical characterization of functional groups via Fourier Transform Infrared Spectroscopy (FT-IR)

Fourier Transform Infrared Spectroscopy (FT-IR) is a well-known method for basic chemical characterization of polymers based on chemical bonding and functional groups. The FT-IR spectra can indicate the type of atomic bonding and functional groups present in the polymer structure, in which each of them

has a specific adsorption wavelength due to vibration and bending of the molecules in their chemical structure. To characterize PHAs via FT-IR, 0.2 g of each PHA was casted into a thin film. A Perkin-Elmer Spectrum-GX NIR FT-IR (Maryland, USA) was used to collect FT-IR reflectant spectrum of each PHA film in the interval of 6500-500 cm^{-1}, at spectral resolution of 8 cm^{-1} resolution, and 128 scans per sample. The peak of ester carbonyl functional group of PHAs should appear at 1730 to 1625 cm^{-1} and the peak of C-H bending at around 3000 cm^{-1} (Duarte *et al*., 2009).

4.2.1.6 Molecular weight analysis via Gel Permeation Chromatography (GPC)

Gel Permeation Chromatography (GPC) is one of the most widely used techniques to determine the molecular weight and molecular weight distribution of polymeric materials such as PHAs (i.e. PHB, P(HB-*co*-5%HV), and P(HB-*co*-12%HV)) samples. Gel Permeation Chromatography (GPC) analyses were carried out on a Waters e2695 instrument equipped with Model 3580 refractive index detectors, Model 270 differential viscometer/light scattering detector and two 10 μm PL gel columns. Two columns of GPC were in series and a refractive index detector, with chloroform as the elution solvent (flow rate, 0.6 mL min^{-1}) at 40°C. The polymer samples were dissolved in chloroform (0.1% w/v) and injection volume was 60 μl. A polystyrene standard dissolved in chloroform (0.1% w/v) was used to construct the calibration curve (Wu *et al*., 2005). In order to measure the molecular weight of P(HB-*co*-65%HV), the dissolving and elution solvents were changed to tetrahydrofuran (THF) (Reignier & Huneault, 2006).

4.2.1.7 Thermal analysis of PHAs via Differential Scanning Calorimeter (DSC)

PHAs were characterized via DSC in order to evaluate their thermal properties. This method was used to detect melting temperature (T_m) and glass transition temperature (T_g) of each polymer. T_m is a temperature required for all of crystalline bodies in the polymer to be destroyed, resulting in the melting of the polymer chains, whereas T_g is a temperature, in which there is a change in the heat capacity as the polymer matrix goes from the glassy state to the rubbery state. All

PHAs were characterized for their T_m and T_g via DSC (DSC 822e, Mettler Toledo, Switzerland) under nitrogen atmosphere. To do this, around 5 mg of PHAs were weighed and put into a DSC aluminum pan. The polymer was heated at 10°C/min until 25°C to 200°C for melting point temperature measurement, and maintained temperature at 200°C for 10 min. After that, PHAs were allowed to slowly crystallize by decreasing temperature gradually to -20°C at 10°C/min, and finally heated at 10°C/min until -20°C to 200°C for detecting the glass temperature (Mittal *et al*., 2010).

4.2.1.8 Hydrophilicity evaluation of PHAs via Contact Angle Measurement (CAM)

The surface hydrophilicity of PHA film was measured by a sessile drop method at room temperature using the Contact Angle instrument (DM-CE1, Kyowa Interface Science Co., Ltd., Saitama, Japan) optical bench-type contact angle goniometry. To do this, the PHAs film samples were prepared by dissolved 0.2 g of each polymer into 5 mL chloroform. Then, poured the polymer solution in a circle glass plate with 5 cm in diameter and covered with the lid to allowed slowly evaporation of chloroform. Drops of purified water were deposited onto the film surfaces and direct microscopic measurement of the contact angle was done with the goniometry (Rathbone *et al*., 2010).

4.2.1.9 Mechanical properties measurement of PHA film

The PHA film was prepared based on a method that described previously. Then, the PHAs film was cut to the size of 1 cm x 5 cm and 0.1 mm thickness. The tensile property was determined by the Instron Univesal tensile tester (Model 5566 H1612, USA). Tensile force was applied by to PHAs film at strain rate of 5 mm/min using 100 N load cell (Chen & Wu, 2005). The tensile strength was calculated as below:

Tensile strength (N/mm^2) = Breaking force (N) / cross-section area of sample (mm^2)

4.2.2 Preparation and characterization of bare PHA nanoparticles and p-THPP-loaded PHA nanoparticles

4.2.2.1 Nanoparticles preparation

The PHA nanoparticles were prepared by a method based on an emulsification-diffusion method as previously described elsewhere (Konan *et al*., 2003), which could be summarized as a diagram in Figure 3.1. Firstly, the known weight of PHA was dissolved in chloroform as a stock solution at 1 g/L. Next, the organic phase was prepared by blending the polymer stock solution with ethanol for a certain volume ratio with final volume of 3 mL, while an aqueous phase was prepared by dissolving a certain amount of PVA, which was used as a stabilizer, in ultrapure water to a final concentration of 0.5%. The organic phase (1 mL each time) was continuously then added into the magnetic stirred aqueous phase (30 mL, 500 rpm). Subsequently, the mixed solution was subjected to ultrasonication using an ultrasonicating machine (DT 2200, Bandelin Sonopuls, Germany) with a booster horn SH 213 G and titanium flat tip TT13 positioning its tip at the half height of the solution at the middle for 2 min for 5 times with 1 min break for emulsification. The output power of ultrasonicator was at 50 watt constantly. Finally, the solvent diffusion step was conducted by adding 30 mL ultrapure water rapidly into the magnetic stirring emulsified solution at 300 rpm.

To study the effect of %HV content of PHAs and the effect of stabilizer on the physicochemical properties (i.e. size, zeta potential, % drug loading, % encapsulation efficiency), and later on the cytotoxicity and photocytotoxicity of drug-loaded polymeric nanoparticles used for PDT, four different PHA polymers; PHB, P(HB-*co*-5%HV), P(HB-*co*-12%HV) and P(HB-*co*-65%HV), and two types of poly(vinyl alcohol) (PVA) (i.e. low molecular weight PVA (MW 13,000-23,000) (Jia-Gen *et al*., 2011) and high molecular weight PVA (MW 30,000-70,000) (Govender *et al*., 1999)) with a same degree of hydrolysis of 87-89% as a shell stabilizer were employed for making the nanoparticles under the same procedure.

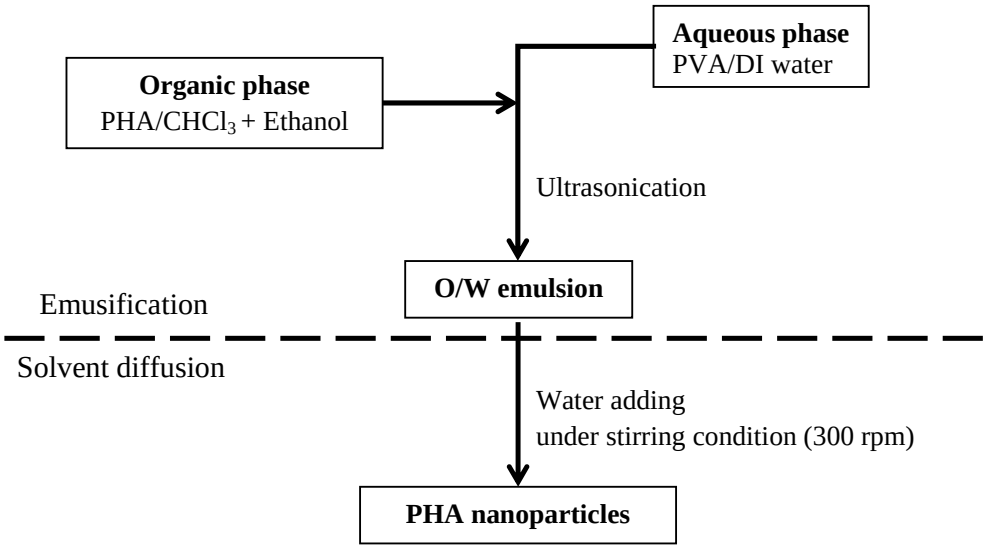

Figure 4.1 Schematic representations of the emulsification-diffusion methods.

For producing p-THPP-loaded PHA nanoparticles, one of the most popular second generation photosensitizer molecules, meso-tetra(p-hydroxyphenyl)porphyrin (p-THPP) was chosen as a photosensitizing (PS) agent in this study. The structure of p-THPP was shown in Figure 3.3. To prepare the p-THPP-loaded nanoparticles, 0.75, 1.5 and 3 mg of p-THPP, which was calculated as 5, 10 and 20% initial drug loading, respectively, was dissolved in organic phase before the emulsification. To protect the p-THPP-loaded nanoparticle formulations from light, all containers of each step were covered from the light all along the preparation process. Furthermore, after solvent diffusion step of all formulations, the PHA nanoparticles prepared by the modified emulsification-diffusion were then filtered through a Sartorius membrane-filter with a pore-size 0.45 µm using syringes as a way to reduce the number of contaminants prior to the evaluation of the cytotoxicity and photocytotoxicity of PHA nanoparticles on cancer cells.

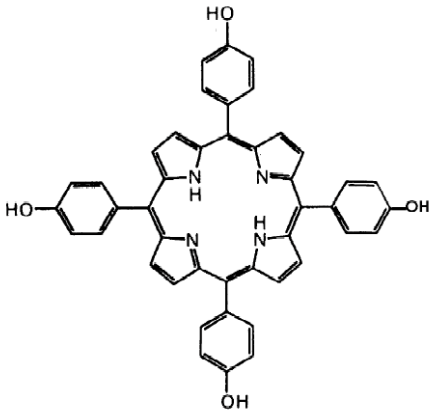

Figure 4.2 Structural formula of p-THPP (Konan *et al*., 2003).

4.2.2.2 Study of size, polydispersity index and zeta potential of PHA nanoparticles

All formulations of the PHA nanoparticles were analyzed in term of particles' mean size, size distribution and zeta potential. The mean size and polydispersity index or PDI was measured by dynamic light scattering (DLS) using Zetasizer Nano ZS (Malvern instruments, UK). Generally, polydispersity index is a parameter to define the particle size distribution of nanoparticles obtained from photon correlation spectroscopic analysis. It is a dimensionless number extrapolated from the autocorrelation function and ranges from a value of 0.01 for monodispersed particles and up to values of 0.5-0.7. The nanoparticles having very broad size distribution typically have the polydispersity index values > 0.7 (Sreeram *et al*., 2009). In this study, zeta potential, which is a term used to describe the nature of the electrostatic potential near the surface of a nanoparticle, was also determined for various types of PHA nanoparticles in 0.1 M sodium acetate by electrophoretic mobility using Zetasizer Nano ZS. The measurement condition was set as 25°C, water and polystyrene latex spheres were also used as a standard.

4.2.2.3 Measurement of % drug loading and % entrapment efficiency of various PHA nanoparticles

The p-THPP-encapsulated nanoparticles were characterized for drug loading content and the entrapment efficiency. The drug-loaded polymeric nanoparticles were subjected to a freeze-drying process in order to obtain dried weight of the nanoparticles. Briefly, the filtered drug-loaded nanoparticles were collected from a 25-mL solution by centrifugation at speed 12,500 rpm in order to separate unencapsulated p-THPP drugs from the drug-loaded PHA nanoparticles. The obtained pellet was then washed twice using 0.25% (w/v) PVA solution, and last with DI water. The suspensions of nanoparticles were then collected in pre-weighed 2.0-mL microcentrifuge tubes and kept in a -80°C freezer for 1 h. Freeze-drying of nanoparticles was carried out using a lyophilize machine at 0.001 bar without addition of any lyoprotectant in order to measure accurate weight of dried drug-encapsulated nanoparticles. The freeze-dried samples were then weighed and stored at 4°C in the dark before performing the drug loading analysis.

To calculate the % drug loading, a known amount of freeze-dried drug-loaded PHA nanoparticles was dissolved in 1 mL tetrahydrofuran (THF) and continuously mixed by using a vortex mixer for 2 min until the drug and PHA polymer were complexly dissolved into THF. Then, the amount of drug present in the solvent was measured using a spectrophotometer (Helios alpha, England) at wavelength of 421 nm. At 421 nm, it is known to be one of specific adsorption wavelengths at which the p-THPP drug can absorb the most light as shown in Figure 3.3. By comparing to a standard curve of various concentrations of pure p-THPP dissolved in THF (Figure 3.4), the % drug loading and the % entrapment efficiency of each drug-loaded PHA nanoparticles could be calculated as the following equations.

Extinction coefficient of p-THPP in THF = 0.5826, THF volume = 1 mL

MW of p-THPP = 678.76

$$\text{Weight of p-THPP in the nanoparticles (μg)} = \frac{\text{Absorbance} \times \text{Dilution factor} \times 678.76 \times 0.5\ \text{mL}}{0.0221 \times 1000\ \text{mL}}$$

$$\%\ \text{Drug loading} = \frac{\text{Amount of photosensitizer in nanoparticles}}{\text{Amount of nanoparticles}} \times 100$$

$$\%\ \text{Entrapment efficiency} = \frac{\text{Drug loading}}{\text{Theoretical drug loading}} \times 100$$

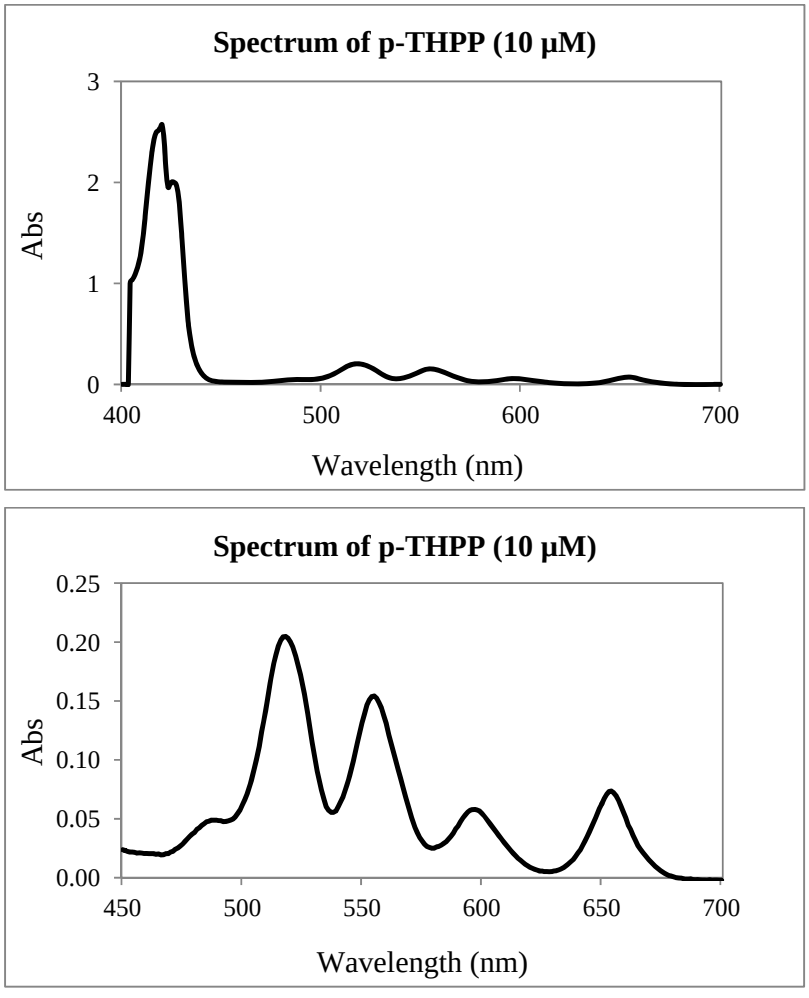

Figure 4.3 Absorption spectra of p-THPP dissolved in THF (10 μM).

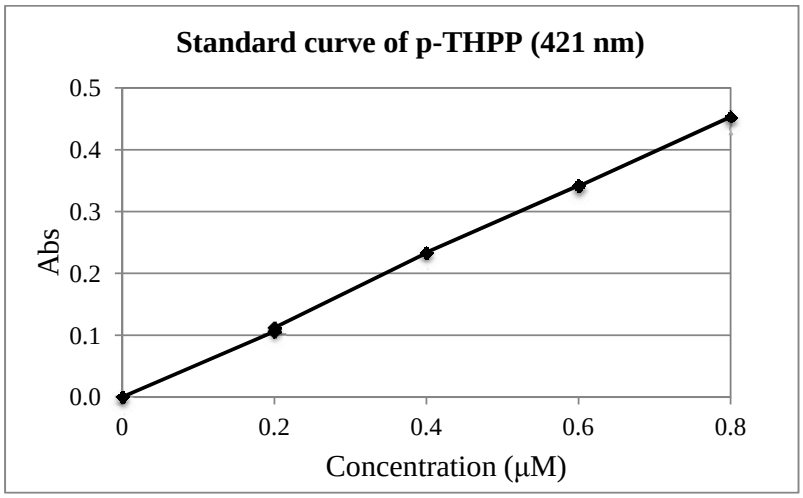

Figure 4.4 Standard curve of p-THPP in THF (λ_{abs} = 421 nm).

4.2.2.4 Characterization of p-THPP-loaded PHA nanoparticles via Transmission Electron Microscopy (TEM)

The morphology of p-THPP-loaded PHA nanoparticles was observed by Transmission electron microscopy (TEM). To do this, the nanoparticles solution was dropped onto a carbon coated copper grid and allowed to be air-dried. Next, the samples were negatively stained using 1.5% phosphotungstic acid (PTA). The excess solution was blotted off using a filter paper. The stained grid was then air-dried, and subsequently visualized under TEM.

4.2.3 Analysis of *in vitro* cytotoxicity and photocytotoxicity of PHA nanoparticles

To analyze the cytotoxicity and photocytotoxicity of p-THPP-loaded PHA nanoparticles for PDT of cancer, HT-29 human adenocarcinoma cell line was tested for cell viability under photodynamic activity of p-THPP-loaded PHA nanoparticles compared to free p-THPP. Our preliminary on the cell study focused on the influence of drug concentration encapsulated in the nanoparticles, pre-incubation time and light dose on the *in vitro* photocytotoxicity of p-THPP.

4.2.3.1 Cell culture

The human colon adenocarcinoma cell line HT-29 was maintained according to an established protocol as previously described elsewhere (Kummalue *et al*., 2009). Typically, a monolayer culture of human colon adenocarcinoma cell line HT-29 was grown in Dulbecco's Modified Eagle's Medium (DMEM) supplemented with 10% (v/v) fetal bovine serum, 100 U/mL penicillin, 100 μg/mL streptomycin and 125 ng/mL amphotericin B under humidified atmosphere with 5% (v/v) CO_2 at 37°C.

4.2.3.2 Study the influence of p-THPP concentrations on cell viability

As a mean to choose proper p-THPP concentration for photocytotoxicity assay of drug-loaded PHA nanoparticles, the p-THPP drug alone was firstly tested to evaluate its cytotoxic effect at various concentrations according to a previous study (Konan *et al*., 2003). Briefly, the 100-μL aliquot of $1x10^4$ cells per well of HT-29 cells in DMEM culture medium was seeded into each well of a 96-well clear bottom black plate in 100 μL of culture medium. The plate was incubated under 5% CO_2 atmosphere for 24 h at 37°C to allow the cells to attach the bottom of each well. The fresh culture medium containing p-THPP were then added into the well to get the final drug concentration of 2, 4, 8 and 16 μg/mL and further pre-incubated at 37°C for 1 h. Then, the culture plate was washed once with serum-free DMEM and 100 μL of fresh culture medium were added into each well, following incubation either without exposure to light (i.e. for evaluating the dark toxicity assay) or exposed to red light at wavelength 653 nm (i.e. for evaluating the phototoxicity assay used in PDT treatment) at a specific light dose of 6 J/cm^2 using LED lamp (Acnelamp, Dima-Tech, Inc., USA) with the exposure time of 12 min 45 sec. The treated cells were further incubated for 24 h with a fresh culture medium by covered with foil to prevent exposure to light. Lastly, the viability of treated HT-29 cells was performed using a standard cell proliferation assay with 3-(4,5-dimethyl-thiazol-2-yl-2,5-diphenyl tetrazolium bromide) or MTT assay in order to measure the number of viable cells left after PDT irradiation as a previously described protocol elsewhere (Lirdprapamongkol *et al*., 2009). Briefly, after removing the culture medium, the wells were replaced and

incubated with fresh culture medium containing MTT (0.5 mg/mL) for 2 h at 37°C. Finally, 100 μL DMSO was added into each well right after removing the media containing MTT, and then measured spectrophotometrically at 550 nm with a background subtraction at 650 nm in a microplate reader. The % cell viability from each condition was calculated and used to assess the cell activities comparing with the controls.

4.2.3.3 Study of the influence of light dose on cell viability

In an attempt to obtain the optimal conditions for the comparative study for different formulations of p-THPP-loaded PHA nanoparticles versus free p-THPP drugs, our preliminary investigation was carried out with an aqueous solution of p-THPP after the known amount of effective dose of p-THPP was obtained. The effect of light dose on p-THPP photocytotoxicity was then evaluated at 1 h pre-incubation with a certain concentration of drug. The HT-29 cancer cells cultivation technique was performed the same as previously described. Briefly, aliquots of $1x10^4$ cells per well of the HT-29 cell line was seeded into each well of 96-well clear bottom black plates in 100 μL of culture medium. The plate was incubated under 5% CO_2 atmosphere for 24 h at 37°C. After the spent medium was removed, the 100 μL fresh medium containing p-THPP were added into the well to get the final concentration of 2, 4 and 8 μg/mL and further pre-incubated for 1 h. Then, the culture plate was washed once with serum-free DMEM, and added with 100 μL of fresh medium. The plate was then exposed to the red light source with wavelength 653 nm, with a specific light dose of either 6 or 9 J/cm^2. The plate was incubated for another 24 h before evaluating the final cell viability with the standard MTT assay as previously described above.

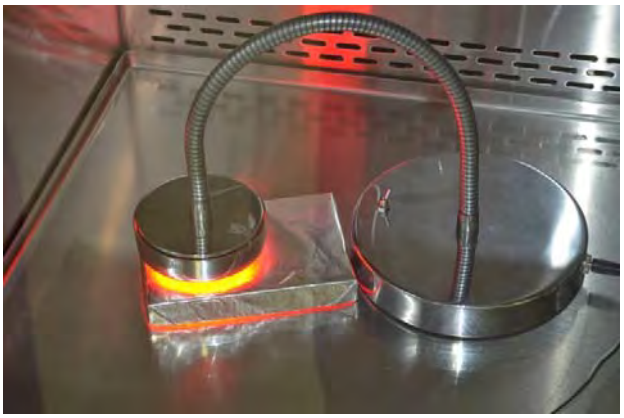

Figure 4.5 Radiation of the LED red light (λ = 653 nm) on HT-29 cancer cells treated with various concentration of p-THPP.

3.2.3.4 Photocytotoxicity assay of the p-THPP-loaded PHA nanoparticles

After obtaining the proper p-THPP concentration and light dose, we further evaluated the effect of the pre-incubation time of cells with either free drug or drug-loaded PHA nanoparticles prior to irradiation with light in order to observe any enhancement on the photocytotoxicity of p-THPP-loaded PHA nanoparticles on cell death. In this experiment, only p-THPP-loaded P(HB-*co*-65%HV) nanoparticles was used as a representative of all other p-THPP-loaded PHA nanoparticles, in which the drug-loaded nanoparticles formulation was prepared by using10% initial p-THPP loading.

Briefly, $1x10^4$ of HT-29 cancer cells were seeded into each well of the 96-well clear bottom black plate with 100 μL of culture medium. The plate was incubated under 5% CO_2 atmosphere for 24 h at 37°C before the photocytotoxicity assay. Then, the cells were incubated with 8 μg/mL of free drug, and also with the equivalent drug of 1.5, 3 and 6 μg/mL of p-THPP-loaded P(HB-*co*-65%HV) nanoparticles under different pre-incubation times ranging from 5 min to 6 h. Following the pre-incubation, the cells in each well were washed once with serum-free DMEM, and subjected to 100 μL of fresh medium. Finally, the plate was exposed to the specific light (λ = 653 nm) with a light dose of 6 J/cm^2. The plate was then incubated for 24 h before prior to MTT assay to observe the cell viability. The dark

toxicity of all formulations (i.e. the toxic of free p-THPP and p-THPP-loaded PHA nanoparticles when no light irradiation) were also performed as negative.

4.2.4 Statistical analysis

The data were subjected to a statistical analysis using SPSS 17.0 software package for windows. Means were compared using the student's t-test and one-way ANOVA (Duncan or Scheffe test). Significant differences were reported for $p \leq 0.05$.

V. RESULTS AND DISCUSSION

5.1 Biosynthesis and characterization of P(HB-*co*-HV) copolymers

5.1.1 Effect of carbon sources on biomass and PHA accumulation by *C. necator* H16

It is generally known that the *C. necator* H16 can accumulate PHA polymers at high level per cell dried weight (CDW) (Lee *et al*., 2008). The appropriate type of carbon source for each PHA-producing bacterium is one of the important factors for obtaining high biomass and PHA content. Different types of carbon sources were studied in MS media. As shown in **Figure 5.1**, when using glucose, fructose and sodium gluconate at 20 g/L, we found that sodium gluconate appears to be the best carbon substrate for obtaining the highest biomass at 6.7 g/L, but only resulting into 30.51% PHA content per CDW. On the other hand, fructose was found to be the best for obtaining high % PHA content at 90.33% per CDW also with suitable biomass at 4.3 g/L, thus leading to the most highest in the overall PHA production at 3.70 g/L. In this experiment, we found that using glucose as the sole carbon source leading to a very low biomass at 0.7 g/L as well as very low % PHA content at 3.02% per CDW, thus resulting in the PHA production at only 0.02 g/L.

It appears that *C. necator* H16 cannot utilize glucose for its growth, which might be due the fact that *C. necator* H16 is lacking of a 6-phosphofructokinase enzyme (E.C. 2.7.1.11) located in the Embden-Meyerhof-Parnas (EMP) pathway that convert fructose-6-phosphate to fructose-1,6-bisphosphate. In order for this strain to metabolize hexoses, Entner-Doudoroff (ED) pathway is utilized rather than the EMP pathway (Park *et al*., 2011; Raberg *et al*., 2011). Furthermore, the strain has no genes encoding a PEP-dependent phosphotransferase system (PTS) or transporters specific for glucose in its genome, while it possesses genes for both fructokinase and glucokinase, as well as all other genes encoding enzymes of the ED pathway for further catabolism of glucose-6-phosphate. Thus, fructose and sodium gluconate are

more readily taken up by the bacterial cells and better utilized than glucose when supplied as the sole carbon source in the media. *C. necator* H16 is also capable of utilizing various organic compounds, but its ability to metabolize sugars appears to be restricted to fructose and the amino sugar *N*-acetylglucosamine and gluconate (Sichwart *et al*., 2010). Nevertheless, the type of PHAs produced by *C. necator* H16 when supplying glucose, fructose, and sodium gluconate as the single carbon source is polyhydroxybutyrate (PHB) homopolymer. These results suggested that our strain could utilize these three types of carbon substrates for the homopolymer production via glycolytic pathway leads to the increase of acetyl-CoA which is a precursor for 3-HB monomer.

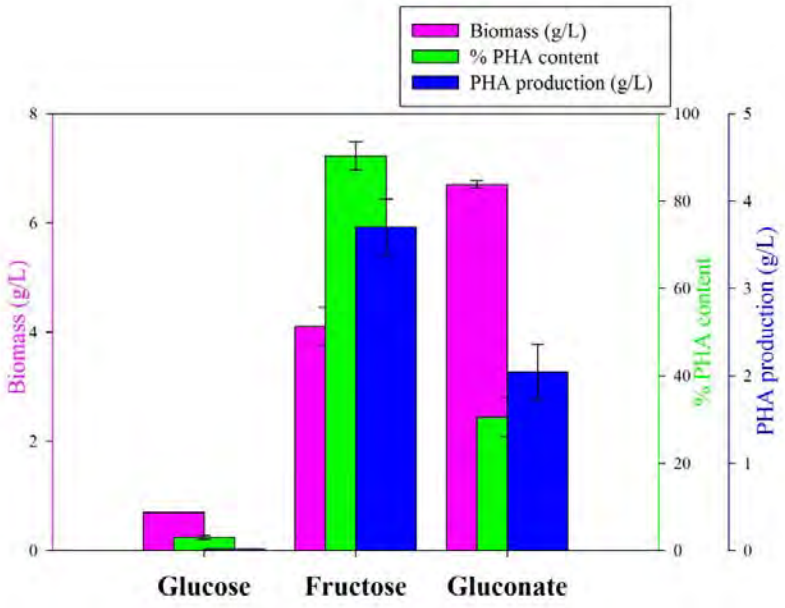

Figure 5.1 Growth and PHA accumulation by *C. necator* H16 when culturing in MS media with 20 g/L of various carbon sources under shaking condition at 200 rpm and 30˚C for 48 h. All experiments were done in duplicate at each condition (mean ± SD, n=2).

5.1.2 Effect of sodium propionate and sodium valerate concentration on biomass and PHA accumulation by *C. necator* H16

The sodium propionate and sodium valerate are the other two carbon substrates that can be metabolized for the production of P(HB-*co*-HV) by *C. necator* H16. In this experiment, the fructose was already provided at 10 g/L, while supplementing with 10 g/L of either sodium propionate or sodium valerate. The results showed that the biomass of both conditions are nearly equal at 3.25 and 3.30 g/L, respectively, while the % PHA content per CDW was found to be 46.78 and 97.04, respectively, and thus resulting in the overall PHA production of 1.54 and 3.22 g/L, respectively (**Figure 5.2**).

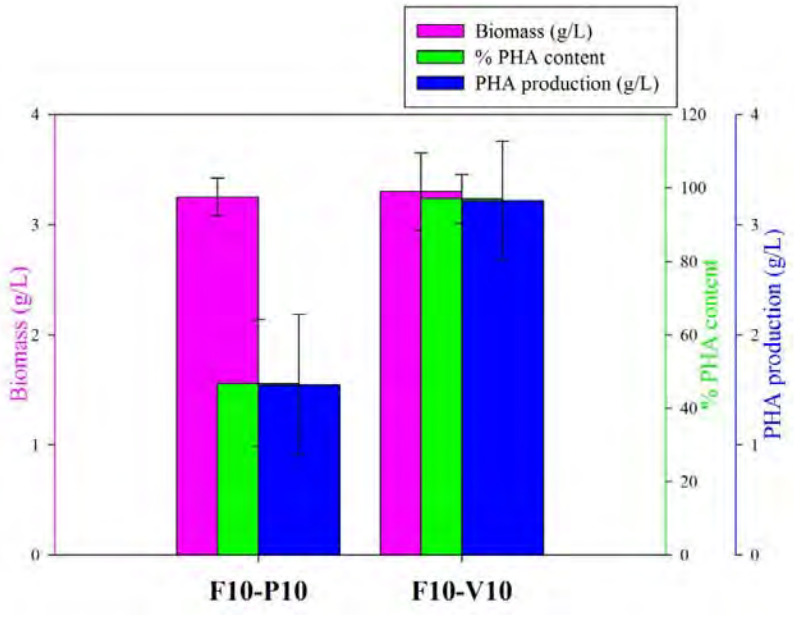

Figure 5.2 Growth and PHA accumulation by *C. necator* H16 when culturing in MS media with 10 g/L fructose together with 10 g/L of either sodium propionate or sodium valerate under shaking condition at 200 rpm and 30˚C for 48 h. All experiments were done in duplicate at each condition. (NOTE: F10-P10 and F10-V10 are representing fructose at 10 g/L combined with sodium propionate at 10 g/L and fructose at 10 g/L combined with sodium valerate at 10 g/L, respectively) (mean ± SD, n=2).

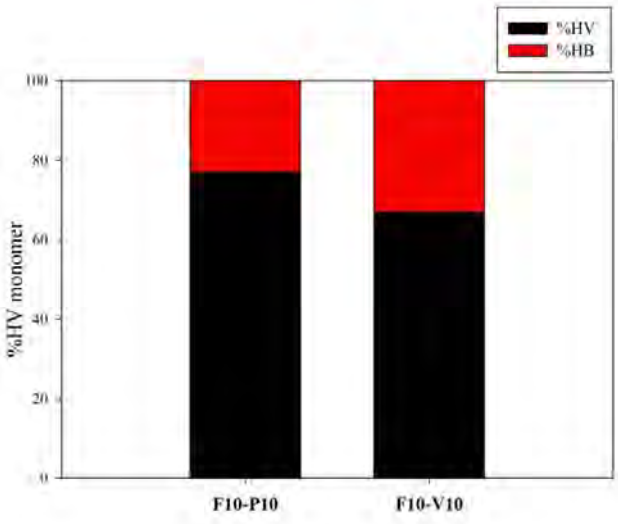

Figure 5.3 %HB and %HV monomer content in the PHA polymer by *C. necator* H16 when culturing in MS media with different combinations of carbon sources.

When adding either sodium propionate or sodium valerate, the %HV mole fraction in the P(HB-*co*-HV) copolymer was found to be 77% and 66%, respectively (**Figure 5.3**). It is important to note that feeding propionate to the culture of *C. necator* leads to propionyl-CoA formation, which then can be condensed with acetoacetyl-CoA to generate 3-ketovaleryl-CoA, a main precursor for 3-HV subunit as shown in Figure 2.15. Addition of sodium valerate directly leads to the increase of 3-ketovaleryl-CoA precursor via *β*-oxidation by the enzyme enoyl-CoA hydratase and L-(+)-3-hydroxyacyl-CoA dehydrogenase, which can directly convert valeryl-CoA to 3-ketovaleryl-CoA as found in *Azotobacter salinestris* (**Figure 5.4**). Although our results showed that co-feeding fructose with either of these two carbon substrates could result in the production of P(HB-*co*-HV) copolymer. However, this bacterial strain prefers using sodium valerate more than sodium propionate for introducing 3-HV monomer into the PHB polymer based on the overall production of PHA in this study. Our results are similar with a previous observation by Kemavongse *et al.* (2007) showed that a bacterial mutant strain identified as *Rhodobacter sphaeroides* could produce P(HB-*co*-HV) in the medium with acetate as a carbon source supplemented with either valeric acid or propionic acid. They found that valeric acid exhibited a better co-substrate as it gave higher HV monomer fraction than propionic acid. The highest % HV monomer at 84% was reported when used valeric acid, while only 20% was

observed when propionic acid was used as a co-carbon substrate (Kemavongse *et al*., 2007). Bhubalan *et al.* (2008) studied the biosynthesis of P(3HB-*co*-3HV-*co*-3HHx) terpolymers from mixtures of palm kernel oil and 3-HV-precursors by using the recombinant strain of *C. necator* (Bhubalan *et al*., 2008). Sodium valerate and sodium propionate have evaluated as a 3-HV precursors for the generation of 3-HV monomers. The results suggested that sodium valerate can be converted more efficiently into 3-HV monomers compared to sodium propionate. Due to propionic acid is need to be converted to propionyl-CoA and it has to be condensed with an acetyl-CoA molecule in order to generate 3-HV monomer. Previous study by Doi and co-workers had made similar findings that valeric acid could generate a 2-fold higher composition of 3-HV monomers compared to propionic acid when it was supplied as the sole carbon substrate (Doi *et al*., 1990)

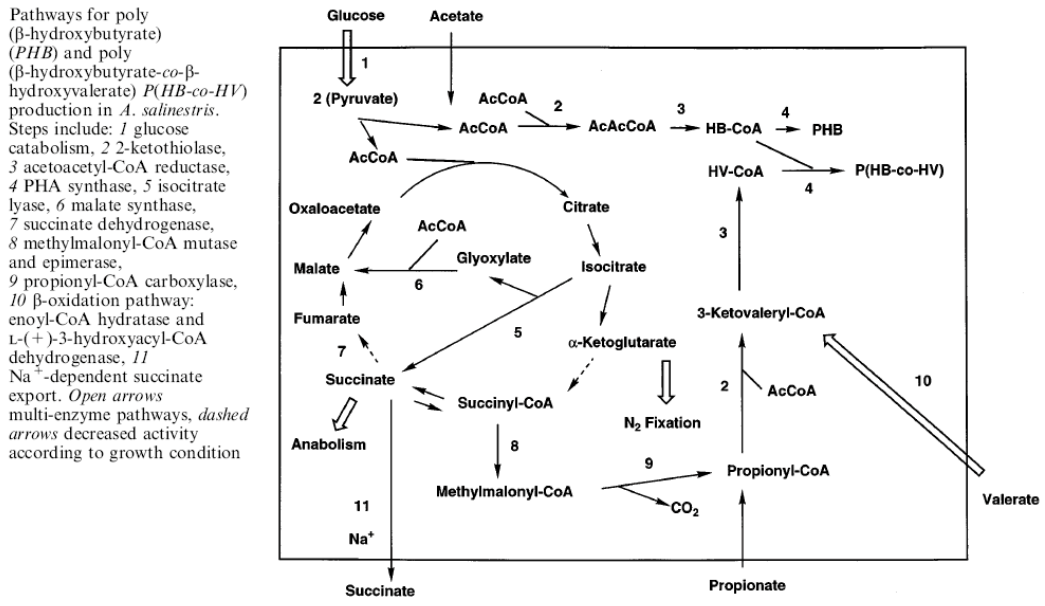

Pathways for poly (β-hydroxybutyrate) (*PHB*) and poly (β-hydroxybutyrate-*co*-β-hydroxyvalerate) *P(HB-co-HV)* production in *A. salinestris*. Steps include: *1* glucose catabolism, *2* 2-ketothiolase, *3* acetoacetyl-CoA reductase, *4* PHA synthase, *5* isocitrate lyase, *6* malate synthase, *7* succinate dehydrogenase, *8* methylmalonyl-CoA mutase and epimerase, *9* propionyl-CoA carboxylase, *10* β-oxidation pathway: enoyl-CoA hydratase and L-(+)-3-hydroxyacyl-CoA dehydrogenase, *11* Na^+-dependent succinate export. *Open arrows* multi-enzyme pathways, *dashed arrows* decreased activity according to growth condition

Figure 5.4 Pathways for poly(*β*-hydroxybutyrate)(PHB) and poly(*β*-hydroxybutyrate-*co*-(*β*-hydroxyvalerate) P(HB-*co*-HV) production in *Azotobacter salinestris* (Page, 1992).

5.1.3 Effect of varying concentrations of fructose and sodium valerate on biomass and P(HB-*co*-HV) accumulation by *C. necator* H16

Due to the goal of this work is to come up with batch cultivation strategies that leads to the overall production of P(HB-*co*-HV) by *C. necator* H16 with the %HV content in the polymer chain at 50% mole or higher and also with the biomass of at least 1 g/L. The effect of combining fructose and sodium valerate at various concentrations on the bacterial growth and the P(HB-*co*-HV) production by *C. necator* H16 were investigated and the results were shown below.

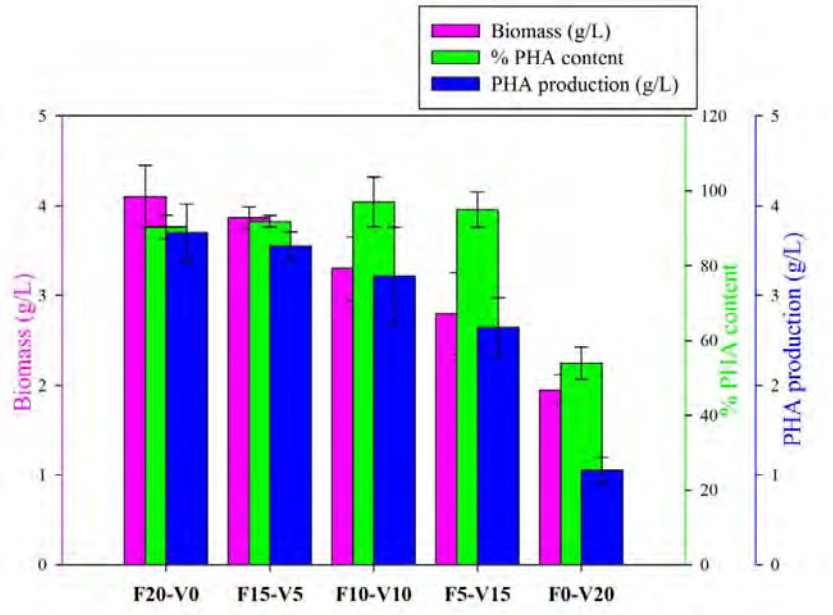

Figure 5.5 Growth and PHA accumulation by *C. necator* H16 when culturing in MS media with various concentrations of fructose and sodium valerate under shaking condition at 200 rpm and 30˚C for 48 h. All experiments were done in duplicate at each condition (mean ± SD, n=2).

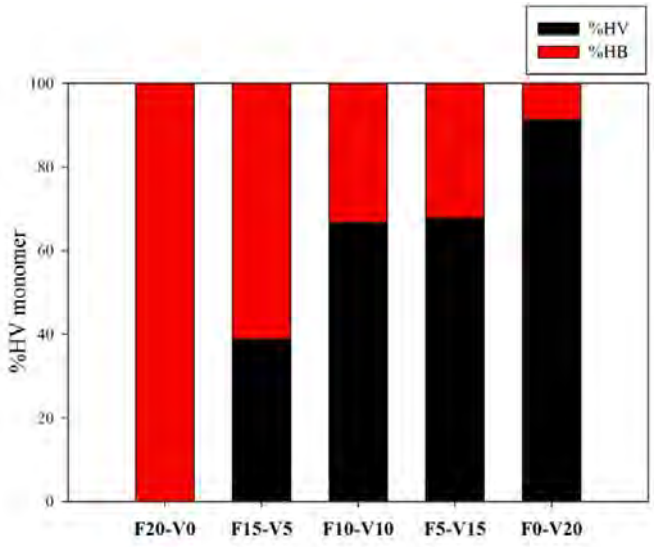

Figure 5.6 %HB and %HV monomer content in the P(HB-*co*-HV) copolymer by *C. necator* H16 when culturing in MS media with various concentrations of fructose and sodium valerate.

As shown in **Figure 5.5**, the results showed that when supplied the mixed substrates between fructose and sodium valerate into the MS media at various combinations of carbon concentration, we were able to obtain high % P(HB-*co*-HV) content at around 90% per CDW at all the culturing conditions except F0-V20 (i.e. the PHA content was at 53.96% per CDW). The biomass from using F20-V0, F15-V5, F10-V10, F5-V15, F0-V20 combinations were at 4.10, 3.87, 3.30, 2.80, and 1.95 g/L, respectively, and thus leading to the overall P(HB-*co*-HV) production at 3.70, 3.55, 3.22, 2.64, 1.05, respectively. These data suggesting that fructose is the most suitable carbon substrate to be up taken and readily metabolized by this bacterial stain leading to higher biomass. Khanna *et al.* (2004) reported that the use of fructose among twelve carbon substrates, *Ralstonia eutropha* (former name of *C. necator*) exhibited a maximum biomass of 3.25 g/L with a PHB concentration of 1.4 g/L at 48 h (Khanna & Srivastava, 2005). Fereidouni *et al.* (2011) obtained up to 92% PHA content after *C. necator* growth on 5 g/L acetate and 40 g/L fructose in an excess carbon source condition (Fereidouni *et al.*, 2011). However, we found that decreasing fructose concentration had no effect on the % P(HB-*co*-HV) content per CDW. This might be due to the fact that another carbon substrate (i.e. sodium valerate) was co-supplied to

maintain the total concentration of carbon source to always be at 20 g/L in the MS media. As shown in **Figure 5.6**, the co-supplying sodium valerate to the MS media could result into the PHA copolymer consisting of HB and HV monomers. We found that increasing of sodium valerate from 5, 10, 15 to 20 g/L (i.e. at the condition: F15-V5, F10-V10, F5-V15, and F0-V20, respectively) could led to the increasing of %HV mole fraction in the P(HB-*co*-HV) copolymers to be at 0.29, 38.97, 66.87, 67.95 and 91.48% mole, respectively. Interestingly, the HB monomer was found to be produced even though supplying only sodium valerate at 20 g/L in the MS medium. This might be due the fact that valerate itself can be metabolized via the fatty acids degradation pathway (i.e. β-oxidation pathway), leading to acetyl-CoA formation, which can be directly diverted to TCA cycle for making ATP as well as used for producing HB monomer as show in Figure 2.15. Similar results were already observed in those studied by Bhubalan *et al.* (2010) that the addition of 10 g/L sodium valerate in the presence of 10 g/L fructose, the CDW was found to be at 3.0 g/L. On the other hand, the % HV monomer was found to be at 35%, which is much lower comparing with our production (Bhubalan *et al.* 2010).

A common method used to observe PHA granules inside the bacterial cells is by observing under fluorescence microscope after staining the bacterial cells with a lipophilic Nile-blue A dye. **Table 5.1** showed the morphology of *C. necator* H16 that produced various types of PHA using different carbon substrates. Light microscope images showed that the cell shape of this strain was also changed after PHA accumulated, in which when they produce PHAs, they appear to be shorter rod and more round. The fluorescent intensity of stained cells was found to be depended strongly on the % PHA content accumulated inside the cells, which was further confirmed by gas chromatography analysis. When *C. nectar* H16 grown with glucose 20 g/L as the sole carbon substrate, they did not produce significant amount of PHA polymers, thus they were only lightly fluorescent when staining with Nile-blue A. Our results are similar with those studies by Chanprateep *et al.* (2008) that reported the morphology variation of PHA-accumulating *R. eutropha* strain A-04 that they become short rod cells ranging from 0.6 to 1.0 μm under transmission electron micrograph of ultra-thin section (Chanprateep *et al.*, 2008). It could be observed by TEM that some cells of recombinant *E. coli* JM109 contained granules of various sizes and some cells

contained mainly smaller granules which resulted in the variation of cell shape as well (Bhubalan *et al.*, 2011).

Table 5.1 Light (A) and fluorescent (B) microscope images of Nile blue A-stained *C. necator* cells in different culture conditions.

Polymer types	**Culturing conditions**	**Bright field**	**Fluorescent field**
PHB (Control)	LB agar		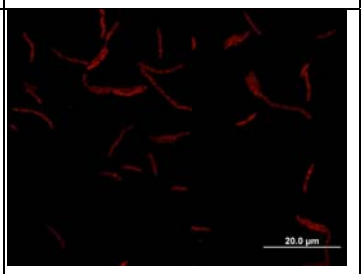
PHB (Negative)	Glucose 20 g/L	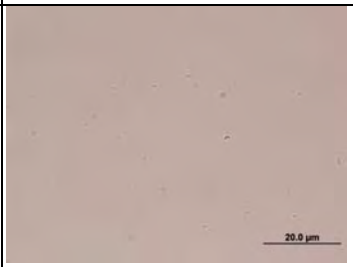	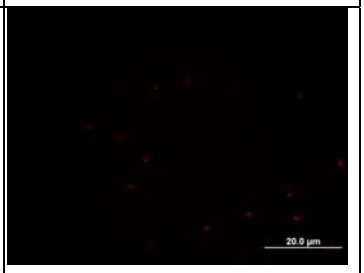
PHB (Positive)	Fructose 20 g/L	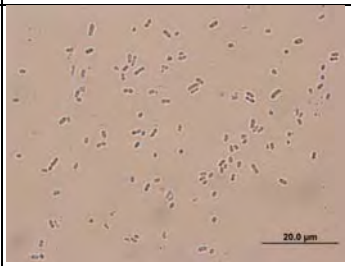	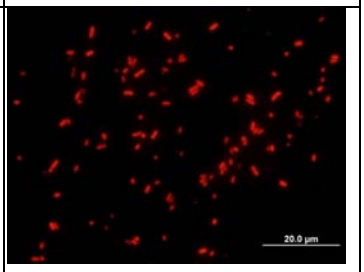
P(HB-*co*-35%HV)	Fructose 15 g/L Sodium valerate 5 g/L		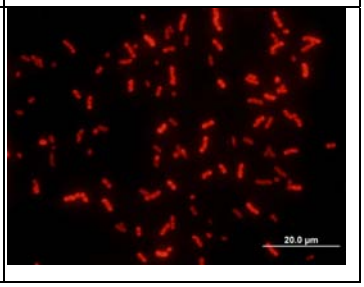

Table 5.1 (Cont.) Light (A) and fluorescent (B) microscope images of Nile blue A-stained *C. necator* cells in different culture conditions.

Polymer types	Culturing conditions	Bright field	Fluorescent field
P(HB-*co*-65%HV)	Fructose 5 g/L Sodium valerate 15 g/L	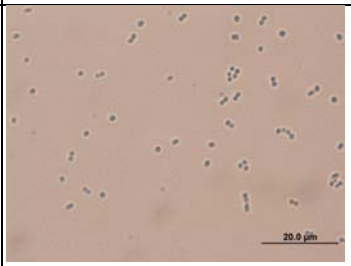	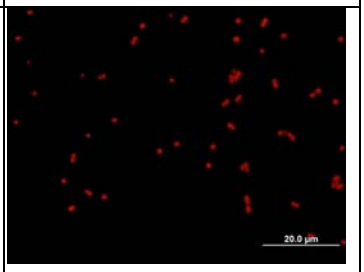
P(HB-*co*-90%HV)	Sodium valerate 20 g/L	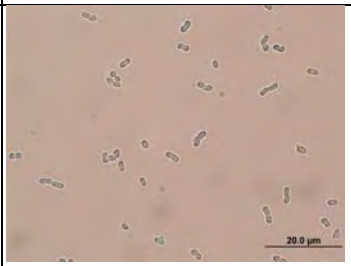	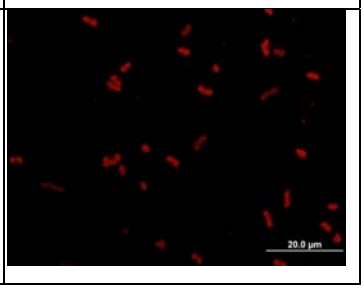

5.1.4 Effect of sodium valerate concentrations on biomass and P(HB-*co*-HV) accumulation by *C. necator* H16

In this experiment, the effect of two different concentrations of sodium valerate (i.e. 10 and 20 g/L) was investigated in the MS media without the presence of fructose. We found that when sodium valerate was increased from 10 to 20 g/L, the biomass was found to be decreased from 4.45 to 1.95 g/L. In addition, the % PHA content was also found to be decreased as well from 91.01 and 53.96% per CDW. Overall, increasing the concentration of sodium valerate from 10 to 20 g/L led to almost 4-fold decrease in the PHA production by *C. necator* H16, resulting in 4.06 and 1.05 g/L, respectively (**Figure 5.7**). These finding suggests that more sodium valerate might result in the decrease of cell growth and PHA production. Our results were found to be similar with a previous work done by Bhubalan *et al.* (2008). They found that increasing 3-HV precursors' concentration could result in the decrease of polymer content per CDW (Bhubalan *et al*., 2008). In their study, palm kernel oil and sodium valerate were co-supplied to produce P(3HB-*co*-3HV-*co*-3HHx) by using the recombinant strain of *C. necator*. Their results showed that using 5 g/L of sodium

valerate could lead to 4.8 g/L biomass, but when 10 g/L of sodium valerate was used, a very low biomass at 0.7 g/L was obtained. Ramsay *et al.* (1989) found that there is toxic concentration of carboxylic acid that could lead to the death of bacteria (Ramsay *et al.*, 1989). This might be a reason for our findings about the toxic effect of using sodium valerate at high concentration at 20 g/L. The result is reasonable to our case that high concentration of carbon source is beneficial in order to obtain high polymer content, but too high concentration can obstructs the multiplication of the cells, resulting in maximum polymer content at the balanced concentration of carbon source. However, increasing the concentration of sodium valerate was found to lead to an increase in the HV monomer incorporation as showed in **Figure 5.8**. The %HV monomer was increased from 67% to 91% when culturing with sodium valerate at 10 and 20 g/L in MS media, respectively. This might be due to the higher accumulation of HV monomer than HB monomer at the high concentration of 20 g/L sodium valerate.

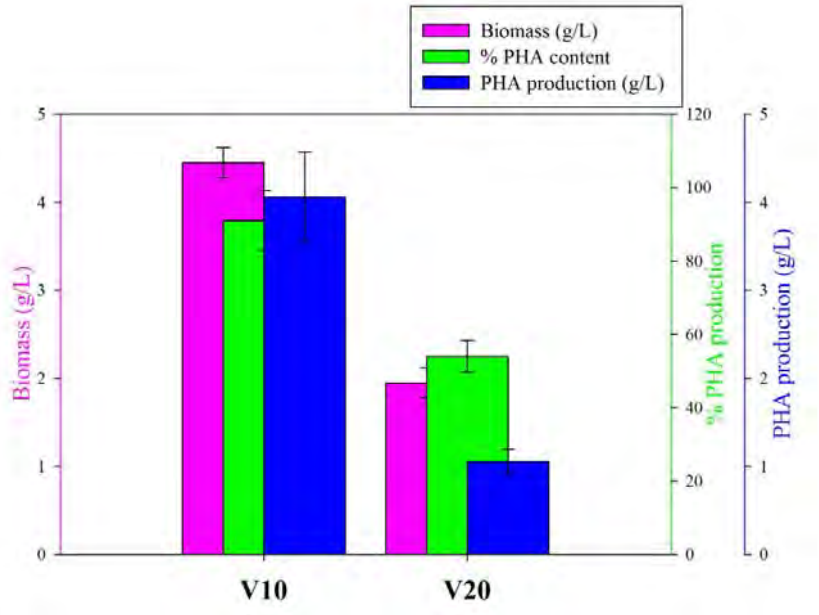

Figure 5.7 Growth and PHA accumulation by *C. necator* H16 when culturing in MS media with various concentrations of sodium valerate under a shaking condition at 200 rpm and 30˚C for 48 h. All experiments were done in duplicate at each condition (mean ± SD, n=2).

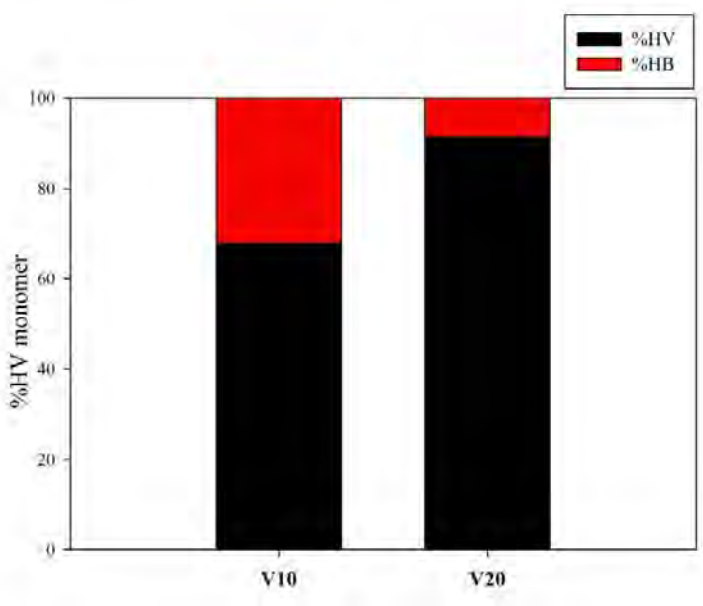

Figure 5.8 %HB and %HV monomer content in the P(HB-*co*-HV) copolymer by *C. necator* H16 when culturing in MS media with various concentrations of sodium valerate.

In summary, *C. necator* H16 could produce P(HB-*co*-HV) with various %HV monomer by utilizing different carbon sources as shown in **Table 5.2**. We finally were able to find suitable culturing conditions of *C. necator* H16 that could lead to the biosynthesis of P(HB-*co*-HV) with the %HV monomer composition at greater than 50% (i.e. ranging from 65 to 91%) and also at the overall production at above 1 g/L. Our results showed that supplying sodium valerate at 10 g/L into the MS media yields the highest P(HB-*co*-HV) production at 4.06 g/L with 65% HV monomer mole incorporation. This culturing condition allows us to culture enough biomass of *C. necator* H16 for the P(HB-*co*-65%HV) extraction and purification step.

Table 5.2 Types of P(HB-*co*-HV) production from different carbon sources by *C. necator* H16 (n=2).

Type of PHA polymer	Types of carbon source	Biomass (g/L)	% PHA content	PHA Production (g/L)
PHB	20 g/L Sodium gluconate	6.7	30.5	2.04
PHB	20 g/L Fructose	4.10	90.32	3.70
P(HB-*co*-12%HV)	20 g/L Fructose 2 g/L Sodium valerate	6.35	97.58	6.20
P(HB-*co*-16%HV)	10 g/L Fructose 2 g/L Sodium valerate	4.93	91.54	4.51
P(HB-*co*-38%HV)	15 g/L Fructose 5 g/L Sodium valerate	3.87	91.85	3.55
P(HB-*co*-65%HV)	10 g/L Sodium valerate	4.45	91.01	4.06
P(HB-*co*-66%HV)	10 g/L Fructose 10 g/L Sodium valerate	3.30	97.04	3.22
P(HB-*co*-67%HV)	5 g/L Fructose 15 g/L Sodium valerate	2.80	94.93	2.64
P(HB-*co*-75%HV)	10 g/L Glucose 5 g/L Sodium propionate	2.50	6.31	0.16
P(HB-*co*-77%HV)	10 g/L Glucose 7 g/L Sodium propionate	2.65	10.59	0.27
P(HB-*co*-81%HV)	10 g/L Glucose 2 g/L Sodium valerate	1.4	23.14	0.31
P(HB-*co*-91%HV)	20 g/L Sodium valerate	1.95	53.96	1.05

5.1.5 PHA extraction

Solvent extraction has been one of the most extensively studied and widely used techniques in the laboratory to purify and recover PHAs from the dried cell because of its simplicity of operation and effectiveness (Jacquel *et al*., 2008; Ramsay *et al.*, 1994). There are two main steps involved. First, the extraction process allows the cell breakage, resulting into the release and solubilization of PHA polymers into the heated organic solvent such as chloroform, and following by filtration to separate the cellular debris from the dissolved PHA polymers. Second, the method involves the precipitation of PHAs by another type of solvent such as methanol or ethanol, in which the PHA polymers are not generally dissolvable. In general, the solvent extraction has several advantages over other methods of purified PHAs from biomass in terms of efficiency and high % purity of PHA polymers. This method is also able to remove bacterial endotoxins (Jacquel *et al*., 2008), thus suitable for medical applications. Moreover, this extraction process also causes negligible degradation to the polymers, so lead to very pure PHAs with high molecular weights (Valappil *et al*., 2007).

In our study, the extraction of P(HB-*co*-65%HV) was performed by a standard solvent extraction technique as shown in **Figure 5.9**. The results from **Table 5.3** showed that the %HV mole composition of PHAs determined from the dried bacterial cells was not significantly different from the extracted polymer. As a result, the determination of %HV mole composition in the dried cells was quite accurate for the determining the %HV content in polymer. Moreover, there were no PHAs being detected in the residual bacterial cells after extraction, indicating the efficiency of the solvent extraction process. The purity of P(HB-*co*-65%HV) polymer was also determined to be closed to 100%.

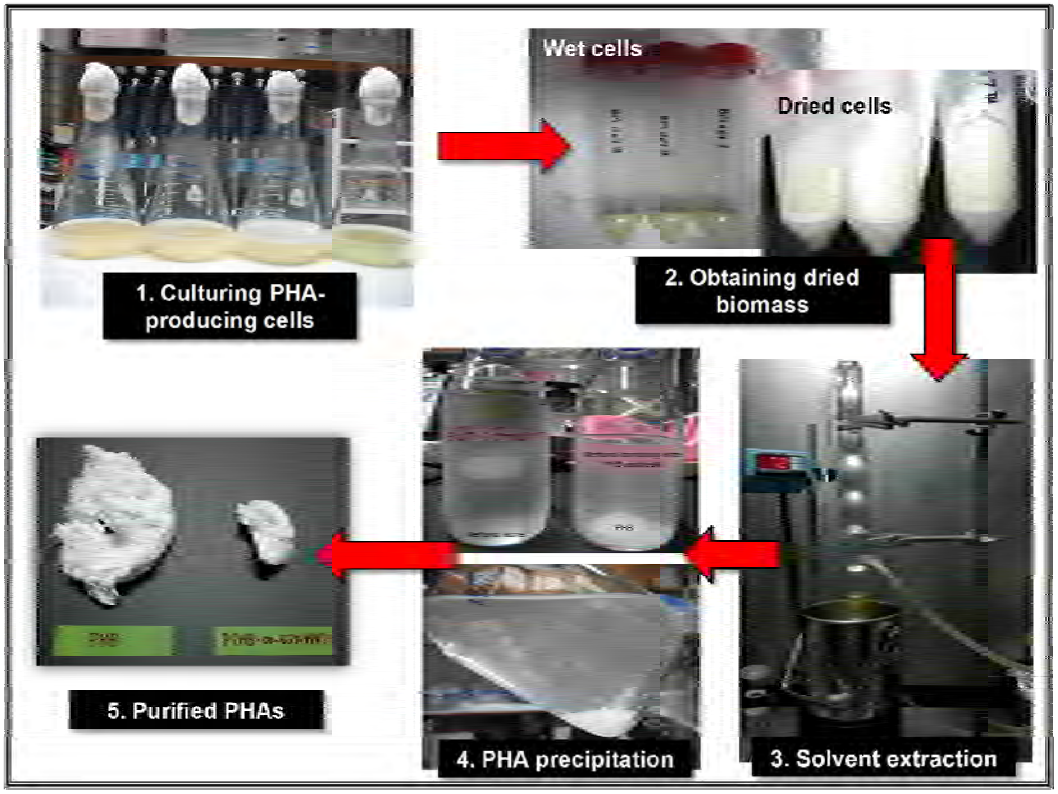

Figure 5.9 PHA extractions by solvent extraction method.

Table 5.3 Average %HV content and PHAs mass of dried cells and polymer from the solvent extraction process.

	Dried cells before extraction	**Residual cells after extraction**	**Extracted PHA polymers**
%HV content Average ± SD	66.75 ± 1.73	Not detected	64.36 ± 1.35

5.1.6 Characterization of PHB, P(HB-*co*-5%HV), P(HB-*co*-12%HV) and P(HB-*co*-65%HV) via Fourier Transform Infrared spectroscopy (FT-IR)

P(HB-*co*-65%HV) was chemically characterized its organic functional groups to compare with commercial PHB, P(HB-*co*-5%HV) and P(HB-*co*-12%HV). Due to all PHAs are polyesters, their FT-IR spectra shows the outstanding peak of ester carbonyl group (C=O stretching) at 1730 to 1625 cm^{-1} (**Figure 5.10**). However, PHAs spectra are different at the peak of C-H stretching which is located at around 3000 to 2800 cm^{-1} as well as their fingerprint region (i.e. 1500 to 1000 cm^{-1}). There are similar in functional groups peaks found among PHAs. However, it is also important to note the differences in %HV contents in these three PHA polymers; P(HB-*co*-5%HV), P(HB-*co*-12%HV) and P(HB-*co*-65%HV, could not be revealed by FT-IR. In previous studies by Lau *et al*. (2011), the FT-IR spectra of PHB and P(HB-*co*-77%HV) were similar to our results (Lau *et al*., 2011).

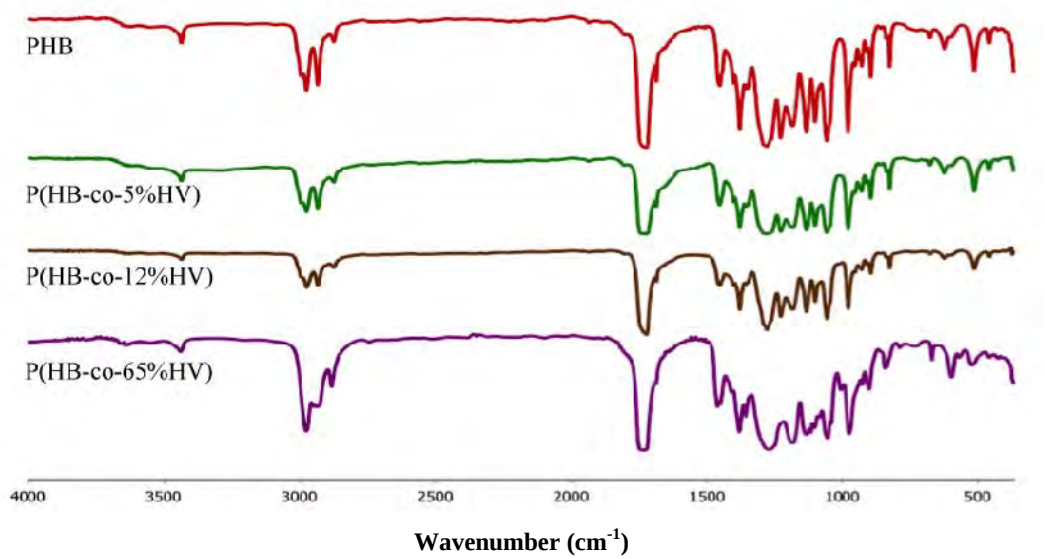

Figure 5.10 The FT-IR spectra of PHB (---), P(HB-*co*-5%HV) (---), P(HB-*co*-12%HV) (---) and P(HB-*co*-65%HV) (---).

5.1.7 Physical characterization of PHA polymers

Our produced copolymer P(HB-*co*-65%HV) was characterized for its physical properties including molecular weight and thermal properties by Gel Permeation Chromatography (GPC) and Differential Scanning Calorimetry (DSC),

respectively. The results of commercial PHAs, P(HB-*co*-5%HV) and P(HB-*co*-12%HV) were obtained from literatures elsewhere (Chanprateep, 2010). **Table 5.4** showed that the molecular weight of all four PHAs, PHB, P(HB-*co*-5%HV), P(HB-*co*-12%HV) and P(HB-*co*-65%) are considered to be high molecular weight molecules in a range of 10^5 to 10^6 g/mol. In addition, the polydisperisity index (PDI) of these four PHA polymers is quite uniform in the range of 1.48 to 2.11.

Table 5.4 Physical properties of PHB, P(HB-*co*-5%HV), P(HB-*co*-12%HV), and P(HB-*co*-65%HV).

Types of polymer	Source	Molecular weight analysis			Thermal properties	
		M_w (g/mol)	M_n (g/mol)	PDI	T_m (°C)	T_g (°C)
PHB	Aldrich	3.95 x $10^{6(*)}$	1.08 x $10^{6(*)}$	1.80$^{(*)}$	175.0	10.0$^{(*)}$
P(HB-*co*-5%HV)	Aldrich	2.04 x $10^{5\,(*)}$	1.05 x $10^{5\,(*)}$	1.94$^{\,(*)}$	164.0	-1.5$^{(*)}$
P(HB-*co*-12%HV)	Aldrich	2.49 x $10^{5\,(*)}$	1.18 x $10^{5\,(*)}$	2.11$^{\,(*)}$	155.0	-2.4$^{(*)}$
P(HB-*co*-65%HV)	Our laboratory	1.69 x 10^6	1.14 x 10^6	1.48	73.0	-34.0

(* Chanprateep, 2010)

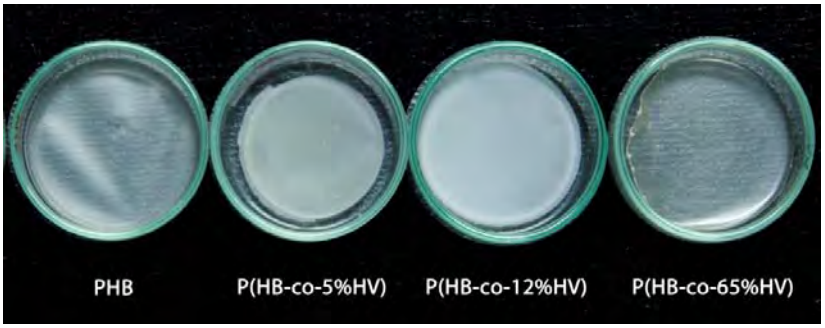

Figure 5.11 The appearance of 2D films casting from PHB, P(HB-*co*-5%HV), P(HB-*co*-12%HV) and P(HB-*co*-65%HV).

After the 2D films of all four different types of PHAs were prepared via a solvent casting technique (**Figure 5.11**), all films were also subjected to the measurement of thermal properties, which are one of physical properties that can differentiate each type of PHA polymer based on the configuration of polymer chains and % crytallinity of the polymer materials. Among PHAs, PHB has the highest melting temperature (T_m) and glass transition temperature (T_g) which are 175.0°C and 10.0°C, respectively. While P(HB-*co*-65%HV) has the lowest T_m and T_g which are 72.0°C and -34.0°C, respectively. As the thermal properties of PHAs reported elsewhere, the T_m and T_g are depended mainly on the %HV incorporation in the polymer chain. The increased of %HV monomer resulted in a decreased of melting temperature, indicating that the copolymers have less crystallinity and become more ductile and flexible than the PHB homopolymer. Chen *et al.* (2005) reported the thermal properties of PHB, P(HB-*co*-10%HV), and P(HB-*co*-20%HV), in which the thermal properties of both PHB and P(HB-*co*-10%HV) were quite similar to our current findings (Chen & Wu, 2005). Bengtsson and colleques recently reported the molecular weight of PHA containing 78 % HV monomer produced from a glycogen-accumulating bacteria had a weight average molecular weight of 6.2×10^5 g/mol with the polydispersity index of 3.9, indicating that a wide range of molecular weight distribution for this particular PHA. Thermal properties of the produced polymer such as melting temperature and glass transition temperature were 98.1 °C and -12.3 °C, respectively (Bengtsson *et al*., 2010). In another study, P(HB-*co*-67%HV) produced by *Burkholderia cepacia* D1 from valeric acid exhibited M_n of 2.65×10^5 g/mol with PDI value of 2.9. The melting point and glass transition of the copolymer were found to be 81°C and -11°C, respectively (Mitomo *et al*., 1999).

5.1.8 Mechanical properties and hydrophobicity characterization of PHA polymers

Table 5.5 Mechanical property and hydrophilicity of PHAs 2D films.

Types of polymers	Mechanical property		Hydrophilicity
	Tensile strength (N/mm^2)	%Elongation at break	Water contact angle (°)
PHB	34.90 ± 2.11^{c}	100 ± 0.00^{a}	70.2 ± 3.5^{a}
P(HB-*co*-5%HV)	34.94 ± 0.61^{c}	102 ± 16.07^{a}	69.8 ± 4.5^{a}
P(HB-*co*-12%HV)	30.73 ± 2.77^{b}	185 ± 49.50^{a}	67.9 ± 2.1^{a}
P(HB-*co*-65%HV)	12.53 ± 1.79^{a}	450 ± 141.42^{c}	76.8 ± 1.8^{b}

Data are the mean and standard deviation derived from three and tenth dependent repeats for mechanical propertyies and surface hydrophilicity of PHA polymers. Mean with different superscript letters within the same column are significantly different ($p \leq 0.05$) as determined by Scheffe's test.

PHAs were characterized for their mechanical properties and hydrophobicity. The surface hydrophobicity of all four types of PHAs 2D film was examined by measuring contact angles using the sessile-drop technique via a Contact Angle instrument (CAM). As shown in **Table 5.5**, the surface contact angle value of PHB, P(HB-*co*-5%HV), P(HB-*co*-12%HV) and P(HB-*co*-65%HV) were found to be 70.2°, 69.8°, 67.9° and 76.8°, respectively. There appears to have no statistical difference in the contact angle value among PHB, P(HB-*co*-5%HV) and P(HB-*co*-12%HV) 2D film, indicating that the hydrophobicity of these three polymer films was nearly the same. Interestingly, the contact angle value of P(HB-*co*-65%HV) was found to be only one that is significantly different ($p \leq 0.05$) from others. Our findings suggests that the % HV monomer in P(HB-*co*-HV) copolymers might have an effect on the surface hydrophobicity as the contact angle value of P(HB-*co*-65%HV) was found to be the highest (76.8°) among all PHAs. The hydrophobicity of the PHA surface appears to be increased with increasing %HV monomer. The certain amount of %HV incorporation (i.e. at 65%) could contribute to more hydrophobicity due to

the presence of more ethyl groups in the polymer side chain. However, when comparing to other hydrophobic polymeric films such as polystyrene or polyethylene, their contact angle values are more than 100°. As a result, our PHAs films are still considered to be quite hydrophilic since the value of their contact angle are much less than 90°. Biresaw *et al*. (2001) reported the contact angles values of the commercial P(HB-*co*-12%HV) was around 61.4°. The commercial P(HB-*co*-8%HV) copolymers studied by Tezcaner *et al*. (2003) showed the contact angle value at 68.3°, which appear to be in similar range with our observation in P(HB-*co*-5%HV) and P(HB-*co*-12%HV) (Tezcaner *et al*., 2003). On the other hand, Rathbone *et al*. (2010) reported the contact angles value of P(HB-*co*-8%HV) copolymer extracted from *R. eutropha* was at 84° (Rathbone *et al*., 2010). Their result is slightly higher than our result observed in P(HB-*co*-5%HV) and P(HB-*co*-12%HV), but the value of PHB are nearly similar to our finding at 63°.

All PHAs 2D films were also measured their tensile strength and elongation at break as shown in **Table 5.5**. The tensile strength of PHB, P(HB-*co*-5%HV), P(HB-*co*-12%HV), and P(HB-*co*-65%HV) were 34.90, 34.94, 30.73 and 12.53 N/mm^2, respectively. The elongation at break values were found to be 100, 102, 185 and 450%, respectively. Both PHB and P(HB-*co*-5%HV) 2D film exhibited the highest tensile strength and the lowest %elongation at break among four types of PHAs, while P(HB-*co*-65%HV) has the greatest flexibility due to its lowest tensile strength and highest value of %elongation at break. In addition, our data also suggests that the tensile strength is decreased as %HV increased in the PHA copolymer. This finding indicates that PHAs become more ductile when increasing HV mole fraction in the copolymer chain. The elongation at break of P(HB-*co*-65%HV) was found to be much higher over another three types of PHAs. The results indicate that the flexibility of PHAs strongly depends on the structure of side chain such as ethyl branch of HV unit that might contribute to improve the brittleness of PHA films. Chen *et al*. (2005) reported the tensile strength of various types of PHAs. Their results also showed similar values of tensile strength to our experiment (Chen & Wu, 2005). The value of PHB was reported to be at 43 MPa, which is slightly higher than our value (i.e. 34.90 N/mm^2). The tensile strength value of our P(HB-*co*-12%HV) is also found to be quite similar to P(HB-*co*-10%HV) (25 N/mm^2). Bhubalan *et al*. (2008) investigated the

tensile strength and elongation at break of P(38%HB-*co*-60%HV-*co*-2%HHx) terpolymer produced by recombinant *C. necator*. The result of 60%HV mole incorporation led to the tensile strength and elongation at break at 14 N/mm^2 and 421%, respectively, which were similar to our P(HB-*co*-65%HV) (Bhubalan *et al*., 2008).

5.2 Preparation and characterization of PHA nanoparticles

5.2.1 Effect of types of PHA and PVA polymers on size of bare PHA nanoparticles

Core-shell nanoparticles are self-assembled nanostructures that are often composed of two different polymers, one at a core and the other at a shell orientation. These nanoparticles have many attractive features including their hydrophobic core, allowing them to be capable of carrying highly hydrophobic drugs with high loading capacity, while their hydrophilic shell providing steric protection and functional groups for surface modification. In general, drug release from the core-shell nanoparticles can be manipulated by choosing biodegradable polymers with different surface erosion rates. The method for preparation of core-shell nanospheres is simply via polymer-polymer phase separation of two immiscible polymers in solution (Srinivasan *et al*., 2005). Emulsion-solvent evaporation is one of the commonly used methods to formulate this type of polymeric nanoparticles and poly(vinyl alcohol) (PVA) is the emulsifier most commonly used to stabilize the emulsion since it forms particles of relatively small size and uniform size distribution (Scholes *et al*., 1993). The binding of PVA on the particle surface is likely to happen during the organic solvent is removed from the interface, in which the interpenetration of PVA onto the surface of core polymer takes place. In making core-shell nanoparticles, 87-90% mol hydrolyzed PVA is commonly used, since it is a copolymer consisting of 87-90% mole of vinyl alcohol unit and the rest with vinyl acetate unit. The hydrophobic vinyl acetate part generally serves as an anchor point towards the hydrophobic interface of core polymer during the formulation (Lee *et al*., 1999). There are many studies reported the use of low MW PVA (MW 13,000-23,000) or high MW PVA (MW 30,000-70,000) to prepared various types of polymeric nanoparticles. For example, Zambaux *et al*. (1998) investigated the parameters on the preparation of PLA

nanoparticles by using low MW PVA (Zambaux *et al*., 1998) and also Soares *et al*. (2010) formulated the PLA nanoparticles with Zinc (II) phthalocyanine-encapsulated using these low MW PVA (Soares *et al*., 2010). The effect of residual PVA using high MW PVA on the size of PLGA nanoparticles were investigated by Sahoo *et al*. (2002). In another study, the anti-cancer drug paclitaxel was encapsulated into PLGA nanoparticles with high MW PVA used as a particles stabilizer as well (Joo *et al*., 2009). Thus far, previous studies employed the partial hydrolyzed PVA as a shell stabilizer with biodegradable polymer such as PLA or PLGA, but there have been no reports about the investigation of the effect of using low MW PVA in comparison with high MW PVA on the properties of any polymeric nanoparticles functions, such as particles' diameter size, drug loading, and rate of degradation.

To facilitate intravenous administration of polymeric nanoparticles to human system for drug delivery, the expected size of nanoparticles should be around 200 nm in diameter or less, which is the ideal size of an engineered nanoparticle to prolong the circulation by reducing the mononuclear phagocyte system clearance and to avoid entrapment in the spleen or other tissues (Moghimi *et al*., 2001). Elsabahy *et al*. (2010) suggested investigated the size of polymeric nanoparticles that should be designed for application for drug delivery and suggested that the size of polymeric nanoparticles should be around 20-200 nm to possess the highest potential for *in vivo* applications (Elsabahy & Wooley, 2010). According to previous research works, there have been many options for modifying the size of nanoparticles by selecting appropriate polymer composition, polymer's molecular weight, stabilizer's molecular weight, solvent diffusion time, surface hydrophobicity/hydrophilicity and also the surface tension of ethanol in organic phase (Dunne *et al*., 2010). Our previous work showed that we have successfully developed the modified emulsification-diffusion technique by studying the different formulation parameters (i.e. PVA concentration, ethanol concentration and solvent diffusion time). The suitable amount of both PVA and ethanol must be added during the preparation of PHA core-shell nanoparticles in order to make the nanoparticles stable in aqueous solutions as well as to obtain the nanoparticles with diameter size at below 200 nm [Data not shown].

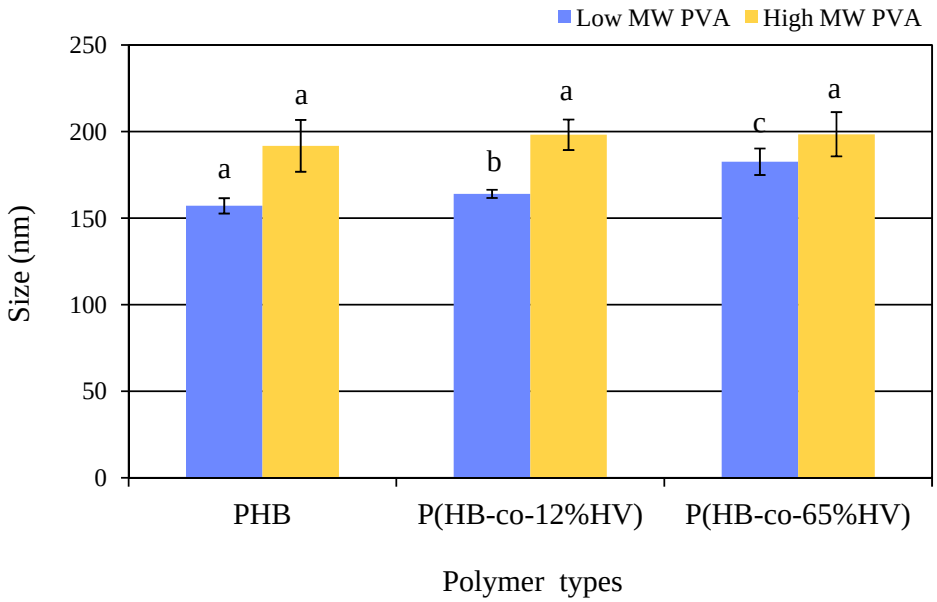

Figure 5.12 Effect of types of PHA and PVA polymers on the size of bare PHA nanoparticles with PDI < 0.2 (mean ± SD, n=3). Mean with different superscript letters within the same bar are significantly different ($p \leq 0.05$) as determined by Duncan's test.

Therefore, our aim in this study is to evaluate the effect of the nature of the PHA polymers (i.e. %HV monomer) and PVA (i.e. molecular weight and polydispersity index) on the size of PHA nanoparticle. Three different types of PHAs were selected: PHB, P(HB-*co*-12%HV) and P(HB-*co*-65%HV) with the same range of molecular weight but different in %HV monomer. Two types of PVA: low molecular weight PVA (MW 13,000-23,000) and high molecular weight PVA (MW 30,000-70,000) with the same degree of hydrolysis of 87-89% were also chosen for this study. We found that when using the low MW PVA as a shell stabilizer, the size of PHA nanoparticles prepared from PHB, P(HB-*co*-12%HV) and P(HB-*co*-65%HV) were found to be 157.1 ± 4.4, 164.0 ± 2.37 and 182.6 ± 7.7, respectively. There was a statically significant difference in size when compared to these three PHAs ($p \leq 0.05$) (**Figure 5.12**). These findings indicates that the increase in %HV in the copolymer can affect the polymer packing of PHA nanoparticles leading to an increase in the overall

size of PHA nanoparticles when the low MW PVA is used as a shell stabilizer. On the other hand, when using high MW PVA as a stabilizer, we found that the particles mean size made of PHB, P(HB-*co*-12%HV) and P(HB-*co*-65%HV) were found to be 191.7 ± 14.9, 198.1 ± 8.8 and 198.5 ± 12.8 nm, respectively, which were not statistically differences ($p \leq 0.05$). In addition, we found that with the high MW PVA as a shell stabilizer, the size of each PHA nanoparticles were always higher than with the low MW PVA. These findings strongly suggest that using the different MW of PVA as the nanoparticles' shell stabilizer has an important effect on increasing the overall size of PHA nanoparticles. The %HV in PHA also has an effect on increasing the overall size of PHA nanoparticles as well, but only seen in the system using the low MW PVA.

From our experiments thus far, we found two important observations. First, the effect of %HV on the size of PHA nanoparticles could only been seen when used the low MW PVA as a stabilizer. The bigger size of nanoparticles obtained when using the polymer with high %HV might be possibly due to the fact that less packing of PHA polymers might be occurred due to the presence of more %HV when forming into the spherical nanoparticles. From our previous experiments in Section 5.1.7, the effect of %HV on the polymer chain packing has already been shown to have a great effect on the melting temperature of the PHA copolymers (i.e. % crystallinity). Increasing %HV can hinder the polymer chain packing hence less crystalline bodies can be formed, resulting into decreasing in the melting temperature.

Second, by comparing between two types of PVA used as the shell stabilizer, we found that the molecular weight of PVA seems to have the effect on the overall size of PHA nanoparticles, in which using higher MW PVA often results into bigger size of PHA nanoparticles. The packing of PVA molecules onto the surface of PHA nanoparticles can be somewhat different when changing PVA types in the system as illustrated in **Figure 5.13**. In particular, the high MW PVA would lead to bigger size of PVA structure assembled onto the surface of PHA nanoparticle. In addition, the high MW PVA also has a wider range of MW distribution (i.e. high polydispersity index) at MW 30,000-70,000, while the low MW PVA has a much narrower molecular weight distribution range at MW of 13,000-23,000. We suspected that the difference in the molecular weight distribution of PVA might also have an

influence on how the PVA molecules can be assembled onto the surface of PHA nanoparticles. The packing of the high MW PVA molecules onto the surface of PHA nanoparticles would be more difficult to occur, since the size of their MW are highly varied and thus often yield a larger size of nanoparticles. Our findings are similar with those reported by Shaffie *et al.*, (2010) that studied the kinetics of emulsion polymerization of vinyl acetate using different MW of PVA (i.e. 9,000, 34,000 and 125,000) and found that increasing the MW of PVA resulting in the increase of polymer particles size values and the number of polymer particles per unit volume of water decreased (Shaffie *et al*., 2010). Furthermore, the same trends were observed by Nabiyouni *et al.*, (2011) that ZnO nanoparticles absorbed PVA with two different MW, 40,000 and 70,000-100,000. Thus, the size of nanoparticles increases as the MW of the adsorbing material increased (Nabiyouni *et al*., 2011).

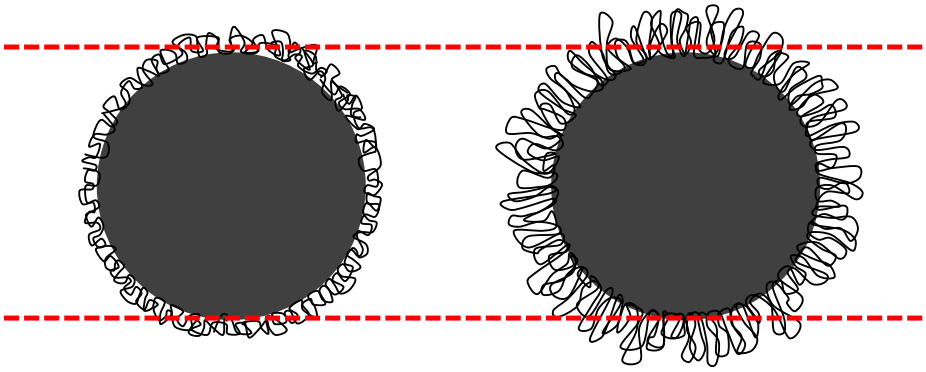

Figure 5.13 The proposed models of how two different types of PVA packed onto the surface of PHA nanoparticles; (A) Low MW PVA (MW 13,000-23,000), (B) High MW PVA (MW 30,000-70,000).

5.2.2 Effect of types of PHA and PVA polymers on the size, % drug loading and % entrapment efficiency of p-THPP-loaded PHA nanoparticles

The ability to modulate and/or control drug releasing from polymeric nanoparticles often becomes one of desired properties when formulating any drug encapsulation system (Dunn *et al*., 1988). In general, the drug release profile from any

encapsulating nanocarriers has been known to be influenced by four important parameters; 1) the amount of drug loaded into the polymeric nanoparticles (i.e. % drug loading), 2) the efficiency of drug being encapsulated in the nanoparticles (i.e. % encapsulation efficiency), 3) the degradation rate of the polymer used as drug carrier, and 4) the physiological environments where the drug-carriers would be localized (i.e. pH, the presence of certain enzymes).

In the present study, a hydrophobic PS, the *meso*-tetra(*p*-hydroxyphenyl)porphyrin (p-THPP), which is a well known second generation PS drug used as a photosensitizing agent. Since p-THPP drug is hydrophobic molecule and does not dissolve in water, thus it is required the encapsulation into polymeric nanoparticles to enhance its bioavailability as well as photodynamic activity (Vargas *et al*., 2004). According to the preparation of p-THPP-loaded PHA nanoparticles, a PS drug was dissolved in the organic phase before the emulsification step. The absorption spectrum that use in PDT is at a wavelength of 653 nm.

Since we hope to understand whether there would be any influence derived from the native properties of both PHA polymers (i.e. chemical structures) and PVA stabilizers (i.e. molecular weight) on the properties of formulated PHA nanoparticles for the controlled-release of PS drugs in PDT, three different types of PHAs similar in their molecular weights but different in their structure (i.e. various %HV mole incorporation in the polymer chain) and two different set of molecular weight of PVA were employed in our nanoparticles formulation in order to investigate whether the differences in the PHA chemical structures would have any influence on % drug loading and % entrapment efficiency. Different p-THPP-loaded PHA nanoparticles were fabricated at the same initial drug loading at 10%, since this value has been wildly used (Ma *et al*., 2012).

In this study, three different types of PHAs with the same range of molecular weight; PHB, P(HB-*co*-12%HV) and P(HB-*co*-65%HV) were employed to investigate the effect of different types of PHAs (i.e. different in %HV) would have on the % drug loading, the % entrapment efficiency and later on the drug release profile under physiological environments. Besides the effect of PHA structure, we suspected that the PVA stabilizing polymer on the surface of PHA nanoparticles might also have some influences on those parameters as well. According to many research studies,

although the high MW PVA comes with a wider range of molecular weight, this type of PVA has often been used as a nanoparticle stabilizer because of the possibility of size-controlled (Son & Kim, 2007). However, we proposed to use the low MW PVA as well, since from our previous results from Experiment 5.2.1 using low MW PVA allowed us to observe the effect of %HV on the size of nanoparticles. As a result, two types of PVA systems; low molecular weight PVA (MW 13,000-23,000) and high molecular weight PVA (MW 30,000-70,000), were also selected to investigate their effects on the drug-encapsulation properties.

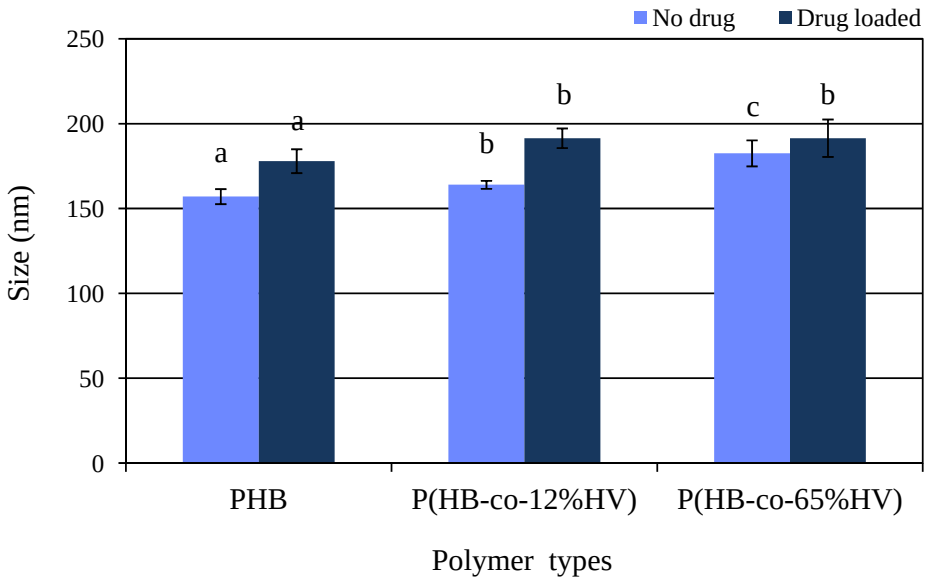

Figure 5.14 Effect of types of PHA polymers on the size of bare and p-THPP-loaded PHA nanoparticles when using low MW PVA as a shell stabilizer with PDI < 0.2 (mean ± SD, n=3). Mean with different superscript letters within the same bar are significantly different ($p \leq 0.05$) as determined by Duncan's test.

From our previous results, when the low MW PVA was used as a stabilizer, the mean size of unloaded nanoparticles prepared form PHB, P(HB-*co*-12%HV) and P(HB-*co*-65%HV) were found to be 157.1 ± 4.4, 164.0 ± 2.37 and 182.6 ± 7.7, respectively. After p-THPP-encapsulated, the particles size were found to be increased as 178.0 ± 7.0, 191.5 ± 5.8, and 191.5 ± 11.0, respectively. With the low

MW PVA, there is a statistically difference in the particle mean size (t-test, $p \leq 0.05$) after drug encapsulation only for PHB and P(HB-*co*-12%HV) nanoparticles. These findings suggest that the presence of p-THPP could cause an increase in the overall size of nanoparticles. However, when compared among the drug-loaded PHA nanoparticles, there appears to have no statistical difference in the particle mean size when compared between the nanoparticles made from P(HB-*co*-12%HV) and P(HB-*co*-65%HV). Interestingly, the particle size of PHB was found to be only one that is significantly different ($p \leq 0.05$) when compared to P(HB-*co*-12%HV) and P(HB-*co*-65%HV) (**Figure 5.14**).

Table 5.6 % Drug loading and % entrapment efficiency of p-THPP-loaded PHA nanoparticles when using low MW PVA as a shell stabilizer (mean ± SD, n=3).

PVA types	**Polymer types**	**Drug loading (%)**	**Entrapment efficiency (%)**
Low MW	PHB	3.99 ± 0.03^{b}	39.91 ± 0.31^{b}
	P(HB-*co*-12%HV)	3.95 ± 0.05^{b}	39.48 ± 0.5^{b}
	P(HB-*co*-65%HV)	2.50 ± 0.82^{a}	29.57 ± 1.07^{a}

Mean with different superscript letters within the same column are significantly different ($p \leq 0.05$) as determined by Duncan's test.

As shown in **Table 5.6**, when using the low MW PVA as a particle shell stabilizer, the % drug loading of PHA nanoparticles prepared from PHB, P(HB-*co*-12%HV) and P(HB-*co*-65%HV) were found to be 3.99 ± 0.03, 3.95 ± 0.05 and 2.50 ± 0.82, respectively, while the % entrapment efficiency were found to be 39.91 ± 0.31, 39.48 ± 0.5 and 29.57 ± 1.07, respectively. From these results, there seems to have no statistical difference in % drug loading and % entrapment efficiency values when compared between the nanoparticles made from PHB and P(HB-*co*-12%HV), however the % drug loading and % entrapment efficiency values of P(HB-*co*-65%HV) was the only one found to be significantly different ($p \leq 0.05$) from the other two PHA polymers. The drug loading data for the P(HB-*co*-65%HV) system appears to be in agreement with the particle mean size data, since we found that there was less increase

in the diameter size after the drug encapsulation into the P(HB-*co*-65%HV) nanoparticles when compared to the other two PHA nanoparticles as shown in Figure 5.14.

Figure 5.15 shows our proposed model demonstrates the presence of drug in the PHA nanoparticles can cause an increase in the overall size of PHA nanopartilces when the low MW PVA was used as a shell stabilizer. The packing of PVA molecules onto the surface of PHA nanoparticles can be assumed that the packing is the same to when there is no drug in the nanoparticles.

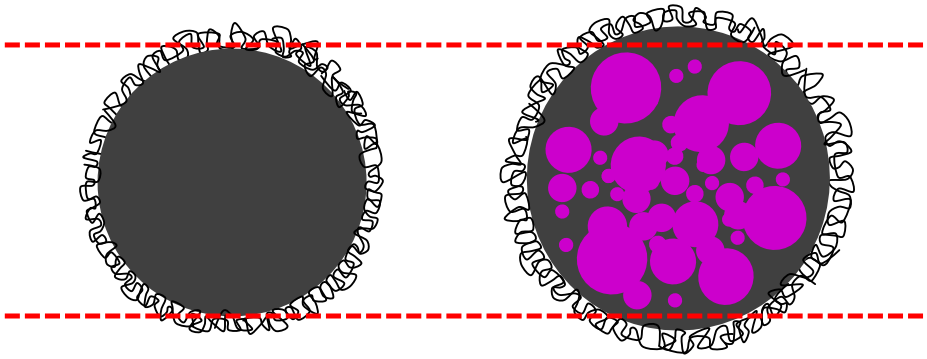

(A) (B)

Figure 5.15 The proposed models of how p-THPP drug are encapsulated into the PHA nanoparticles and causing an increase in the overall particle mean size when the low MW PVA was used as a shell stabilizer; (A) Bare nanoparticles. (B) p-THPP-loaded PHA nanoparticles.

According to the previous results, when the high MW PVA was used as a stabilizer, the size of bare PHA nanoparticles prepared from PHB, P(HB-*co*-12%HV) and P(HB-*co*-65%HV) were found to be at 191.7 ± 14.9, 198.1 ± 8.8 and 198.5 ± 12.8 nm, respectively. As shown in **Figure 5.16**, after the p-THPP encapsulation, the average mean size of PHA nanoparticles were found to be 208.3 ± 3.1, 198.2 ± 3.4 and 199.7 ± 5.9, respectively. From these results, the particle mean size among the nanoparticles made from P(HB-*co*-12%HV) and P(HB-*co*-65%HV) showed no statistical difference between before and after the drug being loaded, while only the

PHB nanoparticles were found to be only one that showed significantly different ($p \leq 0.05$) between before and after the drug loaded when using the high MW PVA.

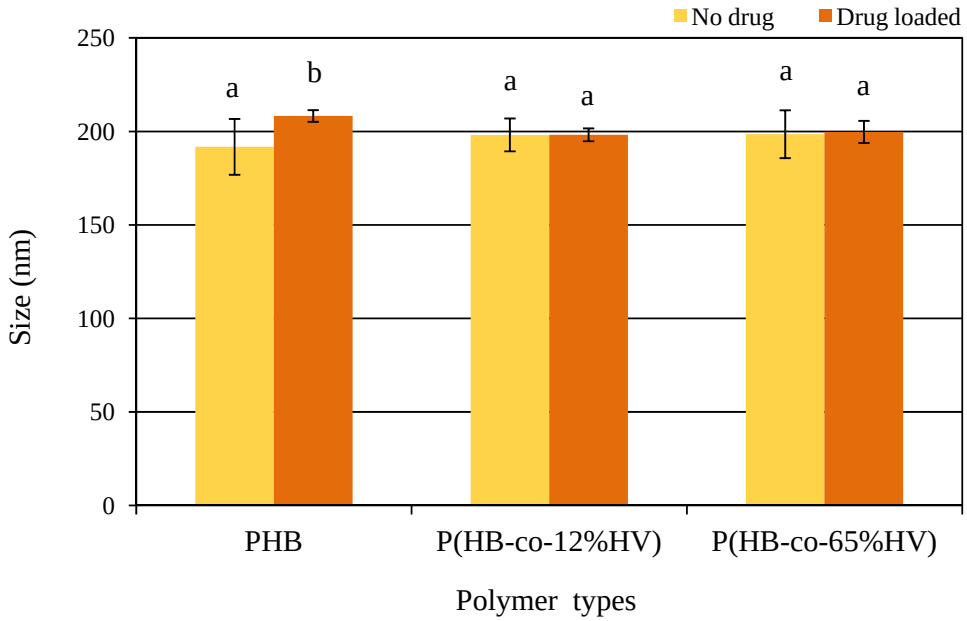

Figure 5.16 Effect of types of PHA polymers on the size of bare and p-THPP-loaded PHA nanoparticles when using high MW PVA as a shell stabilizer with PDI < 0.2 (mean ± SD, n=3). Mean with different superscript letters within the same bar are significantly different ($p \leq 0.05$) as determined by Duncan's test.

Table 5.7 % Drug loading and % encapsulation efficiency of p-THPP-loaded PHA nanoparticles when using high MW PVA as a stabilizer (mean ± SD, n=3).

PVA types	**Polymer types**	**Drug loading (%)**	**Entrapment efficiency (%)**
High MW	PHB	2.34 ± 0.50^{a}	23.44 ± 4.96^{a}
	P(HB-*co*-12%HV)	4.10 ± 1.18^{b}	41.05 ± 11.78^{b}
	P(HB-*co*-65%HV)	4.17 ± 0.45^{b}	41.71 ± 4.53^{b}

Mean with different superscript letters within the same column are significantly different ($p \leq 0.05$) as determined by Duncan's test.

Table 5.7 shows that when high MW PVA was used as a stabilizer, the % drug loading of PHA nanoparticles prepared from PHB, P(HB-*co*-12%HV) and P(HB-*co*-65%HV) were found to be 2.34 ± 0.50, 4.10 ± 1.18 and 4.17 ± 0.45, respectively. The % entrapment efficiency of these three types of PHAs were 23.44 ± 4.96, 41.05 ± 11.78 and 41.71 ± 4.53, respectively. From these results, the results of the % drug loading and % entrapment efficiency were appears to be in similar range when compared between the nanoparticles made from P(HB-*co*-12%HV) and P(HB-*co*-65%HV), however the % drug loading and % entrapment efficiency values of PHB was the only one found to be significantly different ($p \leq 0.05$) from the other two PHA systems. According to these findings, it might possibly be that the high MW PVA might also interact with the hydrophobic p-THPP drugs localized at the core PHA polymer, thus leading to the possible rearrangement of PVA molecules on the surface of PHA nanoparticle (i.e. better packing of PVA) when the drug is present. This is because the particle size at before and after drug loaded were nearly the same (i.e. at around 200 nm), even at the 40% entrapment efficiency.

These phenomena could not be clearly observed in term of the particle size or % entrapment efficiency. Another possible reason is due to the fact that this high MW PVA already has a wide range of molecular weight distribution among themselves (MW 30,000-70,000). As a result, some of them might pack themselves better and onto the surface of PHA nanoparticle when the drug is present as shown in the proposed model of drug-encapsulated PHA nanoparticles (**Figure 5.17**). This might imply that there might be an interaction between PVA and the p-THPP drug molecules in such a way that only smaller MW PVA molecules would bind tighter onto the surface of PHA nanoparticles causing the lost of larger MW PVA molecules from the surface of PHA nanoparticles resulting in the same particle size observed while the drugs are being entrapped. A report by Mallapragada *et al*. (2000) also showed that the high percentage of residual PVA on the surface of nanoparticle were related to the presence of the amount of encapsulated photosensitizer drug inside the nanoparticles (Mallapragada & McCarthy-Schroeder, 2000). Indeed, the p-THPP drug seems to demonstrate a certain affinity to the PVA shell polymer since certain portion of PVA is considered hydrophobic (i.e. acetylene and methylene units in the PVA chain), thus inducing the adsorption of PVA on the hydrophobic surface of

nanoparticles. The amount of PVA on the nanoparticles used in drug delivery should be acceptable due to the widespread use of PVA polymers in various encapsulation applications for human use (Wan & Lim, 1992). Nevertheless, more studies (i.e. measuring residual PVA on the PHA naopartilces) have to be performed in order to gain a better understanding and reasoning for our current observations in our research.

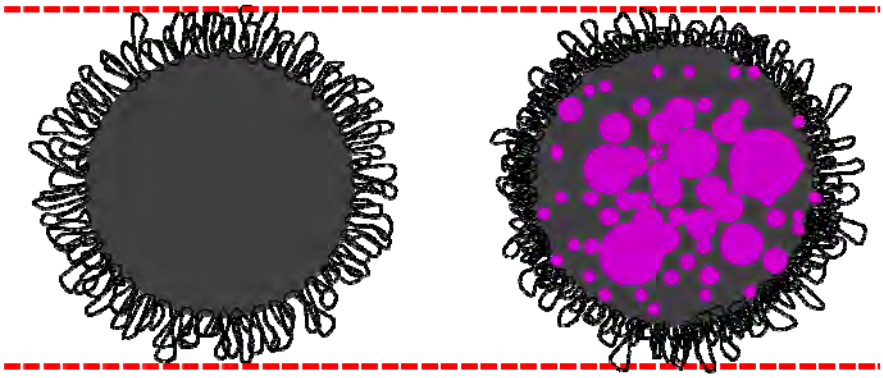

(A) (B)

Figure 5.17 The proposed models of how p-THPP drug are encapsulated into the PHA nanoparticles and causing an increase in the overall particle mean size when the high MW PVA was used as a shell stabilizer; (A) Bare nanoparticles. (B) p-THPP-loaded PHA nanoparticles.

The surface morphology of p-THPP- loaded PHA nanoparticles using low MW PVA as particles stabilizer was also observed by TEM. **Figure 5.18** showed that the nanoparticles prepared were found to be spherical in shape at around 200 nm size range.

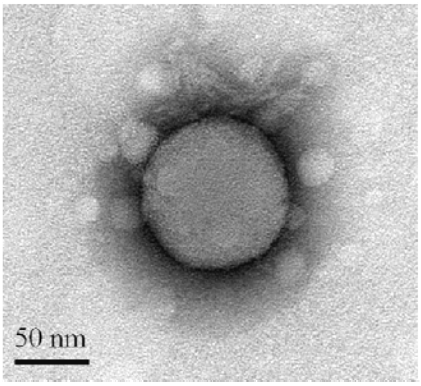

Figure 5.18 TEM image of p-THPP-loaded PHA nanoparticles using low MW PVA as a stabilizer.

5.2.3 Evaluation of size and zeta potential values after redispersing in cell culture media

It has been generally known that the nanoparticles do not behave in solution as inert objects or soluble small molecules, but they often undergo aggregation processes, leading to the formation of a new range of various size and unknown molecular entities (Murdock *et al.*, 2008). The change of physicochemical properties of the nanoparticles (i.e. size, shape and surface charge) might causes different biological responses and thus an lead to incorrect estimation of cytotoxicity (Park *et al.*, 2009). A characterization of the dispersion state of nanomaterials as well as knowledge of the experimental parameters controlling such surface changes or also known as zeta potential have a important implication for the development of reliable *in vitro* toxicity protocols (Shaw *et al.*, 2008).

In order to gain a better evaluation whether our PHA nanoparticles are suitable as anti-cancer drug carriers for PDT, other characterizations of our drug encapsulation systems besides the size of nanoparticles, % drug loading and % entrapment efficiency must also be evaluated including the surface charge (i.e. zeta potential). The zeta potential of nanoparticle is the value that indicates the particle surface charge, which is an important parameter to be evaluated. Moreover, both size and zeta potential characterization of nanoparticles after the resuspension in DMEM

cell culture medium containing 10% (v/v) FBS were also performed to mimic the similar environment where the p-THPP-loaded PHA nanoparticles would be with cancer cells during *in vitro* PDT study. All three types of the PHA nanoparticles with two different PVA systems were also characterized for their size after resuspension in the cell culture medium. The size of various PHA nanoparticles was shown in **Table 5.8**. The slightly increased in particle size of all p-THPP-loaded PHA nanoparticles formulation was observed which might be due to surface adsorption of proteins from the cell culture media according to previous reported by Bhattacharjee *et al*. (2012) (Bhattacharjee *et al*., 2012). It was found that the zeta potential values of the p-THPP-loaded nanoparticles for all polymers used were also in the range of -0.7 to -1.6 mV which exhibited a slight negative charge close to 0 for all formulations. The slightly negative zeta potential values should be due to the presence of carboxylate end groups from PHA polymers. Generally, the presence of uncapped end carboxyl groups on the polyester chain ends has been known to cause some negative zeta potential values. (Manangana & Shawaphuna, 2010). However, in this study, the zeta potential values close to zero should be due to the presence of PVA covering onto the entire PHA nanoparticle surface, creating a shield between the nanoparticle surface and the surrounding medium. The PVA layer at the surface of PHA nanopartticles also probably shields the negative surface charge of PHAs. (Huijberts *et al*., 1994; Valappil *et al*., 2007). The previous study from Zeisser-Labouebe *et al*. (2006) reported that the zeta potential of PLA and PLGA nanoparticles were similar to our current results, which were -3.7 to -7.9 (Zeisser-Labouebe *et al*., 2006).

The increase of the zeta potential values was observed for all p-THPP-loaded nanoparticles formulation after redispersing in the DMEM, it might be possibly due to surface adsorption of other components from the cell culture medium such as serum proteins. The serum proteins might adsorb onto the nanoparticles surface, resulting into an increase in negative charges on the surface of nanoparticles. Nevertheless, it is important to mention that our results are in contrast with those reported by Sabuncu *et al*. (2012) (Sabuncu *et al*., 2012) that the zeta potential of the nanoparticles suspended in DMEM solutions were lower than those suspended in DI water.

Table 5.8 Size and zeta potential of p-THPP-loaded PHA nanoparticles (mean ± SD, n=2).

PHA nanoparticles types		**Nanoparticles solution**		**Resuspension in DMEM**	
Stabilizer	**Polymer types**	**Size (nm)**	**Zeta P (mV)**	**Size (nm)**	**Zeta P (mV)**
Low MW	PHB	211.6 ± 2.4	-0.7 ± 0.4	192.4 ± 1.6	-3.9 ± 0.2
	P(HB-*co*-12%HV)	199.7 ± 7.9	-1.2 ± 0.2	222.9 ± 1.9	-4.3 ± 0.1
	P(HB-*co*-65%HV)	191.1 ± 3.1	-1.4 ± 0.2	197.6 ± 3.7	-3.2 ± 0.3
High MW	PHB	206.8 ± 3.0	-1.6 ± 0.5	207.3 ± 0.6	-3.7 ± 0.1
	P(HB-*co*-12%HV)	201.5 ± 3.3	-1.0 ± 0.0	206.5 ± 1.3	-4.3 ± 0.1
	P(HB-*co*-65%HV)	207.8 ± 2.1	-1.2 ± 0.1	205.8 ± 2.4	-3.8 ± 0.2

At current, the relationship between the increasing of %HV in PHA copolymers and the size of bare and drug-loaded PHA nanoparticles depending on the MW of PVA used as the nanoparticles' shell stabilizer. Using the low MW PVA appears to affect the overall size of both bare and drug-loaded PHA nanoparticles. In particular, it also allowed us to observe the effect of %HV monomer in the copolymer chain that leads to an increase in the size of PHA nanoparticles. When using the high MW PVA as a stabilizer, the size of drug-loaded PHA nanoparticles were found to be in the similar size range among all types of PHA as well as when compared to the unloaded ones. As a result, with high MW PVA, we could not observe the effect of %HV in the PHA copolymer on the size of bare and drug-loaded nanoparticles, which may be due to the complicated packing of high MW PVA molecules that also need to be further investigated. Nevertheless, the sizes of all formulations of p-THPP-loaded PHA nanoparticles with both high and low MW PVA were still less or around 200 nm as we desired. Xiong *et al.* (2010) have formulated and investigated the use of RBITC-loaded PHA nanoparticles ranging from 80-200 nm with a mean diameter of 160 nm for evaluating mammalian cell viability as well as finding the drug release rate (Xiong *et al*., 2010). As a result, the current formulation of our PHA nanoparticles with either high and low MW PVA with this similar size range should be ready to be used for our next *in vitro* cancer cells testing experiments.

5.2.4 Optimization of % drug loading and % entrapment efficiency

Thus far, our results exhibited around 40 % entrapment efficiency from using 10% initial drug loading. In comparison to previous studies, % entrapment efficiency of PLGA nanoparticles were found to be up to 75% when using the same % initial drug loading (Konan *et al*., 2003). Thus, we need to optimize % drug loading and % entrapment efficiency of our PHA nanoparticles formulation system.

In addition, the possibility of modulating the drug release and the degradation rate of the particles is not only offered by choosing the appropriate polymer and particle stabilizer, but the influence of the theoretical drug loading and entrapment efficiency must also be investigated. In this study, our starting approach involved the production of PHA nanoparticles using two types of PVA with p-THPP at 10% initial drug. In order to establish the maximum amount of drug that could be incorporated into nanoparticles at such conditions, the initial procedure involving decreasing and increasing the theoretical initial drug loading of p-THPP in the formulation from 5 to 20% (w/w) were performed.

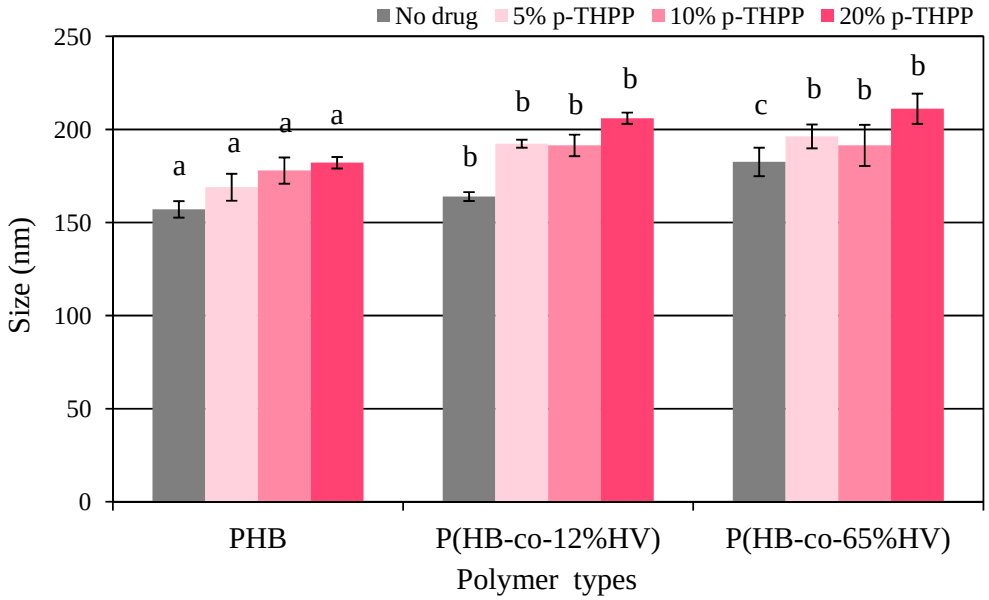

Figure 5.19 Effect of initial drug loading at various type of PHAs on size of bare and p-THPP-loaded PHA nanoparticles when using low MW PVA as a stabilizer with PDI < 0.2 (mean ± SD, n=3). Mean with different superscript letters within the same bar are significantly different ($p \leq 0.05$) as determined by Duncan's test.

As seen in **Figure 5.19**, when using low MW PVA as a shell stabilizer, the size of PHA nanoparticles made of PHB, P(HB-*co*-12%HV) and P(HB-*co*-65%HV) at 5, 10 and 20 % initial drug loading were found to be similar to their bare PHA nanoparticles that have been reported previously. The increasing of particles size with an increase in the %HV monomer at each % initial drug loading was also observed. However, there appears to have no statistical difference in the particle size at each % initial drug loading between the P(HB-*co*-12%HV) and P(HB-*co*-65%HV) nanoparticles. However, the particle size of PHB was found to be only one that is significantly different ($p \leq 0.05$) among three types of PHA nanoparticles when low MW PVA was used.

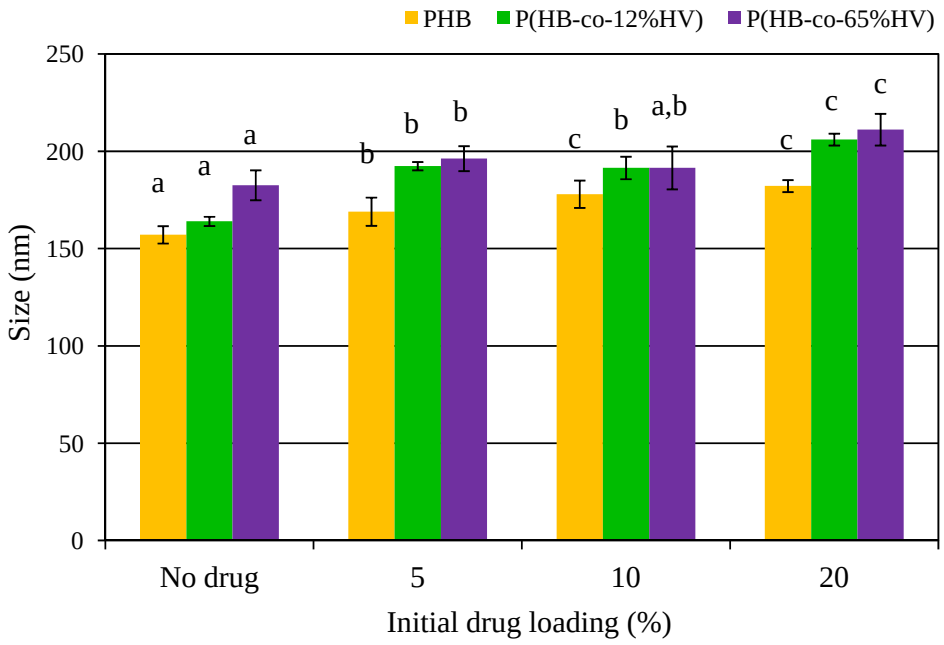

Figure 5.20 Effect of polymer types at various % initial drug loading on size of bare and p-THPP-loaded PHA nanoparticles when using low MW PVA as a stabilizer with PDI < 0.2 (mean ± SD, n=3). Mean with different superscript letters within the same bar are significantly different ($p \leq 0.05$) as determined by Duncan's test.

We found that the particle size of bare and the p-THPP-loaded PHA nanoparticles at 5, 10 and 20 % initial drug loading were increased in all polymer types when using low MW PVA. The increase in drug content of the nanoparticles

with increasing initial drug loading may have resulted in an increase in the particle size (Figure 5.20). There appears to have statistical differences in size at all % initial drug loading among the nanoparticles made from PHB, P(HB-*co*-12%HV) and P(HB-*co*-65%HV) ($p \leq 0.05$).

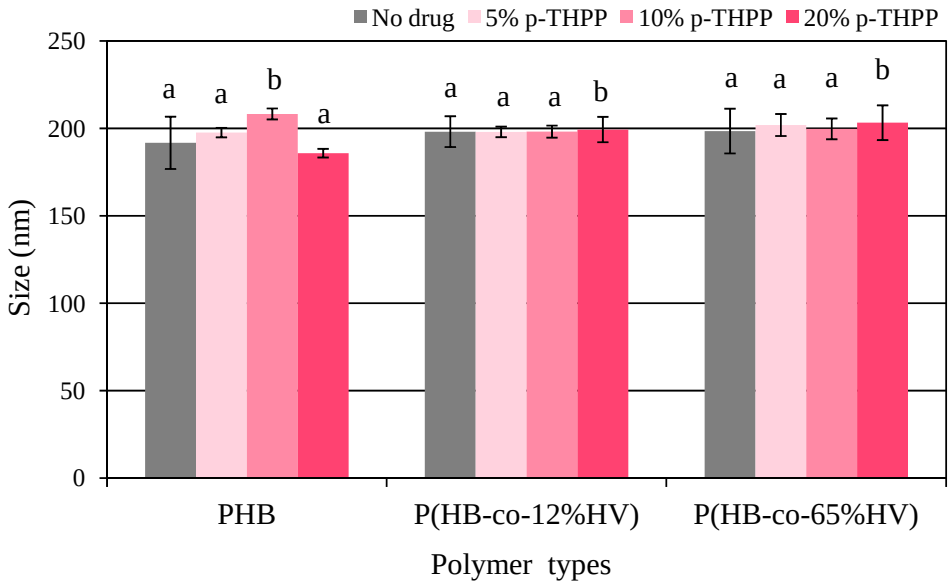

Figure 5.21 Effect of initial drug loading at various type of PHAs on size of bare and p-THPP-loaded PHA nanoparticles when using high MW PVA as a stabilizer with PDI < 0.2 (mean ± SD, n=3). Mean with different superscript letters within the same bar are significantly different ($p \leq 0.05$) as determined by Duncan's test.

Figure 5.21 showed that when using high MW PVA as stabilizer, the size of PHA nanoparticles made of PHB, P(HB-*co*-12%HV) and P(HB-*co*-65%HV) at the initial amount of p-THPP loading of 5, 10 and 20% (w/w) were also found to be in the same trend with the bare PHA nanoparticles. Here, the effect of the %HV monomer on the size of drug-loaded nanoparticles could be observed at certain % initial drug loading. At 5% initial drug loading, there appears to have no statistical difference in the particle mean size among the nanoparticles made from P(HB-*co*-12%HV) and P(HB-*co*-65%HV) ($p \leq 0.05$). At 10 and 20% initial drug loading, there is a significantly difference in the particle mean size of only PHB nanoparticles ($p \leq 0.05$).

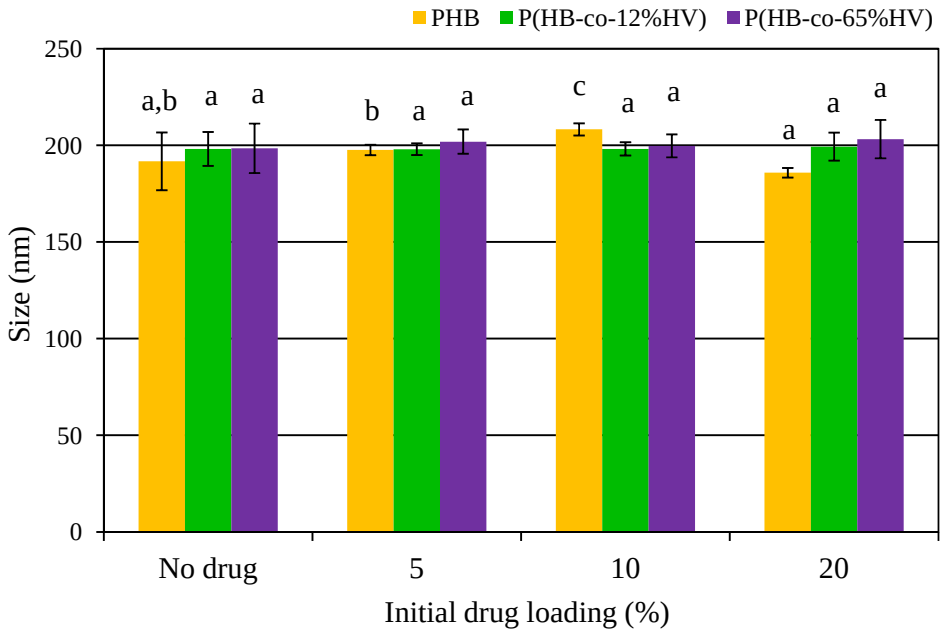

Figure 5.22 Effect of polymer types at various % initial drug loading on size of bare and p-THPP-loaded PHA nanoparticles when using high MW PVA as a stabilizer with PDI < 0.2 (mean ± SD, n=3). Mean with different superscript letters within the same bar are significantly different ($p \leq 0.05$) as determined by Duncan's test.

When using high MW PVA as a shell stabilizer, the particle size of bare and p-THPP-loaded PHA nanoparticles at 5, 10 and 20% initial drug loading were found to be in the same rage. The increasing of % initial drug loading did not lead to any significant increase of the particle size (**Figure 5.22**). There appears to have no statistical difference in size at all % initial drug loading among the nanoparticles made from P(HB-*co*-12%HV) and P(HB-*co*-65%HV) ($p \leq 0.05$). But, the particles size of PHB nanoparticles was found to be significant different at all % initial drug loading ($p \leq 0.05$).

Table 5.9 Effect of the theoretical drug loading on the effective drug loading and entrapment efficiency of p-THPP-PHA nanoparticles.

Type of PVA	Initial drug loading (%)	PHB		P(HB-*co*-12%HV)		P(HB-*co*-65%HV)	
		Drug loading (%)	Entrapment efficiency (%)	Drug loading (%)	Entrapment efficiency (%)	Drug loading (%)	Entrapment efficiency (%)
Low MW	5	1.26 ± 0.03^{a}	25.16 ± 0.61^{a}	1.53 ± 0.04^{a}	30.53 ± 0.85^{a}	1.11 ± 0.19^{a}	22.17 ± 3.73^{a}
	10	$3.99 \pm 0.03^{a,b}$	39.91 ± 0.31^{b}	3.95 ± 0.05^{b}	39.48 ± 0.50^{b}	2.50 ± 0.82^{b}	29.57 ± 1.07^{b}
	20	6.83 ± 2.02^{b}	40.87 ± 1.75^{b}	9.33 ± 0.51^{c}	46.64 ± 2.57^{c}	8.67 ± 0.21^{c}	43.33 ± 1.07^{c}
High MW	5	0.91 ± 0.01^{a}	18.16 ± 0.29^{a}	1.49 ± 0.10^{a}	29.89 ± 1.94^{a}	1.22 ± 0.04^{a}	24.49 ± 0.73^{a}
	10	2.34 ± 0.50^{b}	23.44 ± 4.96^{a}	4.10 ± 1.18^{b}	41.05 ± 11.78^{a}	4.17 ± 0.45^{b}	41.71 ± 4.53^{b}
	20	4.80 ± 0.20^{c}	24.00 ± 1.01^{a}	6.78 ± 0.55^{c}	33.91 ± 2.74^{a}	5.24 ± 0.39^{c}	26.22 ± 1.94^{a}

Mean with different superscript letters within the same column are significantly different ($p \leq 0.05$) as determined by Duncan's test.

To increase the entrapment efficiency in the nanoparticles, the initial amount of p-THPP in the formulations was varied at 5, 10 and 20% (w/w). The results (Table 5.9) showed that when use low MW PVA as a stabilizer, the drug loading of the nanoparticles prepared by PHB, P(HB-*co*-12%HV) and P(HB-*co*-65%HV) were increased from 1.26 up to 6.83% (w/w), 1.53 up to 9.33% (w/w) and 1.11 up to 8.67% (w/w), respectively. They appears to have statistical differences at all % initial drug loading among the nanoparticles made from P(HB-*co*-12%HV) and P(HB-*co*-65%HV). However, for the PHB nanoparticles, the data show statistical differences in % drug loading only when using 5 and 20% initial drug loading ($p \leq 0.05$). From the results, the % drug loading values and % entrapment efficiency among three types of PHA nanoparticles made with low MW PVA are in a similar range to one another. In addition, the results also show to have no trend towards the increasing of %HV in the PHA polymers.

Thus far, the effect of MW of PVA has been shown to have a great affect on the size of drug-loaded PHA nanopaticles for all types. When the high MW PVA was used as a stabilizer, the equal in the particle size was observed for the p-THPP-loaded PHA nanoparticles. Such phenomenon could not be seen when using the low MW PVA. Therefore, it would be interesting to investigate the effect of high MW of PVA on other of nanoparticle's physical parameters mentioned. As shown in **Table 5.9**, with the high MW PVA used, the % drug loading of nanoparticles prepared from PHB, P(HB-*co*-12%HV) and P(HB-*co*-65%HV) at the initial amount of p-THPP in the formulations of 5, 10 and 20% (w/w) were found to be increased from 0.91 up to 4.80% (w/w), 1.49 up to 6.78% (w/w) and 1.22 up to 5.24% (w/w), respectively, while a decrease in the corresponding drug entrapment efficiency was observed. The similar trend was also observed with all types of PHA polymers tested. From these data, we found that the results of % drug loading shows statistical differences at all % initial drug loading among the nanoparticles made from PHB, P(HB-*co*-12%HV) and P(HB-*co*-65%HV) ($p \leq 0.05$). In contrast, the % entrapment efficiency values were found not to be statistically significantly differences from one another, except for P(HB-*co*-65%HV) nanoparticles at 10% initial drug loading. Tsai *et al*. (1986) reported that an increase in the drug loading of mitomycin C into PLA microcapsules ranging from 3.65 to 13.80%, however there was no influence on the mean particle size detected

(Tsai *et al*., 1986). Our finding suggests that there might be an interaction among high MW PVA, drug and PHAs after drug encapsulated, in which it might lead to a change in polymer packing of the PVA chains, resulting into the increase in amount of drug being entrapped, while the particle size was maintained.

However, when comparing between low and high MW PVA systems (**Table 5.9**), we found that the % drug loading values of p-THPP-loaded PHA nanoparticles made with low MW PVA were found to be significantly higher than those PHA nanoparticles made with high MW PVA. There is an earlier study by Prabha *et al*. (2004) showing similar findings to our current work about the effect of MW of PVA (Prabha & Labhasetwar, 2004). They found that the plasmid DNA-encapsulated PLGA nanoparticles formulated with lower MW PVA (13-23 kDa) had a relatively higher % DNA loading than those formulated using high MW PVA (31-50 kDa and 85-146 kDa). They also reported that the residual PVA on the nanoparticles surface resulted in a lower gene transfection. The influence of PVA might affect the release profile of nanoparticles through the difference in their sticking or packing on the surface of nanoparticles (Prabha & Labhasetwar, 2004).

5.3 Analysis of *in vitro* cytotoxicity and photocytotoxicity of p-THPP-loaded PHA nanoparticles

5.3.1 Cytotoxicity and photocytotoxicity of free p-THPP

The concept of PDT is based on the administration of a photosensitizer (PS) drug in the tumor tissues. When illuminate with an appropriate wavelength of light to activate the drug in the presence of oxygen, it results in the generation of reactive oxygen species that leads to cell death and tissue destruction.

In order to find the appropriate conditions for PDT system, the *in vitro* photocytotoxicity of free p-THPP was firstly evaluated on the HT-29 colon cancer cell model for conditions including drug concentration, light dose and pre-incubation time. It was important to show that the laser light alone would not cause a decrease in cell viability under the PDT experiment conditions used for this study (i.e. after 24 h of incubation or irradiation at 6 and 9 J/cm^2).

The HT-29 cells were treated with different concentrations of free p-THPP (i.e. 2, 4, 8 and 16 μg/mL) with a pre-incubation time of 1 h and an irradiated light

dose of 6 J/cm^2. The photocytotoxicity was evaluated at 24 h after the irradiation. As shown in **Figure 5.23**, the MTT test performed at 24 h post irradiation exhibited a substantial decrease of % cell viability in a concentration-dependent manner as when the drug concentration was increased from 2 to 16 μg/mL. The lowest cell viability (i.e. at around 14%) was found at the highest drug concentration tested (i.e. 16 μg/mL). It is also important to note that when compared to the dark controls (i.e. without light) at each drug concentration, the photocytotoxicity of free p-THPP under the influence of light does at 6 J/cm^2 was seen at the drug concentration of 8 μg/mL for the reduction of cell viability observed at the same drug concentration. This finding indicates that the p-THPP, which is one of potent photosensitizers, can cause cell damage only with the light exposure under our PDT testing system. The concentration of free p-THPP at 8 μg/mL offered appropriate photocytotoxic effect leading to around 40-60% cell viability after PDT light irradiation. Therefore, a p-THPP concentration at 8 μg/mL and the cell viability assay performed at 24 h after irradiation were selected as a control condition in the subsequent experiments.

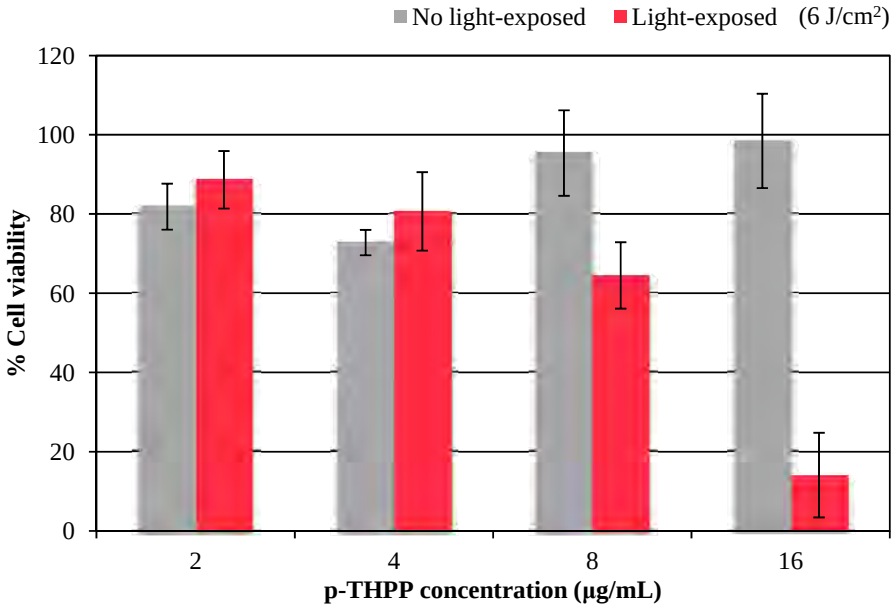

Figure 5.23 Influence of drug concentration on the photocytotoxicity of free p-THPP on the viability of HT-29 cancer cells. The cells were incubated for 1 h at drug dose of 2, 4, 8 and 16 μg/mL and irradiated at a light dose of 6 J/cm^2. MTT assay was performed 24 h after light exposure.

5.3.2 Photocytotoxicity effect of the light dose

The effect of light dose on p-THPP photocytotoxicity was assessed at 1 h pre-incubation time with the drug concentrations at 2, 4 and 8 μg/mL. It has been shown previously in other studies that the effectiveness of photocytotoxic effect on cancer cells depends strongly on the light intensity after treated with p-THPP (Henderson *et al*., 2004). As demonstrated in **Figure 5.24**, the highest light intensity (i.e. 9 J/cm^2) could lead to more photocytotoxic to cancer cells. Our findings were in accordance with a previous study done by Zeisser-Labouebe *et al*. (2006) showing that the photoactivity of hypericin, another type of PS drug, was increased with increasing the light dose (Zeisser-Labouebe *et al*., 2006). In general, an appropriate light dose should be selected at the lowest level as possible, in which it can still be potent enough to kill the cells via PDT, but not harmful when exposing to the cells in the absent of PS drugs (Horfelt *et al*., 2007). This is mainly to help reducing any potential risks and/or side effects towards the cells that might have been caused by the laser light alone at the treatment site. Based from our data in **Figure 5.24**, the 6 J/cm^2 was selected to be the appropriate light dose for our PDT testing system.

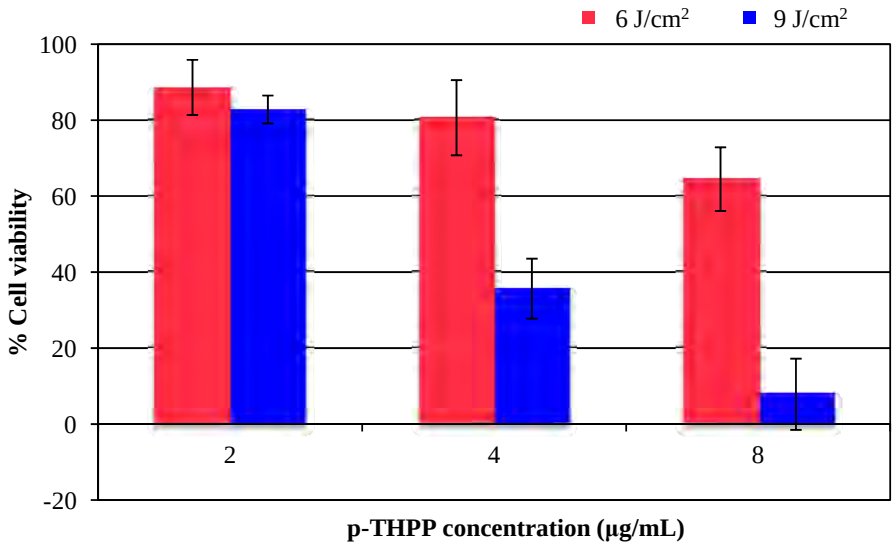

Figure 5.24 Influence of light dose on the photocytotoxicity of free p-THPP on the viability of HT-29 cancer cells. The cells were incubated for 1 h at drug dose of 2, 4 and 8 μg/mL and irradiated with increasing light doses (6 and 9 J/cm^2). MTT assay was performed 24 h after light exposure.

5.3.3 Cytotoxicity and photocytotoxicity effect of p-THPP-loaded PHA nanoparticles

In order to investigate the cytotoxicity and photocytotoxicity of various p-THPP-loaded PHA nanoparticles used in PDT applications, we firstly have to verify that there are no other toxic effects towards the cells from the bare PHA nanoparticles alone. **Figure 5.25** shows that bare PHA nanoparticles did not cause a decrease in cell viability. In addition, we found that the percentage of cell viability of the condition with free p-THPP at 8 μg/mL was not different to when treating the HT-29 cells with p-THPP-loaded P(HB-*co*-65%HV) nanoparticles containing the p-THPP at 6 μg/mL under the same light dose of 6 J/cm^2 (i.e. cell viability at 65% and 54%, respectively). Our current results thus suggested that there should be no toxicity derived from the bare PHA nanoparticles used in our study.

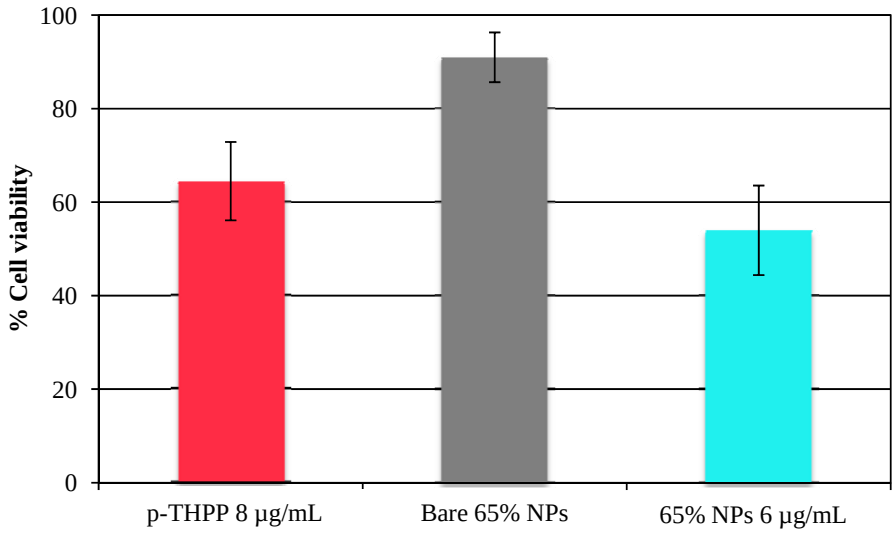

Figure 5.25 Percentage of cell viability of HT-29 cells treated with free p-THPP 8 μg/mL, compared to bare and p-THPP-loaded PHA nanoparticles made from P(HB-*co*-65%HV) at drug dose of 6 μg/mL and irradiated at a light dose of 6 J/cm^2. MTT assay was performed 24 h after light exposure.

Nevertheless, it is important to mention that the *in vitro* drug released behaviors (i.e. burst released and/or gradually released) from p-THPP-loaded PHA nanoparticles need to be performed in future study in order to investigate the effect of

%HV of PHA and type of PVA on the release profile of p-THPP drug overtime under physiological conditions (i.e. pH 7.0 and pH 4.5). Previous studies already reported that the composition of polymer, the molecular weight of polymer and the % drug loading could concurrently affect the degradation of polymeric nanoparticles and the amount of drug released, thus resulting into different patterns of drug released profiles as well as different efficacy in killing cancer cells (Eniola & Hammer, 2005).

At current, we already performed a preliminary study on the time course photocytoactivity of p-THPP-loaded PHA nanoparticles made of only P(HB-*co*-65%HV) copolymers formulated at the 10% initial p-THPP loading compared to free drug in order to investigate whether the drug encapsulated in PHA nanoparticles could give any advantage towards killing HT-29 cancer cells when compared to the free drug alone. In practice, the drug encapsulated in nanoparticles should be beneficial in terms of the stability of drug and possibly the lower dose of drug usage (Mohanra & Chen, 2006). According to previous studies by Konan *et al.* (2003) the period of pre-incubation time of the p-THPP-loaded PHA nanoparticles with the cells prior to the light irradiation could greatly affect to the efficiency of the drug-loaded nanoparticles. The effect of pre-incubation time (i.e. from 5 to 60 min) on photocytotoxicity with various concentrations of p-THPP-loaded PLGA nanoparticles were evaluated (Konan *et al.*, 2003). The molecular weight of PLGA used in their study was about 10-times lower than P(HB-*co*-65%HV). Since we expected that our PHAs polymer might affect the drug released rate due to molecular weight and physical properties that might lead to the slower degradation when compared with PLGA, we decided to investigate further on the appropriate pre-incubation time (i.e. from 5 min to 6 h) for finding the optimized pre-incubation time of our drug-loaded PHA nanoparticles delivery systems against HT-29 cancer cells via PDT. As mentioned previously, the concentration of p-THPP at 8 μg/mL was used as a control for PDT systems at light dose of 6 J/cm^2. Furthermore, the selected equivalent drug doses of p-THPP-loaded PHA nanoparticles prepared by P(HB-*co*-65%HV) were 1.5, 3 and 6 μg/mL which were lower than the control free drug.

As shown in **Figure 5.26(A)**, there was no dark toxicity of either free p-THPP at 8 μg/mL at various pre-incubation times or p-THPP-loaded P(HB-*co*-65%HV) nanoparticles at various concentrations and pre-incubation times. These

findings assure that our PDT system do not have any side effect towards killing cells, especially when the PS drugs are not activated by the light.

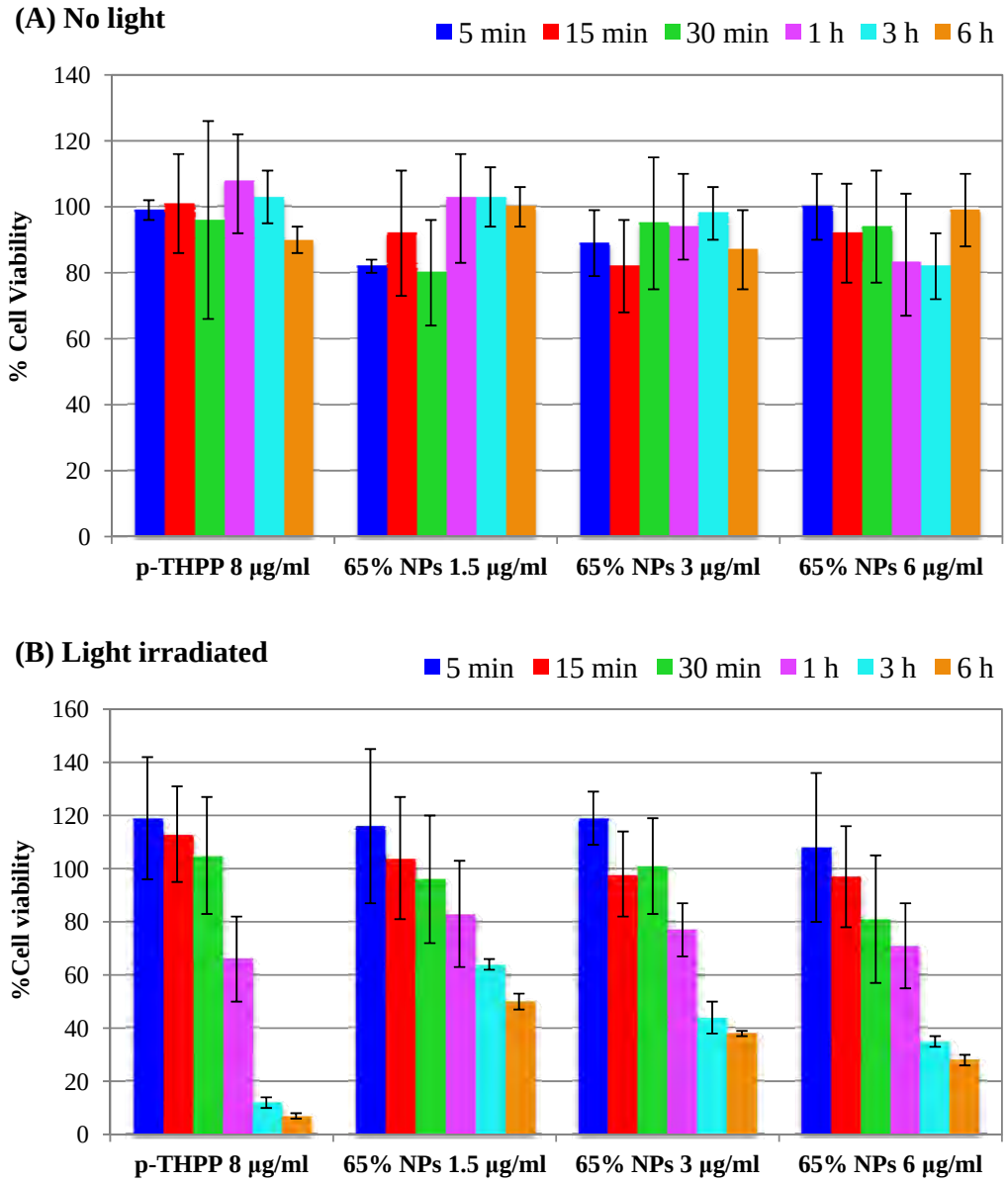

Figure 5.26 Percentage of cell viability of HT-29 cells treated with free-pTHPP at 8 µg/mL compared with p-THPP-loaded PHA nanoparticles made from P(HB-*co*-65%HV) at equivalent drug dose of 1.5, 3 and 6 µg/mL with 5 min to 6 h of pre-incubation time. MTT assay was performed 24 h after light exposure. (**A**) No light irradiation. (**B**) Irradiated at a light dose of 6 J/cm^2.

Figure 5.26(B) exhibited the influence of pre-incubation time on photocytotoxicity evaluated at 8 μg/mL free p-THPP concentrations and three different drug doses of p-THPP-loaded P(HB-*co*-65%HV) nanoparticles (i.e. 1.5, 3 and 6 μg/mL). After irradiation at a dose of 6 J/cm^2, the percentage of cell viability generally decreased when increasing the pre-incubation time. The reduction of % cell viability was found to be a time-dependent manner, since cell death was increased with the increased pre-incubation time from 5 min to 6 h. Furthermore, the p-THPP-loaded P(HB-*co*-65%HV) nanoparticles could cause a decrease of % cell viability in a concentration-dependent manner. The highest photocytotoxic effect was obtained with 6 μg/mL of p-THPP-loaded P(HB-*co*-65%HV) nanoparticles with the pre-incubation time of 6 h, leading to % cell viability at around 28%. Interestingly, our results showed that there were slightly differences in % cell viability at short pre-incubation times (i.e. 5 to 30 min). The signs of photoactivity of free p-THPP and p-THPP-loaded P(HB-*co*-65%HV) nanoparticles were observed after 30 min and the cell viability was still continually decreased until 6 h. At 30 min to 6 h pre-incubation times, the free p-THPP were found to have higher phototoxicity than p-THPP-loaded P(HB-*co*-65%HV) nanoparticles, which might be mainly due to the higher drug used at 8 μg/mL.

Previous studies suggested that the major factor governing the extension of the photo-induced cell damage as well as the mechanism of cell death is due to the subcellular localization of the PS drugs (Kessel & Thompson, 2003). Our results indicated that the efficiency of photoactivation might be dependent on the PS drug cellular uptake mechanism and their subcellular localization. Our cell study results thus far were consistent with the observation found by Konan *et al.* (2003) (Konan *et al*., 2003). Their study investigated the cellular uptake and localization of PLGA nanoparticles in EMT-6 tumor cells by flow cytometry and reported that all formulations entered the cells in a concentration- and time- dependent manner. The p-THPP–loaded PLGA nanoparticles were rapidly internalized within cells to a greater extent relative to the free p-THPP drug at a short pre-incubation times (15-30 min). Moreover, all the formulations tested were observed in both early and late endosomes when observed by fluorescence microscopy resulting in the suggestion that endocytosis might be the major route in cellular uptake mechanism as we suspected

based on our findings.

Furthermore, our results suggested that the effect of P(HB-*co*-65%HV) might facilitate the slow release of p-THPP into the cell culture medium. This might be mainly due to the fact that the molecular weight of PHAs (i.e. 10^5 -10^6 g/mol) are much higher than PLGA or PLA (i.e. 10^3 -10^4 g/mol), which are the most wildly used aliphatic polyesters in the preparation of PS-loaded nanoparticles for PDT system (Konan *et al*., 2003). Many previous research works focusing on the degradation of PLGA microspheres reported that the PLGA polymer with high molecular weight generally exhibits lower degradation rates due to less susceptibility to degradation when compared with the lower one, and more time for the degradation is often required (Park, 1995). The researchers also suggested that when used aliphatic polyester microspheres as drug carriers, the degradation profiles should be careful considered. Moreover, the effect of % drug loading into the polymer matrix was found to be one of the important factors on the rate and duration of drug release. The polymeric matrices with higher amount of drug would give a larger initial burst release than those having lower content due to the less amount of drug encapsulated. The PLGA microspheres with less amount of drug in their matrix can undergo degradation by the biphasic released profile. Thus, the possibility to engineer the controlled-release drug delivery system using aliphatic polyester might be achieved by employing factors that can affect the degradation rate of polymer including type of polymer, type of drug and amount of drug loading (Eniola & Hammer, 2005).

Conclusions and Recommended Future Works

VI. CONCLUSIONS

In the first phase (PHASE I.) of our research, high amount of P(HB-*co*-HV) were successfully biosynthesized by *Cupriavidus necator* H16 in mineral salt media with different types of carbon sources such as fructose, sodium propionate and sodium valerate. According to the copolymer composition determined by gas chromatography, we found that this strain has ability to convert the supplied carbon substrates into HB and HV monomers, resulting into various P(HB-*co*-HV) copolymers with different monomer compositions ranging from 12-90% mole HV incorporation, biomass ranging from 1.4-6.3 g/L, % PHA content per CDW ranging from 10.6-97.6%, and the overall production of P(HB-*co*-HV) ranging from 0.16-6.20 g/L under shake-flask condition. In this research, we found three culturing conditions that could lead to very high production of P(HB-*co*-HV) at above 4 g/L, which are; 1) The production of 6.20 g/L P(HB-*co*-12%HV) using 20 g/L fructose and 2 g/L sodium valerate, 2) The production of 4.51 g/L P(HB-*co*-16%HV) using 10 g/L fructose and 2 g/L sodium valerate and 3) The production 4.06 g/L P(HB-*co*-65%HV) using solely 10 g/L sodium valerate. This might also be worthwhile to mention that there has been no publication thus far reporting about the simple culturing strategy by using sodium valerate as a sole carbon source to obtain P(HB-*co*-65%HV) at almost 94% content per CDW. Nonetheless, the high level of P(HB-*co*-HV) production of different %HV compositions from *C. necator* H16 achieved in our study are also comparable to many literatures (Lee *et al*., 2010). As a result, our study provides an alternative and more simple culturing strategy for the effective production of P(HB-*co*-HV) copolymers by bacteria cultivation with high polymer content. In particular, the P(HB-*co*-HV) copolymers appear to have many favorable physical properties over the pure PHB, including their lower melting and glass-transition temperatures leading to better processability for making plastic films and bags. In addition, the P(HB-*co*-HV) copolymers become more susceptibility to biodegradation due to less chain

packing, thus extending their applications to the area where higher rate of degradation is desired, such as drug carriers and tissue engineering scaffolds in biomedicine.

In the second phase (PHASE II.) of our research, a technique of formulating PHA nanoparticles with the diameter size close to 200 nm has been successfully developed via a modified emulsification-solvent diffusion method using PVA as a shell stabilizer. Here, we demonstrated that this core-shell PHA nanoparticles could be used to carry a hydrophobic p-THPP anti-cancer drug. All PHA nanoparticles formulated are quite uniform in their size distribution with their PDI less than 0.2. In addition, they also have slight negative zeta potential values (i.e. from -0.7 to -1.6), indicating the presence of some slight negative charges on the surface of nanoparticles. The important insights obtained from our research work are based on the investigation into the effect of types of PHA copolymers (i.e. 0, 12 and 65% HV content) and types of PVA stabilizer (i.e. low and high MW) on the size, % drug loading and % entrapment efficiency of the PHA nanoparticles formulated under the same processing condition. By increasing %HV, this could lead to the increasing in the size of nanoparticles, but only with the low MW PVA as a shell stabilizer. This finding was not found when using the high MW PVA, which might be due to the fact that larger PVA molecules assembled onto the surface of nanoparticles, could shield the size changes occurred at the core of PHA nanoparticles. Nevertheless, the final diameter size of p-THPP-loaded PHA nanoparticle made with the highest %HV content (i.e. P(HB-*co*-65%HV)) is still around at 200 nm as desirable for the passive drug delivery in PDT. Interestingly, the effect of increasing %HV on % drug loading and % entrapment efficiency of PHA nanoparticles could also be seen from our research work. The highest drug loading (i.e. 8.67-9.33%) and the highest entrapment efficiency (i.e. 43.33-46.64%) were from when using either P(HB-*co*-12%HV) or P(HB-*co*-65%HV) as the core polymer with the low MW PVA and with 20% initial drug loading in the system. A similar trend of results was also observed with the high MW PVA, however the highest % drug loading and % entrapment efficiency with this PVA system were almost 50% lower than when using the low MW PVA. In summary, the values of % drug loading and % entrapment efficiency of our PHA nanoparticles with the low MW PVA are quite comparable to the values reported in other literatures

that formulated drug-loaded polymeric nanoparticles for PDT from PLA and PLGA polymers (Shah *et al*., 2010).

For the last phase (PHASE III.) of our research, the *in vitro* cytotoxicity evaluation with HT-29 colon cancer cells showed that both of bare PHA nanoparticles and p-THPP-loaded PHA nanoparticles did not cause a concerned cell death when there was no light activation. Interestingly, our preliminary results on the *in vitro* photocytotoxicity study showed that the p-THPP-loaded P(HB-*co*-65%HV) nanoparticles could lead to cell death at lower drug dose when compared to the free p-THPP drug alone, in which almost 70% cell death could be achieved when using p-THPP-loaded nanoparticles at concentration of 6 µg/mL, incubation time of 6 h and light dose of 6 J/cm^2. Thus far, our findings suggest the applicablility of PHA nanoparticles as an anti-cancer drug deliver for PDT, since our PHA nanoparticle system possesses a satisfactory induction of photodynamic damages to HT-29 cancer cells. PHAs might be considered as one of good candidate biomaterials for fabricating prolonged-action drug delivery systems in the form of polymeric nanoparticles. The photo-induced cytotoxicity of the PS is depending on the PDT parameters such as drug concentration, light dose, pre-incubation time and physical properties of the polymer delivery system (i.e. types of polymer, MW, biodegradation). Considering the potential clinical applications of the PHA nanoparticles for photodynamic therapy, a greater understanding about the pharmacokinetic properties of drug-loaded PHA nanoparticles, such as drug-released profile, as well as the interaction between drug-loaded PHA nanoparticles and cancer cells are needed to be more elucidated in the future study.

RECOMMENED FUTURE WORKS

In order to fulfill the overall goals of this research work as well as for high quality scientific publications, additional experiments need to be performed to investigate many factors that involve in our formulated PHA nanoparticles and test their applicability for an anti-cancer drug delivery in PDT system. The suggested future experiments are listed below.

1. Characterization of p-THPP-loaded PHA nanoparticles via Transmission Electron Microscopy (TEM)

According to our findings about the physical properties of drug-loaded PHA nanoparticles, there were some different in particle size and % drug loading of each nanoparticle formulations between two PVA systems, low and high MW, which were used as a shell stabilizer for nanoparticles. In order to investigate the effect of type of PVA shell stabilizer on the size of nanoparticles, Transmission electron microscopy (TEM) will be employed to visualize for how the PVA molecules assembled onto the surface of PHA nanoparticles and to determine the diameter size of the PHA core and the thickness of the PVA shell. Moreover, the differences between morphology (i.e. particles size and different shell packing) of bare PHA nanoparticles compared with p-THPP-loaded PHA nanoparticles using two different PVA systems are *expected* to be observed via TEM. To do this, the nanoparticles solution will be dropped onto a carbon coated copper grid and allowed to air-dried. The samples will be negative stained by using 1.5% phosphotungstic acid (PTA). The grid will be subsequently dried and visualized for TEM image (Su *et al*., 2012).

2. *In vitro* investigation of drug release profile and biodegradation of p-THPP-loaded PHA nanoparticles under various pH conditions

Due to different physical and thermal properties of these three PHA (PHB, P(HB-*co*-12%HV) and P(HB-*co*-65%HV)), when they are used for making drug-encapsulated nanoparticles, we expect that these PHA nanoparticles should contribute to different drug-released behaviors. The difference in drug release profiles is one of important factor for enhancing the effectiveness in killing cancer cells via PDT system. Therefore, we expect to see the differences in the drug released profile from

three different types of PHA nanoparticles formulated in this study. Although PHAs have many merits and great potential for drug release application, more in-depth studies still have to be conducted before the clinical application can be initiated. It is thus important to study the drug release behaviors of p-THPP-loaded PHA nanoparticles.

In vitro drug release behaviors will be carried out using a method as reported by He *et al.* (2011) (He *et al*., 2011). The p-THPP-loaded PHA nanoparticles in buffer solutions of different pH values, sterilized dialysis bags with dialyzer molecular-weight cut-off 10,000 Da will be used to carry out the drug release experiments. Phosphate buffered saline (PBS) of pH 7.4 and acetic buffer solutions (ABS) of pH 4.5 will be used as the drug release media to simulate normal blood/tissues and tumor environments.

3. Determination of singlet oxygen production

In order to investigate of drug release profile from each formulation of p-THPP-loaded PHA nanoparticles that is more directly related to the application in PDT, monitoring the amount of singlet oxygen generated from photosensitizer molecules encapsulated in PHA nanoparticles should be evaluated. The $^1O_2$ generated will be detected through the chemiluminescence of Singlet Oxygen Sensor Green (SOSG) reagent. SOSG has been report to be highly specific for $^1O_2$ and response very little to hydroxyl radicals and peroxide (Flors *et al*., 2006).

The ability of p-THPP-encapsulated into nanoparticles to generate singlet oxygen will be assessed with a SOSG available kit. Briefly, SOSG will be added according to the manufacturer protocol (Molecular Probes Inc., USA). The concentration of free p-THPP and also p-THPP-loaded PHA naoparticles before adding SOSG will be at 2-20 µg/mL in phosphate buffer saline. Sample will be irradiated with LED lamp (λ = 653 nm) and singlet oxygen production will then assayed with fluorescence (excitation/emission = 488/525 nm). Xiao *et al.* (2011) reported the singlet oxygen production by porous Si nanoparticles (function as photosensitizers) that the fluorescence emission intensity after the irradiation of SOSG solution containing porous Si nanoparticles was observed to increase gradually (Figure 5.1) (Xiao *et al*., 2011). An equivalent sample maintained in the dark showed no

increase in fluorescence signal. These findings showed the capacity of singlet oxygen generation of photosensitizer, which can be detected by SOSG.

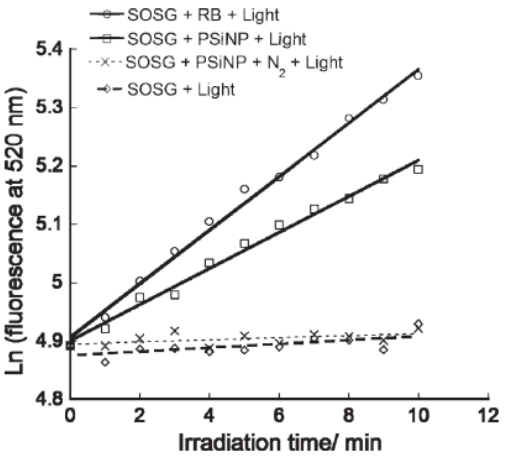

Figure 6.1 Increase in fluorescence intensity of SOSG endoperoxide as a function of irradiation time in the presence of SOSG alone, SOSG with RB, and SOSG with porous Si nanoparticles (PSiNP) in air and in N_2 saturated solution, respectively (Xiao *et al*., 2011).

4. Cytotoxicity and photocytotoxicity studies of p-THPP-loaded PHA nanoparticles against HT-29 cancer cells

According to our preliminary results on the *in vitro* photocytotoxicity studied, only P(HB-*co*-65%HV) nanoparticles using high MW PVA as a stabilizer has been selected. Thus, our future work aims to evaluate the photodynamic activity on HT-29 colon cancer cells using the nanoparticles prepared by all three types of PHA including PHB, P(HB-*co*-12%HV) and P(HB-*co*-65%HV) and also compared between two PVA systems (i.e. low and high MW). The p-THPP-loaded PHA nanoparticles will be selected for further studies at the % initial drug loading that obtained the highest % entrapment efficiency of each PVA type. The appropriate % initial drug loading of p-THPP-loaded PHA nanoparticles prepared by low and high MW PVA were found to be 20% and 10%, respectively.

The cytotoxicity and photocytotoxicity of all nanoparticle formulations will be evaluated with HT-29 cancer cells compared to the free drug. The influence of drug concentration (2-16 mg/mL) and light dose (6-9 J/cm^2) on p-THPP photocytotoxic efficiency will be investigated with all p-THPP formulations tested using the methods that previously described in Section 4.2.3. For time course study, the pre-incubation time should be extended longer (12 h - 3 days) to observe any possible advantage of PHA nanoparticles as it can be retained in the cell longer than the free drug.

In order to elucidate the photodynamic mechanisms of these promising p-THPP-loaded PHA nanoparticles for PDT, we will need to further evaluate their internalization, subcellular localization and efflux in comparison with the free p-THPP drug. The experiments will be carried out by using a method that reported previously by Konan *et al.* (2003) (Konan *et al*., 2003).

6. Cytotoxicity and photocytotoxicity studies of drug-loaded PHA nanopartilces against multidrug resistance cancer cells

The development of multidrug resistance (MDR) is a major impediment to successful cancer treatment. There are many patients suffer from MDR, which can reduce the efficiency of cancer therapy and subsequently lead to treatment failure (Szakacs *et al*., 2006). Cancer cells utilize various mechanisms to reduce the accumulation of the anti-cancer drug at its intracellular site of action. Overexpression of P-glycoprotein (P-gp), a drug efflux transporter, is an important determinant of tumor drug resistance (Leonard *et al*., 2003). Previous studies have shown that biodegradable polymer capsules offered a promising mean to circumvent P-gp-mediated MDR. The capsules were internalized by MDR cells via endocytosis and designed for the subsequent intracellular release of the drugs by enzymatic degradation in lysosomes (Yan *et al*., 2010). According to another strategy, nanoparticle-mediated combination chemotherapy and PDT using doxorubicin and methylene blue as a photosensitizer resulted in an improved cytotoxicity in drug-

resistant breast cancer cells (Khdair *et al*., 2009). Polymeric nanoparticles as photosensitizer carriers appear to be endocytosed and accumulated intracellularly in the cytoplasm, thus indicating additional advantages (Konan *et al.* 2003). Here, the study employing the core-shell p-THPP-loaded PHA nanoparticles for overcoming MDR cancer cells will be investigated. The cytotoxicity and photocytotoxicity of PHA nanoparticles will be studied on *multidrug-resistant colon cancer* cells using the methods previously described in Section 4.2.3. The P-gp expression and also cellular uptake will be performed as described by Li *et al.* (2012) (Li *et al*., 2012).

References

Bengtsson, S., Pisco, A. R., Johansson, P., Lemos, P. C., & Reis, M. A. M. (2010). Molecular weight and thermal properties of polyhydroxyalkanoates produced from fermented sugar molasses by open mixed cultures. *Journal of Biotechnology, 147*(3-4), 172-179.

Bhattacharjee, S., Ershov, D., Fytianos, K., Gucht, J., Alink, G. M., Rietjens, I. M., *et al*. (2012). Cytotoxicity and cellular uptake of tri-block copolymer nanoparticles with different size and surface characteristics. *Particle and Fibre Toxicology, 9*, 11.

Bhubalan, K., Chuah, J. A., Shozui, F., Brigham, C. J., Taguchi, S., Sinskey, A. J., *et al*. (2011). Characterization of the highly active polyhydroxyalkanoate synthase of *chromobacterium* sp. strain USM2. *Applied and Environmental Microbiology, 77*(9), 2926-2933.

Bhubalan, K., Lee, W. H., Loo, C. Y., Yamamoto, T., Tsuge, T., Doi, Y., *et al*. (2008). Controlled biosynthesis and characterization of poly(3-hydroxybutyrate-co-3-hydroxyvalerate-co-3-hydroxyhexanoate) from mixtures of palm kernel oil and 3HV-precursors. *Polymer Degradation and Stability, 93*(1), 17-23.

Chanprateep, S. (2010). Current trends in biodegradable polyhydroxyalkanoates. *Journal of Bioscience and Bioengineering, 110*(6), 621-632.

Chanprateep, S., Katakura, Y., Visetkoop, S., Shimizu, H., Kulpreecha, S., & Shioya, S. (2008). Characterization of new isolated Ralstonia eutropha strain A-04 and kinetic study of biodegradable copolyester poly(3-hydroxybutyrate-co-4-hydroxybutyrate) production. *Journal of Industrial Microbiology & Biotechnology, 35*(11), 1205-1215.

Chen, G. Q., & Wu, Q. (2005). The application of polyhydroxyalkanoates as tissue engineering materials. *Biomaterials, 26*, 6565-6578.

Doi, Y., Segawa, A., Nakamura, S., & Kunioka, M. Production of biodegradable copolyesters by *Alcaligenes eutrophus*. (1990). In: *Novel biodegradable microbial polymers.* (Dawes E. A., ed.) Kluwer Academic Publishers, Netherlands, pp. 37-48.

Duarte, A. R. C., Mano, J. F., & Reis, R. L. (2009). Preparation of chitosan scaffolds loaded with dexamethasone for tissue engineering applications using supercritical fluid technology. *European Polymer Journal, 45*(1), 141-148.

Dunn, R. L., English, J. P., Strobel, J. D., Cowsar, D. R. & Tice, T. R. (1988). Preparation and evaluation of lactic acid/glycoside copolymers for drug delivery. In: *Polymers in medicine III*. (Migliaresi, C. ed.), Elsevier, Amsterdam, pp. 149-159.

Dunne, M., Corrigan, O. I., & Ramtoola, Z. (2000). Influence of particle size and dissolution conditions on the degradation properties of polylactide-co-glycolide particles. *Biomaterials, 21*(16), 1659-1668.

Elsabahy, M., & Wooley, K. L. (2010). Design of polymeric nanoparticles for biomedical delivery applications. *Chemical Society Reviews, 41*(7), 2545-2561.

Eniola, A. O., & Hammer, D. A. (2005). Characterization of biodegradable drug delivery vehicles with the adhesive properties of leukocytes II: effect of degradation on targeting activity. *Biomaterials, 26*(6), 661-670.

Fereidouni, M., Younesi, H., Daneshi, A., & Sharifzadeh, M. (2011). The effect of carbon source supplementation on the production of poly(3-hydroxybutyrate-co-3-hydroxyvalerate) by *Cupriavidus necator*. *Biotechnology and Applied Biochemistry, 58*(3), 203-211.

Govender, T., Stolnik, S., Garnett, M. C., Illum, L., & Davis, S. S. (1999). PLGA nanoparticles prepared by nanoprecipitation: drug loading and release studies of a water soluble drug. *Journal of Controlled Release, 57*(2), 171-185.

He, Q., Gao, Y., Zhang, L., Zhang, Z., Gao, F., Ji, X., *et al*. (2011). A pH-responsive mesoporous silica nanoparticles-based multi-drug delivery system for overcoming multi-drug resistance. *Biomaterials, 32*, 7711-7720.

Henderson, B. W., Gollnick, S. O., Snyder, J. W., Busch, T. M., Kousis, P. C., Cheney, R. T., *et al*. (2004). Choice of oxygen-conserving treatment regimen determines the inflammatory response and outcome of photodynamic therapy of tumors. *The Journal of Cancer Research, 644*(6), 2120-2126.

Horfelt, C., Stenquist, B., Larko, O., Faergemann, J., & Wennberg, A. M. (2007). Photodynamic therapy for acne vulgaris: a pilot study of the dose-response and mechanism of action. *Acta Dermato Venereologica, 87*(4), 325-329.

Huijberts, G. M., Wal, H., Wilkinson, C., & Eggink, G. (1994). Gas-chromatographic analysis of poly(3-hydroxyalkanoates) in bacteria. *Biotechnology Techniques, 8*(3), 187-192.

Jacquel, N., Lo, C. W., Wei, Y. H., Wu, H. S., & Wang, S. S. (2008). Isolation and purification of bacterial poly(3-hydroxyalkanoates). *Biochemical Engineering Journal, 39*(1), 15-27.

Jia-Gen. W., Tingting, G., Hong-Yuan, Z., Yi-Yun, X., Xiu-Zhen, Z., Guo, C., & Yuxiang, C. (2011). Preparation and optimization of PEG-PLGA loaded with vincristine sulfate and its in vitro release. *Journal of Bioequivalence & Bioavailability. 3*(9). 211-214.

Kemavongse, K., Prasertsan, P., Upaichit, A., & Methacanon, P. (2007). Effect of co-substrate on production of poly-b-hydroxybutyrate (PHB) and copolymer PHBV from newly identified mutant *Rhodobacter sphaeroides* U7 cultivated under aerobic-dark condition. *Songklanakarin Journal of Science and Technology, 29*(4), 1101-1113.

Kessel, D., & Thompson, P. (1987). Purification and analysis of hematoporphyrin and hematoporphyrin derivative by gel exclusion and reverse-phase chromatography. *Photochemistry and Photobiology, 46*(6), 1023-1025.

Khdair, A., Handa, H., Mao, G., & Panyamb, J. (2009). Nanoparticle-mediated combination chemotherapy and photodynamic therapy overcomes tumor drug resistance *in vitro*. *European Journal of Pharmaceutics and Biopharmaceutics, 71*, 214-222.

Khanna, S., & Srivastava, A. K. (2005). Statistical media optimization studies for growth and PHB production by *Ralstonia eutropha*. *Process Biochemistry, 40*, 2173-2182.

Konan, Y. N., Berton, M., Gurny, R., & Allemann, E. (2003). Enhanced photodynamic activity of meso-tetra(4-hydroxyphenyl)porphyrin by incorporation into sub-200 nm nanoparticles. *European Journal of Pharmaceutical Sciences, 18*(3-4), 241-249.

Konan, Y. N., Cerny, R., Favet, J., Berton, M., Gurny, R., & Allemann, E. (2003). Preparation and characterization of sterile sub-200 nm meso-tetra(4-hydroxylphenyl)porphyrin-loaded nanoparticles for photodynamic therapy. *European Journal of Pharmaceutics and Biopharmaceutics, 55*(1), 115-124.

Kunasundari, B., & Sudesh, K. (2011). Isolation and recovery of microbial polyhydroxyalkanoates. *eXPRESS Polymer Letters, 5*(7), 620-634.

Lau, N. S., Tsuge, T., & Sudesh, K. (2011). Formation of new polyhydroxyalkanoate containing 3-hydroxy-4-methylvalerate monomer in *Burkholderia* sp. *Applied Microbiology and Biotechnology, 89*(5), 1599-1609.

Lee, S. C., Oh, J. T., Jang, M. H., & Chung, S. I. (1999). Quantitative analysis of polyvinyl alcohol on the surface of poly(D,L-lactide-co-glycolide) microparticles prepared by solvent evaporation method: effect of particle size and PVA concentration. *Journal of Controlled Release, 59*(2), 123-132.

Leonard, G. D., Fojo, T., & Bates, S. E. (2003). The role of ABC transporters in clinical practice. *The Oncologist, 8*(5), 411-424

Li, B., Xu, H., Li, Z., Yao, M., Xie, M., Shen, H., *et al*. (2012). Bypassing multidrug resistance in human breast cancer cells with lipid/polymer particle assemblies. *International Journal of Nanomedicine, 7*, 187-197.

Lirdprapamongkol, K., Kramb, J. P., Suthiphongchai, C., Surarit, R., Srisomsap, C., Dannhardt, G., & Svasti, J. (2009). Vanillin suppresses metastatic potential of

human cancer cells through PI3K inhibition and decreases angiogenesis *in vivo*. *Journal of agricultural and food chemistry, 57*(8), 3055-3063.

Ma, Y., Zheng, Y., Liu, K., Tian, G., Tian, Y., Xu, L., *et al*. (2012). Nanoparticles of poly(lactide-co-glycolide)-d-a-Tocopheryl polyethylene glycol 1000 succinate random copolymer for cancer treatment. *Nanoscale Research Letters, 5*, 1161-1169.

Mallapragada, S. K., & McCarthy-Schroeder, S. (2000). Poly(vinyl alcohol) as a Drug Delivery Carrier, In: *Handbook of Pharmaceutical Controlled Release Technology.* (Wise, D. L. ed.), Marcel Dekker, New York, pp. 31-47,

Manangana, T., & Shawaphuna, S. (2010). Quantitative extraction and determination of polyhydroxyalkanoate accumulated in *Alcaligenes latus* dry cells. *Science Asia, 36*, 199-203.

Mitomo, H., Takahashi, T., Ito, H., & Saito, T. (1999). Biosynthesis and characterization of poly(3-hydroxybutyrate-co-3-hydroxyvalerate) produced by *Burkholderia cepacia* D1. *International Journal of Biological Macromolecules, 24*(4), 311-318.

Mittal, A., Negi, P., Garkhal, K., Verma, S., & Kumar, N. (2010). Integration of porosity and bio-functionalization to form a 3D scaffold: cell culture studies and *in vitro* degradation. *Biomedical Materials, 5*(4), 045001.

Moghimi, S. M., Hunter, A. C., & Murray, J. C. (2001). Long-circulating and target-specific nanoparticles: theory to practice. *Pharmacological Reviews, 53*(2), 283-318.

Mohanraj, V. J., & Chen, Y. (2006). Nanoparticles - A Review *Tropical Journal of Pharmaceutical Research, 5*(1), 561-573.

Murdock, R. C., Braydich-Stolle, L., Schrand, A. M., Schlager, J. J., & Hussain, S. M. (2008). Characterization of nanomaterial dispersion in solution prior to in *vitro* exposure using dynamic light scattering technique. *Toxicological Sciences, 101*(2), 239-253.

Nabiyouni, G., Barati, A., & Saadat, M. (2011). Surface adsorption of polyethylene glycol and polyvinyl alcohol with variable molecular weights on zinc oxide nanoparticles. *Iranian Journal of Chemical Engineering 8*(1), 20-30.

Ostle, A. G., & Holt, J.G. (1982). Nile blue A as a fluorescent stain for poly-beta-

hydroxybutyrate. *Applied and Environmental Microbiology, 44,* 238-241.

Park, M. V. D. Z., Annema, W., Salvati, A., Lesniak, A., Elsaesser, A., Barnes, C., *et al*. (2009). *In vitro* developmental toxicity test detects inhibition of stem cell differentiation by silica nanoparticles. *Toxicology and Applied Pharmacology, 240*(1), 108-116.

Park, J., Kim, T., & Lee, S. (2011). Genome-scale reconstruction and in silico analysis of the *Ralstonia eutropha* H16 for polyhydroxyalkanoate synthesis, lithoautotrophic growth, and 2-methyl citric acid production. *BMC Systems Biology, 5*(1), 101.

Park, T. G. (1995). Degradation of poly(lactic-co-glycolic acid) microspheres: effect of copolymer composition. *Biomaterials, 16*(15), 1123-1130.

Prabha, S., & Labhasetwar, V. (2004). Critical determinants in PLGA/PLA nanoparticle-mediated gene expression. *Pharmaceutical Research, 21*(2), 354-364.

Raberg, M., Peplinski, K., Heiss, S., Ehrenreich, A., Voigt, B., Doring, C., *et al*. (2011). Proteomic and transcriptomic elucidation of the mutant ralstonia eutropha G+1 with regard to glucose utilization. *Applied and Environmental Microbiology, 77*(6), 2058-2070.

Ramsay, B. A., Ramsay, J. A., & Cooper, D. G. (1989). Production of poly-*β*-hydroxyalkanoic acid by *Pseudomonas cepacia*. *Applied and Environmental Microbiology, 55*(3), 584-589.

Ramsay, J. A., Berger, E., Voyer, R., Chavarie, C., & Ramsay, B. A. (1994). Extraction of poly-3-hydroxybutyrate using chlorinated solvents. Biotechnology Techniques, 8(8), 589-594.

Rathbone, S., Furrer, P., Lubben, J., Zinn, M., & Cartmell, S. (2010). Biocompatibility of polyhydroxyalkanoate as a potential material for ligament and tendon scaffold material. *Journal of Biomedical Materials Research Part A, 93A*(4), 1391-1403.

Sabuncu, A. C., Grubbs, J., Qian, S., Abdel-Fattah, T. M., Stacey, M. W., & Beskok, A. (2012). Probing nanoparticle interactions in cell culture media. *Colloids and Surfaces B: Biointerfaces 95*, 96-102.

Sahoo, S. K., Panyam, J., Prabha, S., & Labhasetwar, V. (2002). Residual polyvinyl alcohol associated with poly (D,L-lactide-co-glycolide) nanoparticles affects their physical properties and cellular uptake. *Journal of Controlled Release, 82*(1), 105-114.

Scholes, P. D., Coombes, A. G. A., Illum, L., Daviz, S. S., Vert, M., & Davies, M. C. (1993). The preparation of sub-200 nm poly(lactide-co-glycolide) microspheres for site-specific drug delivery. *Journal of Controlled Release, 25*(1-2), 145-153.

Shaffie, K. A., B.Moustafa, A., Saleh, N. H., & Nasr, H. E. (2010). Effect of polyvinyl alcohol of different molecular weights as protective colloids on the kinetics of the emulsion polymerization of vinyl acetate. *Journal of American Science, 6*(10), 1202-1212.

Shaw, S. Y., Westly, E. C., Pittet, M. J., Subramanian, A., Schreiber, S. L., & Weissleder, R. (2008). Perturbational profiling of nanomaterial biologic activity. *Proceedings of the National Academy of Sciences, 105*(21), 7387-7392.

Sichwart, S., Hetzler, S., Broker, D., & Steinbuchel, A. (2010). Extension of the substrate utilization eange of *Ralstonia eutropha* strain H16 by netabolic engineeringto include mannose and glucose. *Applied and Environmental Microbiology, 77*(4), 1325-1334.

Soares, M. V., Oliveira, M. R., Santos, E. P. d., Gitirana, L. d. B., Barbosa, G. M., Quaresma, C. H., *et al*. (2011). Nanostructured delivery system for zinc phthalocyanine: preparation, characterization, and phototoxicity study against human lung adenocarcinoma A549 cells. *International Journal of Nanomedicine, 6*, 227-238.

Son, H. J., & Kim, J. S. (2007). Therapeutic efficacy of DNA-loaded PLGA microspheres in tumor-bearing mice. *Archives of Pharmacal Research 30*, 1047-1050.

Sreeram, K. J., Nidhin, M., & Nair, B. U. (2009). Synthesis of aligned hematite nanoparticles on chitosan–alginate films. *Colloids and Surfaces B: Biointerfaces, 71*(2), 260-267.

Srinivasan, C., Katare, Y. K., Muthukumaran, T., & Panda, A. K. (2005). Effect of additives on encapsulation efficiency, stability and bioactivity of entrapped lysozyme from biodegradable polymer particles. *Journal of Microencapsulation, 22*(2), 127-138.

Su, W. P., Cheng, F. Y., Shieho, D. B., Yeh, C. S., & Su, W. C. (2012). PLGA nanoparticles codeliver paclitaxel and Stat3 siRNA to overcome cellular resistance in lung cancer cells. *International Journal of Nanomedicine, 7*, 4269–4283.

Sudesh, K., Abe, H., & Doi, Y. (2000). Synthesis, structure and properties of polyhydroxyalkanoates: biological polyesters. *Progress in Polymer Science, 25*(10), 1503-1555.

Tezcaner, A., Bugra, K., & Hasırcı, V. (2003). Retinal pigment epithelium cell culture on surface modified poly(hydroxybutyrate-co-hydroxyvalerate) thin films. *Biomaterials, 24*(25), 4573-4583.

Tsai, D. C., Howard, S. A., Hogan, T. F., Malanga, C. J., Kandzari, S. J., & Ma, J. K. (1986). Preparation and in vitro evaluation of polylactic acid-mitomycin C microcapsules. *Journal of Microencapsulation, 3*(3), 181-193.

Valappil, S. P., Misra, S. K., Boccaccini, A. R., Keshavarz, T., Bucke, C., & Roy, I. (2007). Large-scale production and efficient recovery of PHB with desirable material properties, from the newly characterised *Bacillus cereus* SPV. *Journal of Biotechnology, 132*(3), 251-258.

Vargas, A., Pegaz, B., Debefve, E., Konan-Kouakou, Y., Lange, N., Ballini, J. P., *et al*. (2004). Improved photodynamic activity of porphyrin loaded into nanoparticles: an *in vivo* evaluation using chick embryos. *International Journal of Pharmaceutics, 286*(1-2), 131-145.

Wan, L. S. C., & Lim, L. Y. (1992). Drug release from heat treated polyvinyl alcohol films. *Drug Development and Industrial Pharmacy, 18*, 1895-1906.

Wu, L., Zhang, H., Zhang, J., & Ding, J. (2005). Fabrication of three-dimensional porous scaffolds of complicated shape for tissue engineering. I. Compression molding based on flexible-rigid combined mold. *Tissue Engineering, 11*(7-8), 1105-1114.

Xiao, L., Gu, L., Howell, S. B., & Sailor, M. J. (2011). Porous silicon nanoparticle photosensitizers for singlet oxygen and their phototoxicity against cancer cells. *ACS Nano, 5*(5), 3651–3659.

Xiong, Y. C., Yao, Y. C., Zhan, X. Y., & Chen, G. Q. (2010). Application of polyhydroxyalkanoates nanoparticles as intracellular sustained drug-release vectors. *Journal of Biomaterials Science, Polymer Edition, 21*(1), 127-140.

Yan, Y., Ochs, C. J., Such, G. K., Heath, J. K., Nice, E. C., & Caruso, F. (2010). Bypassi ng multidrug resistance in cancer cells with biodegradable polymer capsules. *Advanced Materials, 22*(47), 5398-5403.

Zambaux, M. F., Bonneaux, F., Gref, R., Maincent, P., Dellacherie, E., Alonso, M. J., *et al*. (1998). Influence of experimental parameters on the characteristics of poly(lactic acid) nanoparticles prepared by a double emulsion method. *Journal of Controlled Release, 50*(1-3), 31-40.

Zeisser-Labouebe, M., Lange, N., Gurny, R., & Delie, F. (2006). Hypericin-loaded nanoparticles for the photodynamic treatment of ovarian cancer. *International Journal of Pharmaceutics, 326*(1-2), 174-181.

APPENDIX A

Standard curve of 3-HB monomer

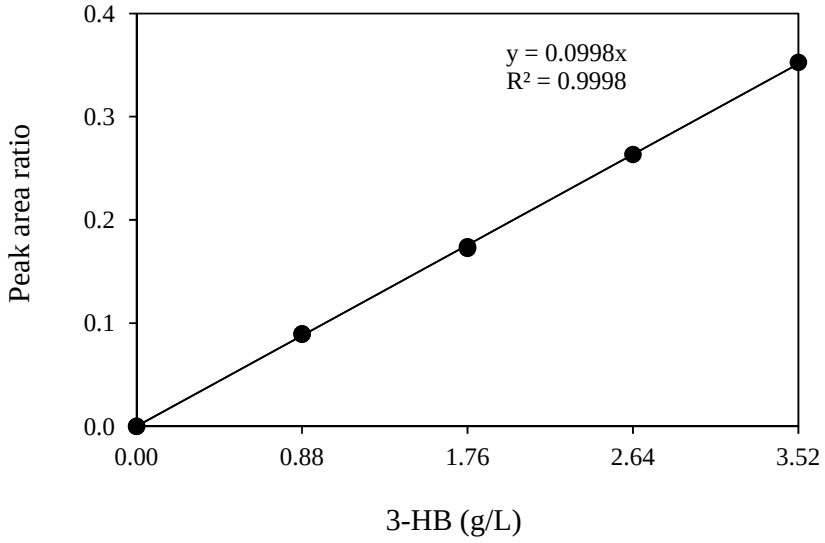

Standard curve of 3-HV monomer

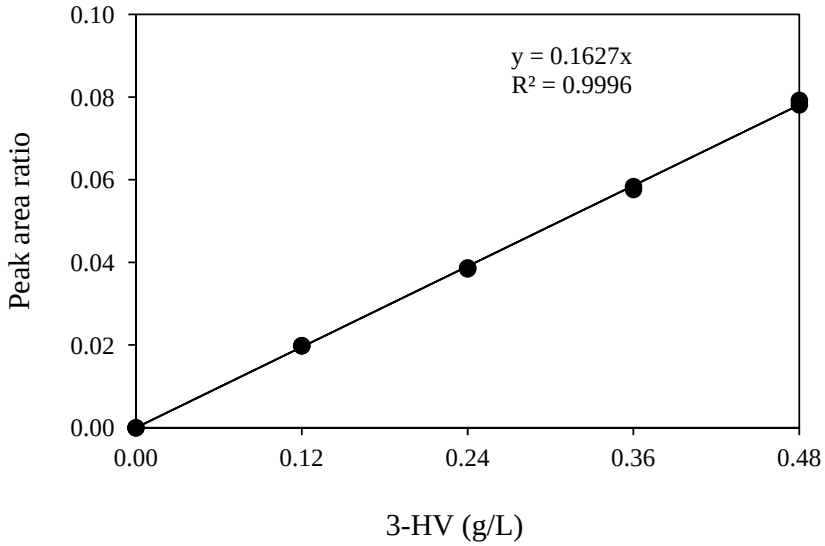

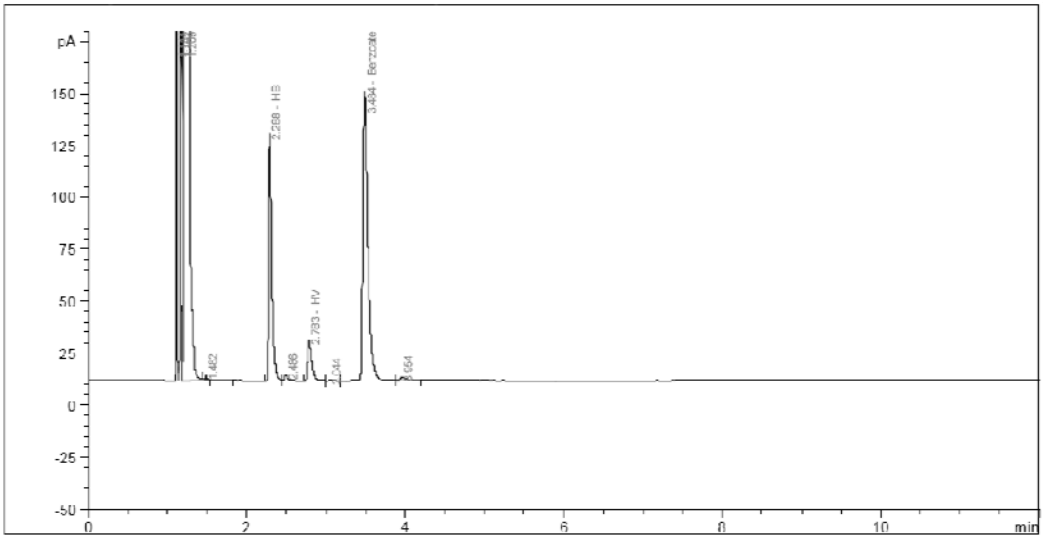

At 1.2 minute Methanol Chromatogram

At 2.2 minute Hydroxybutyrate chromatogram 3.52 g/L (interested peak)

At 2.7 minute Hydroxyvalerate chromatogram 0.48 g/L (interested peak)

At 3.4 minute Benzoate chromatogram (internal standard)

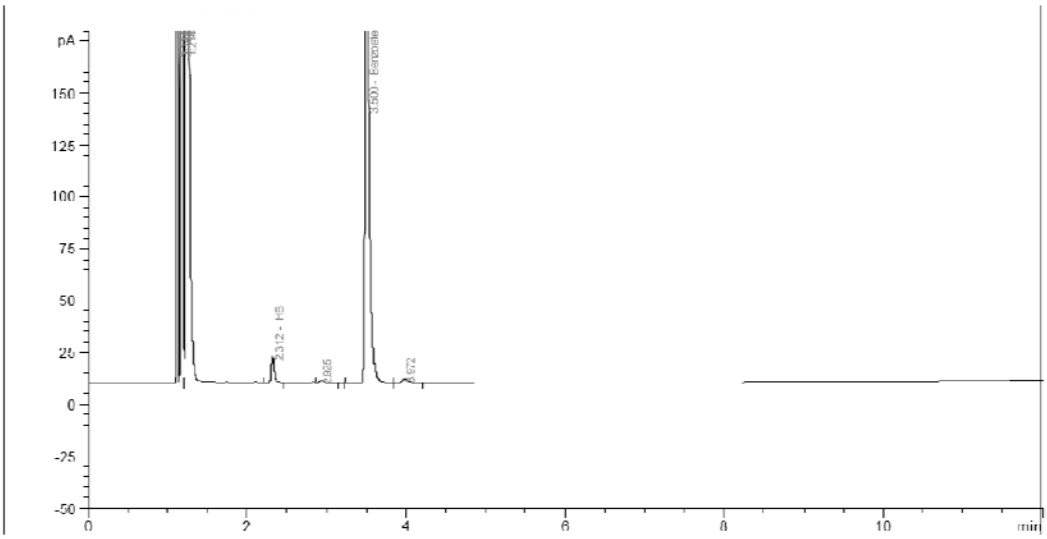

Chromatogram of polymer extract from *C. necator* H16 grown in MS media with 20 g/L glucose at 30°C and 200 rpm for 48 h.

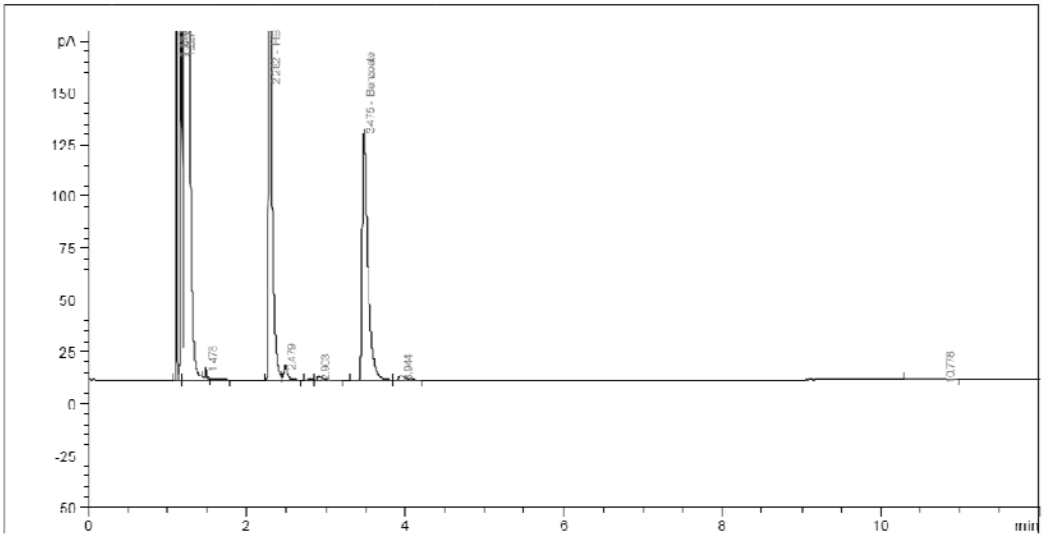

Chromatogram of polymer extract from *C. necator* H16 grown in MS media with 20 g/L fructose at 30°C and 200 rpm for 48 h.

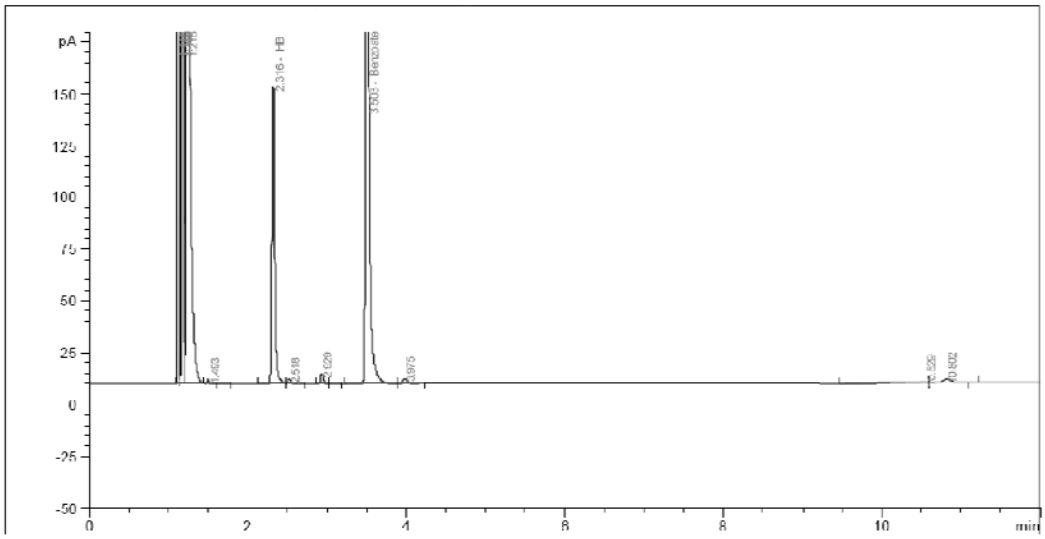

Chromatogram of polymer extract from *C. necator* H16 grown in MS media with 20 g/L gluconate at 30°C and 200 rpm for 48 h.

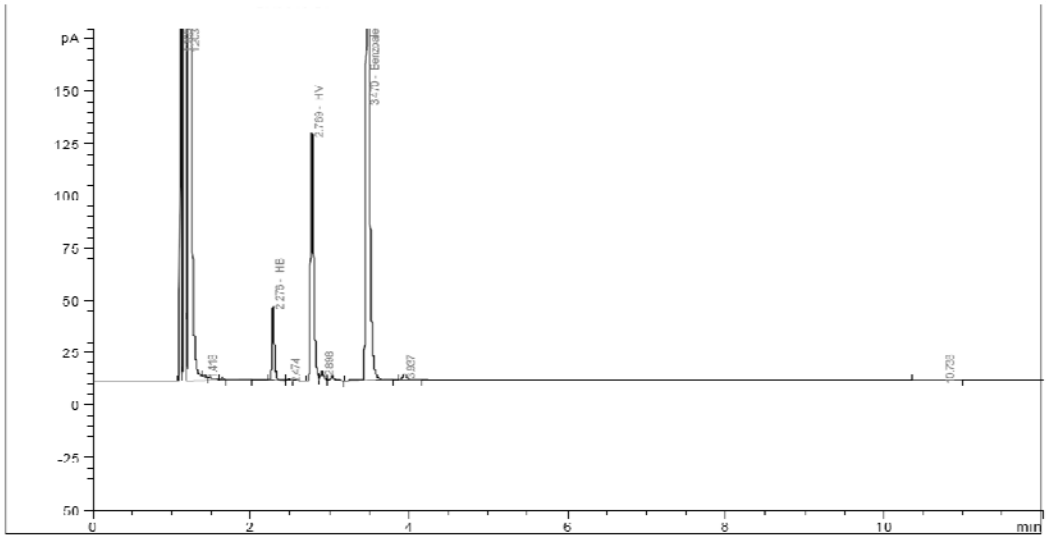

Chromatogram of polymer extract from *C. necator* H16 grown in MS media with 10 g/L fructose and 10 g/L propionate at 30°C and 200 rpm for 48 h.

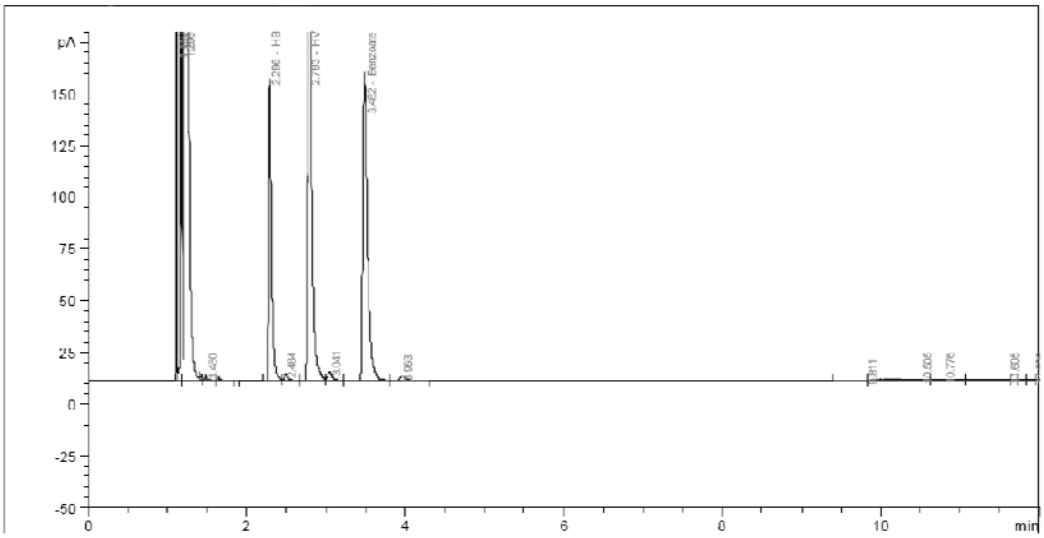

Chromatogram of polymer extract from *C. necator* H16 grown in MS media with 10 g/L fructose and 10 g/L valerate at 30°C and 200 rpm for 48 h.

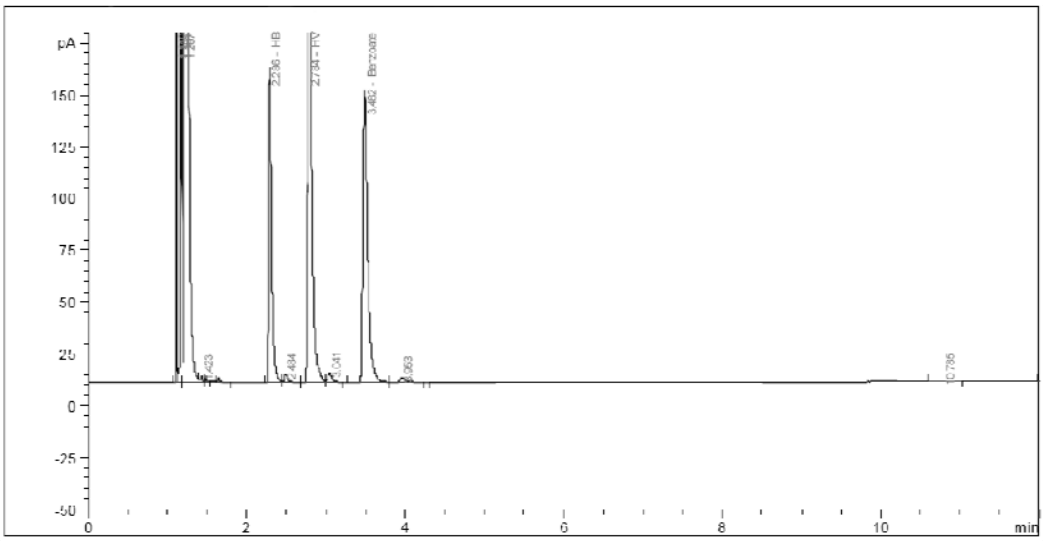

Chromatogram of polymer extract from *C. necator* H16 grown in MS media with 15 g/L fructose and 5 g/L valerate at 30°C and 200 rpm for 48 h.

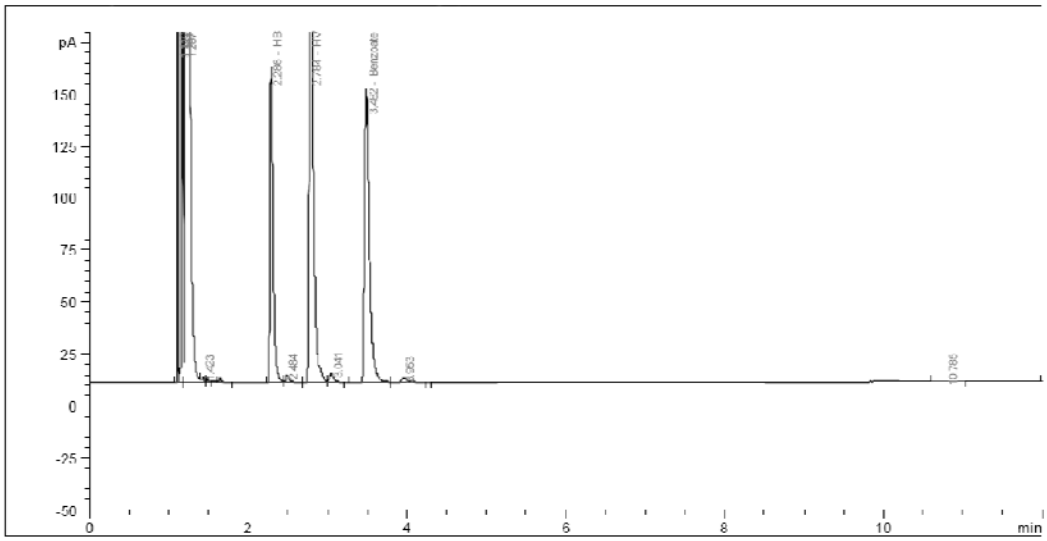

Chromatogram of polymer extract from *C. necator* H16 grown in MS media with 5 g/L fructose and 15 g/L valerate at 30°C and 200 rpm for 48 h.

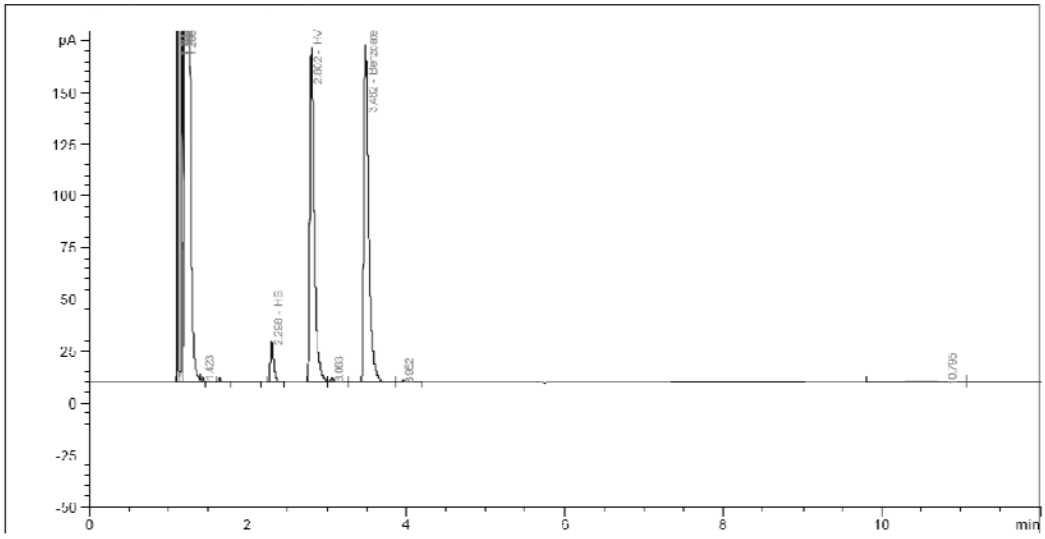

Chromatogram of polymer extract from *C. necator* H16 grown in MS media with 20 g/L valerate at 30°C and 200 rpm for 48 h.

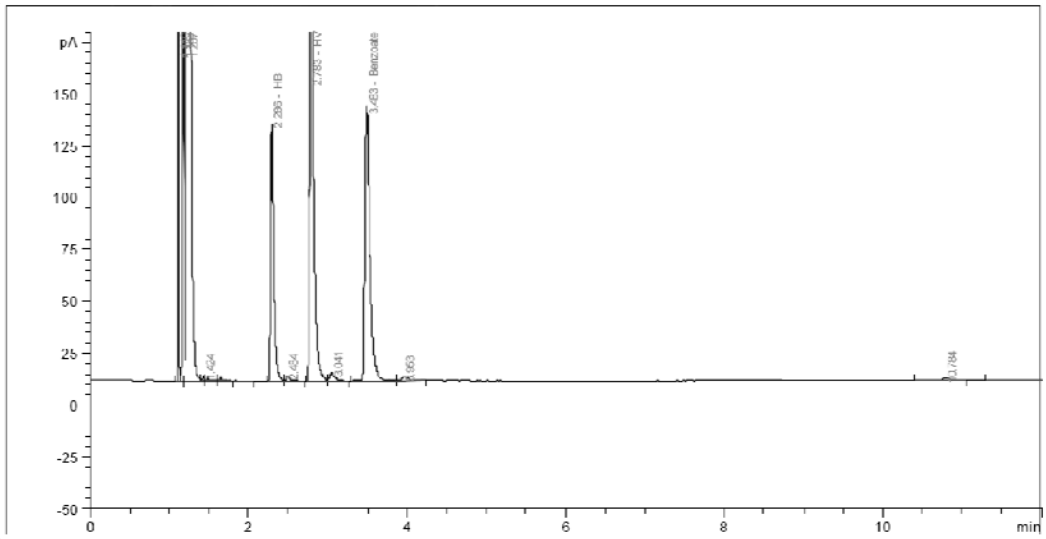

Chromatogram of polymer extract from *C. necator* H16 grown in MS media with 10 g/L valerate at 30°C and 200 rpm for 48 h.

APPENDIX B

Effect of carbon sources on biomass and PHA accumulation by *C. necator* H16.

Growth condition	Biomass (g/L)	% PHA content	PHA production (g/L)	% Mole of monomers	
				HB	HV
Glucose	0.70 ± 0.00	3.01 ± 0.49	0.02 ± 0.00	100	0
Fructose	4.10 ± 0.35	90.33 ± 3.17	3.70 ± 0.32	100	0
Gluconate	6.75 ± 0.07	30.51 ± 4.44	2.04 ± 0.32	100	0

Effect of sodium propionate and sodium valerate concentration on biomass and PHA accumulation by *C. necator* H16.

Growth condition	Biomass (g/L)	% PHA content	PHA production (g/L)	% Mole of monomers	
				HB	HV
F10-P10	3.25 ± 0.17	46.78 ± 17.32	1.54 ± 0.64	22.92	77.08
F10-V10	3.3 ± 0.35	97.04 ± 6.65	3.21 ± 0.54	33.14	66.86

Effect of varying the concentration of fructose and sodium valerate on the biomass and P(HB-*co*-HV) accumulation by *C. necator* H16

Growth condition	Biomass (g/L)	% PHA content	PHA production (g/L)	% Mole of monomers	
				HB	HV
F20-V0	4.10 ± 0.35	90.33 ± 3.17	3.70 ± 0.32	100	0
F15-V5	3.87 ± 0.12	91.85 ± 1.52	3.55 ± 0.16	61.03	38.97
F10-V10	3.3 ± 0.35	97.04 ± 6.65	3.21 ± 0.54	33.14	66.87
F5-V15	2.8 ± 0.46	94.93 ± 4.76	2.64 ± 0.33	32.05	67.95
F0-V20	1.95 ± 0.17	53.96 ± 4.32	1.05 ± 0.14	8.52	91.48

Effect of sodium valerate concentrations on biomass and PHA accumulation by *C. necator* H16.

Growth condition	Biomass (g/L)	% PHA content	PHA production (g/L)	% Mole of monomers	
				HB	HV
V10	4.45 ± 0.17	91.01 ± 8.06	4.06 ± 0.51	32.16	67.84
V20	1.95 ± 0.17	53.96 ± 4.32	1.05 ± 0.14	8.52	91.48

APPENDIX C

Effect of types of PHA polymers and PVA on the size of bare PHA nanoparticles.

Stabilizer	Polymer types	Size (nm)
Low MW	PHB	157.1 ± 4.4[a]
	P(HB-*co*-12%HV)	164.0 ± 2.4[b]
	P(HB-*co*-65%HV)	182.6 ± 7.7[c]
High MW	PHB	191.7 ± 14.9[a]
	P(HB-*co*-12%HV)	198.1 ± 8.8[a]
	P(HB-*co*-65%HV)	198.5 ± 12.8[a]

Effect of types of PHA polymers and PVA on the size of p-THPP-loaded PHA nanoparticles (10% initial p-THPP).

Stabilizer	Polymer types	Size (nm)	
		No drug	p-THPP-loaded
Low MW	PHB	157.1 ± 4.4[a]	178.0 ± 7.0[a]
	P(HB-*co*-12%HV)	164.0 ± 2.4[b]	191.5 ± 5.8[b]
	P(HB-*co*-65%HV)	182.6 ± 7.7[c]	191.5 ± 11.0[b]
High MW	PHB	191.7 ± 14.9[a]	208.3 ± 3.1[b]
	P(HB-*co*-12%HV)	198.1 ± 8.8[a]	198.2 ± 3.4[a]
	P(HB-*co*-65%HV)	198.5 ± 12.8[a]	199.7 ± 5.9[a]

Effect of the theoretical drug loading on size of p-THPP-loaded PHA nanoparticles .

Stabilizer	Polymer types	Size (nm)			
		No drug	5% p-THPP	10% p-THPP	20% p-THPP
Low MW	PHB	157.1 ± 4.4[a]	169.0 ± 7.3[a]	178.0 ± 7.0[a]	182.2 ± 3.1[a]
	P(HB-*co*-12%HV)	164.0 ± 2.4[b]	192.4 ± 2.1[b]	191.5 ± 5.8[b]	206.1 ± 3.0[b]
	P(HB-*co*-65%HV)	182.6 ± 7.7[c]	196.3 ± 6.4[b]	191.5 ± 11.0[b]	211.2 ± 8.1[b]
High MW	PHB	191.7 ± 14.9[a]	197.6 ± 2.7[a]	208.3 ± 3.1[b]	185.8 ± 2.5[a]
	P(HB-*co*-12%HV)	198.1 ± 8.8[a]	198.0 ± 3.0[a]	198.2 ± 3.4[a]	199.3 ± 7.2[b]
	P(HB-*co*-65%HV)	198.5 ± 12.8[a]	201.9 ± 6.3[a]	199.7 ± 5.9[a]	203.2 ± 9.9[b]

Effect of polymer types on size of p-THPP-PHA nanoparticles with and without p-THPP-loaded (5, 10 and 20% initial p-THPP).

Stabilizer	Initial drug loading (%)	Size (nm)		
		PHB	P(HB-*co*-12%HV)	P(HB-*co*-65%HV)
Low MW	No drug	157.1 ± 4.4[a]	164.0 ± 2.4[a]	182.6 ± 7.7[a]
	5	169.0 ± 7.3[b]	192.4 ± 2.1[b]	196.3 ± 6.4[b]
	10	178.0 ± 7.0[c]	191.5 ± 5.8[b]	191.5 ± 11.0[a,b]
	20	182.2 ± 3.1[c]	206.1 ± 3.0[c]	211.2 ± 8.1[c]
High MW	No drug	191.7 ± 14.9[a,b]	198.1 ± 8.8[a]	198.5 ± 12.8[a]
	5	197.6 ± 2.7[b]	198.0 ± 3.0[a]	201.9 ± 6.3[a]
	10	208.3 ± 3.1[c]	198.2 ± 3.4[a]	199.7 ± 5.9[a]
	20	185.8 ± 2.5[a]	199.3 ± 7.2[a]	203.2 ± 9.9[a]

Size, polydispersity index (PDI) and zeta potential of all nanoparticles formulations.

Stabilizer	Polymer types	% p-THPP	Size (nm)	PDI	Zeta potential (mV)
Low MW	PHB	No drug	157.1 ± 4.4	-	-
		5	169.0 ± 7.3		-0.8
		10	178.0 ± 7.0	0.082	-1.1
		20	182.2 ± 3.1	0.090	-1.4
	P(HB-*co*-12%HV)	No drug	164.0 ± 2.4	-	-
		5	192.4 ± 2.1	0.095	-0.8
		10	191.5 ± 5.8	0.069	-1.0
		20	206.1 ±3.0	0.080	-1.2
	P(HB-*co*-65%HV)	No drug	182.6 ± 7.7	-	-
		5	196.3 ± 6.4	0.152	-1.5
		10	191.5 ± 11.0	0.059	-1.2
		20	211.2 ± 8.1	0.154	-0.9
High MW	PHB	No drug	191.7 ± 15.0	-	-
		5	197.6 ± 2.7	0.136	-1.0
		10	208.3 ± 3.1	0.193	-2.1
		20	185.8 ± 2.5	0.123	-1.6
	P(HB-*co*-12%HV)	No drug	198.1 ± 8.8	-	-
		5	198.0 ± 3.0	0.110	-0.8
		10	198.2 ± 3.4	0.120	-1.0
		20	199.3 ± 7.2	0.141	-1.4
	P(HB-*co*-65%HV)	No drug	198.5 ± 12.8	-	-
		5	201.9 ± 6.3	0.177	-0.7
		10	199.7 ± 5.9	0.137	-1.1
		20	203.2 ± 9.9	0.191	-0.6

APPENDIX D

Influence of drug concentration on the photocytotoxicity of free p-THPP on the viability of HT-29 cancer cells.

Conc. (μg/mL)	% Cell viability	
	Light irradiation (6 J/cm^2)	No light irradiation
Control	100 ± 4	100 ± 1
2	89 ± 7	82 ± 6
4	81 ± 10	73 ± 3
8	65 ± 8	95 ± 11
16	14 ± 11	98 ± 12

Influence of light dose on the photocytotoxicity of free p-THPP on the viability of HT-29 cancer cells.

Conc. (μg/mL)	% Cell viability	
	6 J/cm^2	9 J/cm^2
Control	100 ± 4	100 ± 1
2	89 ± 7	83 ± 6
4	81 ± 10	36 ± 3
8	65 ± 8	8 ± 11

Percentage of cell viability of HT-29 cancer cells treated with free p-THPP 8 μg/mL compared to bare and p-THPP-loaded P(HB-*co*-65%HV) nanoparticles.

Conditions	% Cell viability
p-THPP 8 μg/mL	65 ± 8
Bare 65% NPs	91 ± 5
65% NPs 6 μg/mL	54 ± 9

Influence of pre-incubation time on the photocytotoxicity of free p-THPP and p-THPP-loaded P(HB-*co*-65%HV) nanoparticles on the cell viability of HT-29 cancer cells (No light irradiation).

	% Cell viability			
Time	p-THPP 8 μg/mL	65% NPs 1.5 μg/mL	65% NPs 3 μg/mL	65% NPs 6 μg/mL
5 min	99 ± 3	82 ± 2	89 ± 10	100 ± 10
15 min	101 ± 15	92 ± 19	82 ± 14	92 ± 15
30 min	96 ± 30	80 ± 16	95 ± 20	94 ± 17
1 h	108 ± 14	103 ± 13	94 ± 16	83 ± 21
3 h	103 ± 8	103 ± 9	98 ± 8	82 ± 10
6 h	90 ± 4	100 ± 6	87 ± 12	99 ± 11

Influence of pre-incubation time on the photocytotoxicity of free p-THPP and p-THPP-loaded P(HB-*co*-65%HV) nanoparticles on the cell viability of HT-29 cancer cells (Light irradiation at 6 J/cm^2).

	% Cell viability			
Time	p-THPP 8 μg/mL	65% NPs 1.5 μg/mL	65% NPs 3 μg/mL	65% NPs 6 μg/mL
5 min	119 ± 23	116 ± 29	119 ± 10	108 ± 28
15 min	113 ± 18	104 ± 23	98 ± 16	97 ± 19
30 min	105 ± 22	96 ± 24	101 ± 18	81 ± 24
1 h	66 ± 16	83 ± 20	77 ± 10	71 ± 16
3 h	12 ± 2	64 ± 2	44 ± 6	35 ± 2
6 h	7 ± 1	50 ± 3	38 ± 1	28 ± 2

Outputs

จากโครงการวิจัย MRG 5380110

โครงการการพัฒนาอนุภาคระดับนาโนจากสารโพลิไฮดรอกซีบิวทิวเรทให้เป็นตัวส่งถ่ายยาเพื่อใช้ในการบำบัดโรคมะเร็งด้วยวิธีโฟโต้ไดนามิกเทราปี

(Development of Polyhydroxyalkanoate Nanoparticles as Anti-Cancer Drug Carriers for Photodynamic Therapy)

Poster presentations:

- การประชุมนักวิจัยรุ่นใหม่พบเมธีวิจัย สกว. ครั้งที่ 12 วันที่ 10 - 12 ตุลาคม 2555
  - Title "Development of Polyhydroxyalkanoate Nanaoparticles as Anti-cancer Drug Delivers for Photodynamic Therapy"
- Inno Bioplast 2013 ที่ ศูนย์ประชุมฯ สิริกิติ์ วันที่ 24 - 26 มกราคม 2556 โดย National Innovation Agency
  - Title "**Production and Applications of Bacterial P(HB-co-HV) Copolymers in Food Packing and Medicine**"
- 12th International Conference on Polymers for Advanced Technologies, Berlin, Germany วันที่ 29 กันยายน - 2 ตุลาคม 2556
  - Title "**Development of Polyhydroxyalkanoate Nanaoparticles as Anti-cancer Drug Delivers for Photodynamic Therapy**"

Proceeding:

- Sasivimon Pramual, Nungnit Wattanavichean, Apinya Assavanig, and Nuttawee Niamsiri. **Production and characterization of a biodegradable packaging materials: P(HB-co-HV) copolymer**, The 14th FOOD INNOVATION ASIA CONFERENCE 2012 at BITEC Bangna, Bangkok, Thailand, 14th -15th June 2012

Expected publications:

1) Niamsiri, N., Pramual, S., Pholpabu, P., Assavanig, A., Berkvist, M., Batt, C. A., Svasti, J. *Preparation and chracterization of sub-200 nm polyhydroxyalkanoate nanoparticles for drug delivery*. (Manuscript in preparation)
2) Pramual, S., Assavanig, A., Sunintaboon, Panya, Berkvist, M., Lirdprapamongkola, K., Svasti. J., Niamsiri, N. *Development of meso-tetra(p-hydroxyphenyl)porphin-loaded polyhydroxyalkanoate nanoparticles for photodynamic treatment of colon cancer*. (Manuscript in preparation)

Students:

1) Master student:: **Miss Sasivimon Pranual**
    - Miss Sasivimon currently continues studying her PhD in the topic of photodynamic therapy of cancers.
2) Undergraduate student in Distinction program: **Miss Pitirat Pholpabu**